Lecture Notes

Introduction to *Ab Initio* Molecular Dynamics

Jürg Hutter
Physical Chemistry Institute
University of Zurich
Winterthurerstrasse 190
8057 Zurich, Switzerland
hutter@pci.unizh.ch

September 14, 2002

Contents

Lecture 1

Molecular Dynamics

1.1 Introduction

The aim of molecular dynamics is to model the detailed microscopic dynamical behavior of many different types of systems as found in chemistry, physics or biology. The history of molecular dynamics goes back to the mid 1950's when first computer simulations on simple systems were performed[1]. Excellent modern textbooks [2, 3] on this topic can be found and collections of articles from summer schools are a very good source for in depth information on more specialized aspects [4, 5, 6].
Molecular Dynamics is a technique to investigate equilibrium and transport properties of many–body systems. The nuclear motion of the particles is modeled using the laws of classical mechanics. This is a very good approximation for molecular systems as long as the properties studied are not related to the motion of light atoms (i.e. hydrogen) or vibrations with a frequency ν such that $h\nu > k_B T$. Extensions to classical molecular dynamics to incorporate quantum effects or full quantum dynamics (see for example Refs. [7, 8] for a starting point) is beyond the scope of this lecture series.

1.2 Equations of Motion

We consider a system of N particles moving under the influence of a potential function U [9, 10]. Particles are described by their positions $\mathbf{R}$ and momenta $\mathbf{P} = M\mathbf{V}$. The union of all positions (or momenta) $\{\mathbf{R}_1, \mathbf{R}_2, \ldots, \mathbf{R}_N\}$ will be called $\mathbf{R}^N$ ($\mathbf{P}^N$). The potential is assumed to be a function of the positions only; $U(\mathbf{R}^N)$.
The Hamiltonian $\mathcal{H}$ of this system is

$$\mathcal{H}(\mathbf{R}^N, \mathbf{P}^N) = \sum_{I=1}^{N} \frac{\mathbf{P}_I^2}{2M_I} + U(\mathbf{R}^N) \ . \tag{1.1}$$

The forces on the particle are derived from the potential

$$F_I(\mathbf{R}^N) = -\frac{\partial U(\mathbf{R}^N)}{\partial \mathbf{R}_I} \ . \tag{1.2}$$

The equations of motion are according to Hamilton's equation

$$\dot{\mathbf{R}}_I = \frac{\partial \mathcal{H}}{\partial \mathbf{P}_I} = \frac{\mathbf{P}_I}{M_I} \tag{1.3}$$

$$\dot{\mathbf{P}}_I = -\frac{\partial \mathcal{H}}{\partial \mathbf{R}_I} = -\frac{\partial U}{\partial \mathbf{R}_I} = F_I(\mathbf{R}^N) \ , \tag{1.4}$$

from which we get Newton's second law (using $\mathbf{P}_I = M_I \dot{\mathbf{R}}_I$)

$$M_I \ddot{\mathbf{R}}_I = F_I(\mathbf{R}^N) \ . \tag{1.5}$$

The equations of motion can also be derived using the Lagrange formalism. The Lagrange function is

$$\mathcal{L}(\mathbf{R}^N, \dot{\mathbf{R}}^N) = \sum_{I=1}^{N} \frac{1}{2} M_I \dot{\mathbf{R}}_I^2 - U(\mathbf{R}^N) \ , \tag{1.6}$$

and the associated Euler–Lagrange equation

$$\frac{d}{dt} \frac{\partial \mathcal{L}}{\partial \dot{\mathbf{R}}_i} = \frac{\partial \mathcal{L}}{\partial \mathbf{R}_i} \tag{1.7}$$

leads to the same final result. The two formulations are equivalent, but the *ab initio* molecular dynamics literature almost exclusively uses the Lagrangian techniques.

1.3 Microcanonical Ensemble

The following section is slightly shortened from the very clear and concise feature article by Tuckerman and Martyna [10].
The equations of motion are time reversible (invariant to the transformation $t \to -t$) and the total energy is a constant of motion

$$\frac{\partial E}{\partial t} = \frac{\partial \mathcal{H}(\mathbf{R}^N, \dot{\mathbf{R}}^N)}{\partial t} = 0 \ . \tag{1.8}$$

These properties are important to establish a link between molecular dynamics and statistical mechanics. The latter connects the microscopic details of a system the physical observables such as equilibrium thermodynamic properties, transport coefficients, and spectra. Statistical mechanics is based on the Gibbs' ensemble concept. That is, many individual microscopic configurations of a very large system lead to the same macroscopic

properties, implying that it is not necessary to know the precise detailed motion of every particle in a system in order to predict its properties. It is sufficient to simply average over a large number of identical systems, each in a different configuration; i.e. the macroscopic observables of a system are formulated in term of ensemble averages. Statistical ensembles are usually characterized by fixed values of thermodynamic variables such as energy, E; temperature, T; pressure, P; volume, V; particle number, N; or chemical potential μ. One fundamental ensemble is called the microcanonical ensemble and is characterized by constant particle number, N; constant volume, V; and constant total energy, E, and is denoted the NVE ensemble. Other examples include the canonical or NVT ensemble, the isothermal–isobaric or NPT ensemble, and the grand canonical or μVT ensemble. The thermodynamic variables that characterize an ensemble can be regarded as experimental control parameters that specify the conditions under which an experiment is performed.
Now consider a system of N particles occupying a container of volume V and evolving under Hamilton's equation of motion. The Hamiltonian will be constant and equal to the total energy E of the system. In addition, the number of particles and the volume are assumed to be fixed. Therefore, a dynamical trajectory (i.e. the positions and momenta of all particles over time) will generate a series of classical states having constant N, V, and E, corresponding to a microcanonical ensemble. If the dynamics generates all possible states then an average over this trajectory will yield the same result as an average in a microcanonical ensemble. The energy conservation condition, $\mathcal{H}(\mathbf{R}^N, \dot{\mathbf{R}}^N) = E$ which imposes a restriction on the classical microscopic states accessible to the system, defines a hypersurface in the phase space called a constant energy surface. A system evolving according to Hamilton's equation of motion will remain on this surface. The assumption that a system, given an infinite amount of time, will cover the entire constant energy hypersurface is known as the ergodic hypothesis. Thus, under the ergodic hypothesis, averages over a trajectory of a system obeying Hamilton's equation are equivalent to averages over the microcanonical ensemble. In addition to equilibrium quantities also dynamical properties are defined through ensemble averages. Time correlation functions are important because of their relation to transport coefficients and spectra via linear response theory [11, 12].
The important points are: by integration Hamilton's equation of motion for a number of particles in a fixed volume, we can create a trajectory; time averages and time correlation functions of the trajectory are directly related to ensemble averages of the microcanonical ensemble.

1.4 Numerical Integration

In a computer experiment we will not be able to generate the true trajectory of a system with a given set of initial positions and velocities. For all potentials U used in real applications only numerical integration techniques can be applied. These techniques are

based on a discretization of time and a repeated calculation of the forces on the particles. Many such methods have been devised [13] (look for "Integration of Ordinary Differential Equations"). However, what we are looking for is a method with special properties: long time energy conservation and short time reversibility. It turns out that symplectic methods (they conserve the phase space measure) do have these properties. Long time energy conservation ensures that we stay on (in fact close) to the constant energy hypersurface and the short time reversibility means that the discretize equations still exhibit the time reversible symmetry of the original differential equations. Using these methods the numerical trajectory will immediately diverge from the true trajectory (the divergence is exponential) but as they stay on the correct hypersurface they still sample the same microcanonical ensemble. On the other hand, a short time accurate method will manage to stay close to the true trajectory for a longer time and ultimately will also exponentially diverge but will not stay close to the correct energy hypersurface and therefore will not give the correct ensemble averages.
Our method of choice is the velocity Verlet algorithm [14, 15]. It has the advantage that it uses as basic variables positions and velocities at the same time instant t. The velocity Verlet algorithm looks like a Taylor expansion for the coordinates:

$$\mathbf{R}(t+\Delta t) = \mathbf{R}(t) + \mathbf{V}(t)\Delta t + \frac{\mathbf{F}(t)}{2M}\Delta t^2 \ . \tag{1.9}$$

This equation is combined with the update for the velocities

$$\mathbf{V}(t+\Delta t) = \mathbf{V}(t) + \frac{\mathbf{F}(t+\Delta t) + \mathbf{F}(t)}{2M}\Delta t^2 \ . \tag{1.10}$$

The velocity Verlet algorithm can easily be cast into a symmetric update procedure that looks in pseudo code

```
V(:) := V(:) + dt/(2M(:))*F(:)
R(:) := R(:) + dt*V(:)
Calculate new forces F(:)
V(:) := V(:) + dt/(2M(:))*F(:)
```

To perform a computer experiment the initial values for positions and velocities have to be chosen together with an appropriate time step (discretization length) Δt. The choice of Δt will be discussed in more detail in a later chapter about *ab initio* molecular dynamics. The first part of the simulation is the equilibration phase in which strong fluctuation may occur. Once all important quantities are sufficiently equilibrated, the actual simulation is performed. Finally, observables are calculated from the trajectory. Some quantities that can easily be calculated are (for these and other quantities see the books by Frenkel and Smit [3] and Allen and Tildesley [2] and references therein)

- The average temperature

$$\langle \frac{1}{2} M \mathbf{V}^2 \rangle = \frac{1}{2} k_{\mathrm{B}} T \tag{1.11}$$

- The diffusion constant

$$D = \frac{1}{6\tau} = \Delta \mathbf{R}^2(\tau) = \langle (\mathbf{R}(\tau) - \mathbf{R}(0))^2 \rangle \tag{1.12}$$

  for large times τ.

- The pair correlation function

$$g(r) = \frac{V}{N} \langle \sum_i \sum_{j \neq i} \delta(\mathbf{r} - \mathbf{R}_{ij}) \rangle \tag{1.13}$$

- The temporal Fourier transform of the velocity autocorrelation function $\langle \mathbf{V}(t) \cdot \mathbf{V}(0) \rangle$ is proportional to the density of normal modes (in a purely harmonic system).

1.5 Extended System Approach

In the framework of statistical mechanics all ensembles can be formally obtained from the microcanonical NVE ensemble – where particle number, volume and energy are the external thermodynamic control variables – by suitable Laplace transforms of its partition function. Thermodynamically this corresponds to Legendre transforms of the associated thermodynamic potentials where intensive and extensive conjugate variables are interchanged. In thermodynamics, this task is achieved by a "sufficiently weak" coupling of the original system to an appropriate infinitely large bath or reservoir via a link that establishes thermodynamic equilibrium. The same basic idea is instrumental in generating distribution functions of such ensembles by computer simulation. Additional degrees of freedom that control the quantity under consideration are added to the system. The simulation is then performed in the extended microcanonical ensemble with a modified total energy as a constant of motion. This system has the property that after the correct integration over the additional degrees of freedom has been performed the distribution function of the targeted ensemble is recovered. Two important special cases are: thermostats and barostats, which are used to impose temperature instead of energy and / or pressure instead of volume as external control parameters [2, 3, 7, 16, 17, 18, 19].

1.5.1 Barostats

Keeping the pressure constant is a desirable feature for many applications of molecular dynamics. The concept of barostats and thus constant–pressure molecular dynamics was introduced in the framework of extended system dynamics by Andersen [18]. His method was devised to allow for isotropic fluctuations in the volume of the supercell. An extension of Andersen's method consists in allowing for changes of the shape of the computational cell to occur as a result of applying external pressure [17], including the

possibility of non–isotropic external stress; the additional fictitious degrees of freedom in the Parrinello–Rahman approach [17] are the lattice vectors of the supercell. These variable–cell approaches make it possible to study dynamically structural phase transitions in solids at finite temperatures. The basic idea to allow for changes in the cell shape consists in constructing an extended Lagrangian where the lattice vectors $\mathbf{a}_1$, $\mathbf{a}_2$ and $\mathbf{a}_3$ of the simulation cell are additional dynamical variables. Using the 3×3 matrix $\mathbf{h} = [\mathbf{a}_1, \mathbf{a}_2, \mathbf{a}_3]$ (which fully defines the cell with volume $\det\, h = \Omega$) the real–space position $\mathbf{R}_I$ of a particle in this original cell can be expressed as

$$\mathbf{R}_I = \mathbf{h}\mathbf{S}_I \tag{1.14}$$

where $\mathbf{S}_I$ is a scaled coordinate with components $\mathbf{S}_{i,u} \in [0,1]$ that defines the position of the ith particle in a unit cube (i.e. $\Omega_{\rm unit} = 1$) which is the scaled cell [17]. The resulting metric tensor $\mathcal{G} = \mathbf{h}^{\rm t}\mathbf{h}$ converts distances measured in scaled coordinates to distances as given by the original coordinates. The variable–cell extended Lagrangian can be postulated

$$\mathcal{L} = \sum_I^N \frac{1}{2} M_I \left(\dot{\mathbf{S}}_I^{\rm t} \mathcal{G} \dot{\mathbf{S}}_I\right) - U(\mathbf{h}, \mathbf{S}^N) + \frac{1}{2} W \ {\rm Tr}\ \dot{\mathbf{h}}^{\rm t}\dot{\mathbf{h}} - p\,\Omega \ , \tag{1.15}$$

with additional nine dynamical degrees of freedom that are associated to the lattice vectors of the supercell $\mathbf{h}$. Here, p defines the externally applied hydrostatic pressure, W defines the fictitious mass or inertia parameter that controls the time–scale of the motion of the cell $\mathbf{h}$. In particular, this Lagrangian allows for symmetry–breaking fluctuations – which might be necessary to drive a solid–state phase transformation – to take place spontaneously. The resulting equations of motion read

$$M_I \ddot{\mathbf{S}}_{I,u} = -\sum_{v=1}^{3} \frac{\partial U(\mathbf{h}, \mathbf{S}^N)}{\partial \mathbf{R}_{I,v}} \left(\mathbf{h}^{\rm t}\right)^{-1}_{vu} - M_I \sum_{v=1}^{3}\sum_{s=1}^{3} \mathcal{G}^{-1}_{uv} \dot{\mathcal{G}}_{vs} \dot{S}_{I,s} \tag{1.16}$$

$$W \ddot{\mathbf{h}}_{uv} = \Omega \sum_{s=1}^{3} \left(\mathbf{\Pi}^{\rm tot}_{us} - p\,\delta_{us}\right) \left(\mathbf{h}^{\rm t}\right)^{-1}_{sv} \ , \tag{1.17}$$

where the total internal stress tensor

$$\mathbf{\Pi}^{\rm tot}_{us} = \frac{1}{\Omega} \sum_I M_I \left(\dot{\mathbf{S}}_I^{\rm t} \mathcal{G} \dot{\mathbf{S}}_I\right)_{us} + \Pi_{us} \tag{1.18}$$

is the sum of the thermal contribution due to nuclear motion at finite temperature and the internal stress tensor Π derived from the interaction potential. A modern formulation of barostats that combines the equation of motion also with thermostats (see next section) was given by Martyna et al. [19].

1.5.2 Thermostats

Standard molecular dynamics generates the microcanonical or NVE ensemble where in addition the total momentum is conserved [3]. The temperature is not a control variable and cannot be preselected and fixed. But it is evident that also within molecular dynamics the possibility to control the average temperature (as obtained from the average kinetic energy of the nuclei and the energy equipartition theorem) is welcome for physical reasons. A deterministic algorithm of achieving temperature control in the spirit of extended system dynamics [18] by a sort of dynamical friction mechanism was devised by Nosé and Hoover [16, 20], see e.g. Refs. [2, 16, 3] for reviews of this technique. Thereby, the canonical or NVT ensemble is generated in the case of ergodic dynamics.
It is well–known that the standard Nosé–Hoover thermostat method suffers from non–ergodicity problems for certain classes of Hamiltonians, such as the harmonic oscillator [20]. A closely related technique, the so–called Nosé–Hoover–chain thermostat [21], cures that problem and assures ergodic sampling of phase space even for the pathological harmonic oscillator. This is achieved by thermostatting the original thermostat by another thermostat, which in turn is thermostatted and so on. In addition to restoring ergodicity even with only a few thermostats in the chain, this technique is found to be much more efficient in imposing the desired temperature. The underlying equations of motion read

$$\begin{aligned} M_I \ddot{\mathbf{R}}_I &= -\nabla_I E^{\mathrm{KS}} - M_I \dot{\xi}_1 \dot{\mathbf{R}}_I \\ Q_1^{\mathrm{n}} \ddot{\xi}_1 &= \left[\sum_I M_I \dot{\mathbf{R}}_I^2 - g k_{\mathrm{B}} T \right] - Q_1^{\mathrm{n}} \dot{\xi}_1 \dot{\xi}_2 \\ Q_k^{\mathrm{n}} \ddot{\xi}_k &= \left[Q_{k-1}^{\mathrm{n}} \dot{\xi}_{k-1}^2 - k_{\mathrm{B}} T \right] - Q_k^{\mathrm{n}} \dot{\xi}_k \dot{\xi}_{k+1} \left(1 - \delta_{kK}\right) \qquad \text{where } k = 2, \ldots, K \ . \end{aligned} \tag{1.19}$$

By inspection of Eq. (1.19) it becomes intuitively clear how the thermostat works: $\dot{\xi}_1$ can be considered as a *dynamical* friction coefficient. The resulting "dissipative dynamics" leads to non–Hamiltonian flow, but the friction term can aquire positive or negative sign according to its equation of motion. This leads to damping or acceleration of the nuclei and thus to cooling or heating if the instantaneous kinetic energy of the nuclei is higher or lower than $k_{\mathrm{B}}T$ which is preset. As a result, this extended system dynamics can be shown to produce a canonical ensemble in the subspace of the nuclear coordinates and momenta. In spite of being non–Hamiltonian, Nosé–Hoover (–chain) dynamics is also distinguished by conserving an energy quantity of the extended system; see Eq. (1.21).
The desired average physical temperature is given by T and g denotes the number of dynamical degrees of freedom to which the nuclear thermostat chain is coupled (i.e. constraints imposed on the nuclei have to be subtracted). It is found that this choice requires a very accurate integration of the resulting equations of motion (for instance by using a high–order Suzuki–Yoshida integrator [22]). The integration of these equations of motion is discussed in detail in Ref. [22] using the velocity Verlet algorithm. One of the advantages of the velocity Verlet integrator is that it can be easily used together with higher

order schemes for the thermostats. Multiple time step techniques can be used and time reversibility of the overall algorithm is preserved.

```
Integrate Thermostats for dt/2
V(:) := V(:) + dt/(2M(:))*F(:)
R(:) := R(:) + dt*V(:)
Calculate new forces F(:)
V(:) := V(:) + dt/(2M(:))*F(:)
Integrate Thermostats for dt/2
```

The choice of the "mass parameters" assigned to the thermostat degrees of freedom should be made such that the overlap of their power spectra and the ones of the thermostatted subsystems is maximal [22]. The relations

$$Q_1^{\mathrm{n}} = \frac{g k_{\mathrm{B}} T}{\omega_{\mathrm{n}}^2} \ , \qquad Q_k^{\mathrm{n}} = \frac{k_{\mathrm{B}} T}{\omega_{\mathrm{n}}^2} \ , \tag{1.20}$$

assures this if ω_{n} is a typical phonon or vibrational frequency of the nuclear subsystem (say of the order of 2000 to 4000 cm^{-1}). There is a conserved energy quantity in the case of thermostatted molecular dynamics. This constant of motion reads

$$\begin{aligned} E_{\mathrm{cons}}^{\mathrm{NVT}} &= \sum_I \frac{1}{2} M_i \dot{\mathbf{R}}_i^2 + U(\mathbf{R}^N) \\ &\quad + \sum_{k=1}^{K} \frac{1}{2} Q_k^{\mathrm{n}} \dot{\xi}_k^2 + \sum_{k=2}^{K} k_{\mathrm{B}} T \xi_k + g k_{\mathrm{B}} T \xi_1 \end{aligned} \tag{1.21}$$

for Nosé–Hoover–chain thermostatted molecular dynamics.

Lecture 2

Ab initio Molecular Dynamics

In this lecture the two most popular extension of classical molecular dynamics to include first–principles derived potential functions are discussed. The focus is on the Kohn–Sham method of density functional theory [23, 24], as this is the method almost exclusively used in applications. However, most other electronic structure theories can be used as well and it is anticipated that thanks to more powerful computers and wider acceptance of dynamical methods within the quantum chemistry community in the future a larger variety of methods will be applied.
The total ground–state energy of the interacting system of electrons with classical nuclei fixed at positions $\{\mathbf{R}_I\}$ can be obtained

$$\min_{\Psi_0} \{\langle \Psi_0 \,|\mathcal{H}_{\rm e}|\, \Psi_0\rangle\} \;\; = \;\; \min_{\{\phi_i\}} E^{\rm KS}[\{\phi_i\}]$$

as the minimum of the Kohn–Sham energy [25, 26]

$$\begin{aligned} E^{\rm KS}[\{\phi_i\}] \;\; &= \;\; T_{\rm s}[\{\phi_i\}] + \int d\mathbf{r} \;\; V_{\rm ext}(\mathbf{r})\; n(\mathbf{r}) \\ &\quad + \frac{1}{2} \int d\mathbf{r} \;\; V_{\rm H}(\mathbf{r})\; n(\mathbf{r}) + E_{\rm xc}[n] + E_{\rm ions}(\mathbf{R}^N) \;\; , \end{aligned} \tag{2.1}$$

which is an explicit functional of the set of auxiliary functions (Kohn–Sham orbitals) $\{\phi_i(\mathbf{r})\}$ that satisfy the orthonormality relation

$$\langle \phi_i \mid \phi_j \rangle = \delta_{ij} \;\; . \tag{2.2}$$

This is a dramatic simplification since the minimization with respect to all possible many–body wavefunctions $\{\Psi\}$ is replaced by a minimization with respect to a set of orthonormal one–particle functions. The associated charge density

$$n(\mathbf{r}) \;\; = \;\; \sum_i^{\rm occ} f_i \mid \phi_i(\mathbf{r}) \mid^2 \tag{2.3}$$

is obtained from a single Slater determinant built from the occupied orbitals, where $\{f_i\}$ are integer occupation numbers.
The first term in the Kohn–Sham functional Eq. (2.1) is the kinetic energy of a non–interacting reference system

$$T_{\rm s}[\{\phi_i\}] = \sum_i^{\rm occ} f_i \left\langle \phi_i \left| -\frac{1}{2}\nabla^2 \right| \phi_i \right\rangle \tag{2.4}$$

consisting of the same number of electrons exposed to the same external potential as in the fully interacting system. The second term comes from the fixed external potential $V_{\rm ext}(\mathbf{r})$, in most cases the potential due to the classical nuclei, in which the electrons move. The third term is the classical electrostatic energy of the electronic density and is obtained from the Hartree potential

$$V_{\rm H}(\mathbf{r}) \;=\; \int d\mathbf{r}' \; \frac{n(\mathbf{r}')}{\mid \mathbf{r}-\mathbf{r}' \mid} \;, \tag{2.5}$$

which in turn is related to the density through

$$\nabla^2 V_{\rm H}(\mathbf{r}) \;=\; -4\pi n(\mathbf{r}) \tag{2.6}$$

Poisson's equation. The second last contribution in the Kohn–Sham functional, is the exchange–correlation functional $E_{\rm xc}[n]$. The electronic exchange and correlation effects are lumped together and basically define this functional as the remainder between the exact energy and its Kohn–Sham decomposition in terms of the three previous contributions. Finally, the interaction energy of the bare nuclear charges is added in the last term.
The minimum of the Kohn–Sham functional is obtained by varying the energy functional Eq. (2.1) for a fixed number of electrons with respect to the orbitals subject to the orthonormality constraint. This leads to the Kohn–Sham equations

$$\left\{ -\frac{1}{2}\nabla^2 + V_{\rm ext}(\mathbf{r}) + V_{\rm H}(\mathbf{r}) + \frac{\delta E_{\rm xc}[n]}{\delta n(\mathbf{r})} \right\} \phi_i(\mathbf{r}) \;=\; \sum_j \Lambda_{ij}\phi_j(\mathbf{r}) \tag{2.7}$$

$$\left\{ -\frac{1}{2}\nabla^2 + V^{\rm KS}(\mathbf{r}) \right\} \phi_i(\mathbf{r}) \;=\; \sum_j \Lambda_{ij}\phi_j(\mathbf{r}) \tag{2.8}$$

$$H^{\rm KS}\phi_i(\mathbf{r}) \;=\; \sum_j \Lambda_{ij}\phi_j(\mathbf{r}) \;, \tag{2.9}$$

which are one–electron equations involving an effective one–particle Hamiltonian $H^{\rm KS}$ with the local potential $V^{\rm KS}$. Note that $H^{\rm KS}$ nevertheless embodies the electronic many–body effects by virtue of the exchange–correlation potential

$$\frac{\delta E_{\rm xc}[n]}{\delta n(\mathbf{r})} = V_{\rm xc}(\mathbf{r}) \;. \tag{2.10}$$

A unitary transformation within the space of the occupied orbitals leads to the canonical form

$$H^{\mathrm{KS}}\phi_i(\mathbf{r}) = \epsilon_i\phi_i(\mathbf{r}) \tag{2.11}$$

of the Kohn–Sham equations, with the eigenvalues $\{\epsilon_i\}$. This set of equations has to be solved self–consistently in order to yield the density, the orbitals and the Kohn–Sham potential for the electronic ground state. The functional derivative of the Kohn–Sham functional with respect to the orbitals, the Kohn–Sham force acting on the orbitals, can be expressed as

$$\frac{\delta E^{\mathrm{KS}}}{\delta\phi_i^\star(\mathbf{r})} = f_i H_{\mathrm{e}}^{\mathrm{KS}}\phi_i(\mathbf{r}) \ . \tag{2.12}$$

Crucial to any application of density functional theory is the approximation of the unknown exchange–correlation functional. Investigations on the performance of different functionals for different type of properties and applications are abundant in the recent literature. A discussion focused on the framework of *ab initio* molecular dynamics is for instance given in Ref. [27]. Two important classes of functionals are the "Generalized Gradient Approximation" (GGA) functionals

$$E_{\mathrm{xc}}^{\mathrm{GGA}}[n] \ = \ \int d\mathbf{r} \ n(\mathbf{r}) \ \varepsilon_{\mathrm{xc}}^{\mathrm{GGA}}(n(\mathbf{r}); \nabla n(\mathbf{r})) \ , \tag{2.13}$$

where the functional depends only on the density and its gradient at a given point in space, and hybrid functionals, where the GGA type functionals are combined with a fraction of exact exchange energy from Hartree–Fock theory.

2.1 Born–Oppenheimer Molecular Dynamics

The interaction energy $U(\mathbf{R}^N)$ in the molecular dynamics method has the same physical meaning as the Kohn–Sham energy within the Born–Oppenheimer (BO) approximation. The Kohn–Sham energy depends only on the nuclear positions and defines the hypersurface for the movement of the nuclei. The Lagrangian for BO dynamics is therefore

$$\mathcal{L}_{\mathrm{BO}}(\mathbf{R}^N, \dot{\mathbf{R}}^N) = \sum_{I=1}^{N} \frac{1}{2} M_I \dot{\mathbf{R}}_I^2 - \min_{\{\phi_i\}} E^{\mathrm{KS}}[\{\phi_i\}; \mathbf{R}^N] \ , \tag{2.14}$$

and the minimization is constraint to orthogonal sets of $\{\phi_i\}$. The equations of motions are

$$M_I \ddot{\mathbf{R}}_I = -\nabla_I \left[\min_{\{\phi_i\}} E^{\mathrm{KS}}[\{\phi_i\}; \mathbf{R}^N] \right] \ . \tag{2.15}$$

The BOMD program in pseudocode is simply derived from the previous version.

```
V(:) := V(:) + dt/(2M(:))*F(:)
R(:) := R(:) + dt*V(:)
Optimize Kohn-Sham Orbitals (EKS)
Calculate forces F(:) = dEKS/dR(:)
V(:) := V(:) + dt/(2M(:))*F(:)
```

Extensions to other ensembles along the ideas outlined in the last lecture are straight forward. In fact, a classical molecular dynamics program can easily be turned into a BOMD program by replacing the energy and force routines by the corresponding routines from a quantum chemistry program.

2.1.1 Forces in BOMD

The forces needed in an implementation of BOMD are

$$\frac{d}{d\mathbf{R}_I}\left[\min_{\{\phi_i\}} E^{\mathrm{KS}}[\{\phi_i\};\mathbf{R}^N]\right] \quad . \tag{2.16}$$

They can be calculated from the extended energy functional

$$\mathcal{E}^{\mathrm{KS}} = E^{\mathrm{KS}} + \sum_{ij} \Lambda_{ij} \left(\langle\phi_i \mid \phi_j\rangle - \delta_{ij}\right) \tag{2.17}$$

to be

$$\begin{aligned} \frac{d\mathcal{E}^{\mathrm{KS}}}{d\mathbf{R}_I} &= \frac{\partial E^{\mathrm{KS}}}{\partial \mathbf{R}_I} + \sum_{ij} \Lambda_{ij} \frac{\partial}{\partial \mathbf{R}_I} \langle\phi_i \mid \phi_j\rangle \\ &\quad + \sum_i \left[\frac{\partial E^{\mathrm{KS}}}{\partial \langle\phi_i \mid}} + \sum_j \Lambda_{ij} \mid \phi_j\rangle\right] \frac{\partial \langle\phi_i \mid}{\partial \mathbf{R}_I} \quad . \end{aligned} \tag{2.18}$$

The Kohn–Sham orbitals are assumed to be optimized, i.e. the term in brackets is (almost) zero and the forces simplify to

$$F^{\mathrm{KS}}(\mathbf{R}_I) = -\frac{\partial E^{\mathrm{KS}}}{\partial \mathbf{R}_I} + \sum_{ij} \Lambda_{ij} \frac{\partial}{\partial \mathbf{R}_I} \langle\phi_i \mid \phi_j\rangle \quad . \tag{2.19}$$

The accuracy of the forces used in BOMD depends linearly on the accuracy of the minimization (see Fig. 2.1) of the Kohn–Sham energy. This is an important point we will further investigate when we compare BOMD to the Car–Parrinello method.

Figure 2.1: Accuracy of nuclear forces for a system of 8 silicon atoms in a cubic unit cell at 10 Ry cutoff using norm–conserving pseudopotentials

2.2 Car–Parrinello Molecular Dynamics

The basic idea of the Car–Parrinello approach can be viewed to exploit the time–scale separation of fast electronic and slow nuclear motion by transforming that into classical–mechanical adiabatic energy–scale separation in the framework of dynamical systems theory. In order to achieve this goal the two–component quantum / classical problem is mapped onto a two–component purely classical problem with two separate energy scales at the expense of loosing the explicit time–dependence of the quantum subsystem dynamics. This is achieved by considering the extended Kohn–Sham energy functional $\mathcal{E}^{\mathrm{KS}}$ to be dependent on $\{\Phi_i\}$ and $\mathbf{R}^N$. In classical mechanics the force on the nuclei is obtained from the derivative of a Lagrangian with respect to the nuclear positions. This suggests that a functional derivative with respect to the orbitals, which are interpreted as classical fields, might yield the force on the orbitals, given a suitable Lagrangian.
Car and Parrinello postulated the following Lagrangian [28] using $\mathcal{E}^{\mathrm{KS}}$.

$$\mathcal{L}_{\mathrm{CP}}[\mathbf{R}^N, \dot{\mathbf{R}}^N, \{\Phi_i\}, \{\dot{\Phi}_i\}] = \sum_I \frac{1}{2} M_I \dot{\mathbf{R}}_I^2 + \sum_i \frac{1}{2} \mu \left\langle \dot{\Phi}_i \middle| \dot{\Phi}_i \right\rangle - \mathcal{E}^{\mathrm{KS}} \left[\{\Phi_i\}, \mathbf{R}^N \right] \quad (2.20)$$

The corresponding Newtonian equations of motion are obtained from the associated Euler–Lagrange equations

$$\frac{d}{dt} \frac{\partial \mathcal{L}_{\mathrm{CP}}}{\partial \dot{\mathbf{R}}_I} = \frac{\partial \mathcal{L}_{\mathrm{CP}}}{\partial \mathbf{R}_I} \quad (2.21)$$

$$\frac{d}{dt} \frac{\delta \mathcal{L}_{\mathrm{CP}}}{\delta \langle \dot{\Phi}_i \mid} = \frac{\delta \mathcal{L}_{\mathrm{CP}}}{\delta \langle \Phi_i \mid} \quad (2.22)$$

like in classical mechanics, but here for both the nuclear positions and the orbitals. Note that the constraints contained in $\mathcal{E}^{\mathrm{KS}}$ are holonomic [9]. Following this route of ideas, Car–Parrinello equations of motion are found to be of the form

$$M_I \ddot{\mathbf{R}}_I(t) = -\frac{\partial E^{\mathrm{KS}}}{\partial \mathbf{R}_I} + \sum_{ij} \Lambda_{ij} \frac{\partial}{\partial \mathbf{R}_I} \langle \Phi_i \mid \Phi_j \rangle \quad (2.23)$$

$$\mu \ddot{\Phi}_i(t) = -\frac{\delta E^{\mathrm{KS}}}{\delta \langle \Phi_i \mid} + \sum_j \Lambda_{ij} \mid \Phi_j \rangle \quad (2.24)$$

where μ is the "fictitious mass" or inertia parameter assigned to the orbital degrees of freedom; the units of the mass parameter μ are energy times a squared time for reasons of dimensionality. Note that the constraints within $\mathcal{E}^{\mathrm{KS}}$ lead to "constraint forces" in

the equations of motion. In general, these constraints will depend on both the Kohn–Sham orbitals and the nuclear positions through the overlap matrix of basis functions. These dependencies have to be taken into account properly in deriving the Car–Parrinello equations following from Eq. (2.20) using Eqs. (2.21)–(2.22).
The constant of motion is

$$E_{\rm cons} = \sum_I \frac{1}{2} M_I \dot{\mathbf{R}}_I^2 + \sum_i \frac{1}{2}\mu \left\langle \dot{\Phi}_i \middle| \dot{\Phi}_i \right\rangle + E^{\rm KS}\left[\{\Phi_i\}, \mathbf{R}^N\right] \quad . \tag{2.25}$$

According to the Car–Parrinello equations of motion, the nuclei evolve in time at a certain (instantaneous) physical temperature $\propto \sum_I M_I \dot{\mathbf{R}}_I^2$, whereas a "fictitious temperature" $\propto \sum_i \mu \langle \dot{\Phi}_i | \dot{\Phi}_i \rangle$ is associated to the electronic degrees of freedom. In this terminology, "low electronic temperature" or "cold electrons" means that the electronic subsystem is close to its instantaneous minimum energy $\min_{\{\Phi_i\}} E^{\rm KS}$ i.e. close to the exact Born–Oppenheimer surface. Thus, a ground–state wavefunction optimized for the initial configuration of the nuclei will stay close to its ground state also during time evolution if it is kept at a sufficiently low temperature.
The remaining task is to separate in practice nuclear and electronic motion such that the fast electronic subsystem stays cold also for long times but still follows the slow nuclear motion adiabatically (or instantaneously). Simultaneously, the nuclei are nevertheless kept at a much higher temperature. This can be achieved in nonlinear classical dynamics via decoupling of the two subsystems and (quasi–) adiabatic time evolution. This is possible if the power spectra of both dynamics do not have substantial overlap in the frequency domain so that energy transfer from the "hot nuclei" to the "cold electrons" becomes practically impossible on the relevant time scales. This amounts in other words to imposing and maintaining a metastability condition in a complex dynamical system for sufficiently long times. How and to which extend this is possible in practice was investigated in detail in an important investigation based on well–controlled model systems [29] and with more mathematical rigor in Ref. [30].

2.2.1 How to Control Adiabaticity ?

Under which circumstances can the adiabatic separation be achieved, and how can it be controlled? A simple harmonic analysis of the frequency spectrum of the orbital classical fields close to the minimum defining the ground state yields [29]

$$\omega_{ij} = \left(\frac{2(\epsilon_i - \epsilon_j)}{\mu}\right)^{1/2} \quad , \tag{2.26}$$

where ϵ_j and ϵ_i are the eigenvalues of occupied and unoccupied orbitals, respectively. This is in particular true for the lowest frequency $\omega_{\rm e}^{\rm min}$, and an analytic estimate for the lowest possible electronic frequency

$$\omega_{\rm e}^{\rm min} \propto \left(\frac{E_{\rm gap}}{\mu}\right)^{1/2} \quad , \tag{2.27}$$

shows that this frequency increases like the square root of the electronic energy difference E_{gap} between the lowest unoccupied and the highest occupied orbital. On the other hand it increases similarly for a decreasing fictitious mass parameter μ.
In order to guarantee the adiabatic separation, the frequency difference $\omega_{\mathrm{e}}^{\mathrm{min}} - \omega_{\mathrm{n}}^{\mathrm{max}}$ should be large. But both the highest phonon frequency $\omega_{\mathrm{n}}^{\mathrm{max}}$ and the energy gap E_{gap} are quantities that are dictated by the physics of the system. Therefore, the only parameter to control adiabatic separation is the fictitious mass. However, decreasing μ not only shifts the electronic spectrum upwards on the frequency scale, but also stretches the entire frequency spectrum according to Eq. (2.26). This leads to an increase of the maximum frequency according to

$$\omega_{\mathrm{e}}^{\mathrm{max}} \propto \left(\frac{E_{\mathrm{cut}}}{\mu}\right)^{1/2} \quad , \tag{2.28}$$

where E_{cut} is the largest kinetic energy in an expansion of the wavefunction in terms of a plane wave basis set. At this place a limitation to decrease μ arbitrarily kicks in due to the maximum length of the molecular dynamics time step Δt^{max} that can be used. The time step is inversely proportional to the highest frequency in the system, which is $\omega_{\mathrm{e}}^{\mathrm{max}}$ and thus the relation

$$\Delta t^{\mathrm{max}} \propto \left(\frac{\mu}{E_{\mathrm{cut}}}\right)^{1/2} \tag{2.29}$$

governs the largest time step that is possible. As a consequence, Car–Parrinello simulators have to make a compromise on the control parameter μ; typical values for large–gap systems are μ = 500–1500 a.u. together with a time step of about 5–10 a.u. (0.12–0.24 fs). Note that a poor man's way to keep the time step large and still increase μ in order to satisfy adiabaticity is to choose heavier nuclear masses. That depresses the largest phonon or vibrational frequency $\omega_{\mathrm{n}}^{\mathrm{max}}$ of the nuclei (at the cost of renormalizing all *dynamical* quantities in the sense of classical isotope effects). Other advanced techniques are discussed in the literature [22].

2.2.2 Forces in CPMD

The forces needed in a CPMD calculation are the partial derivative of the Kohn–Sham energy with respect to the independent variables, i.e. the nuclear positions and the Kohn–Sham orbitals. The orbital forces are calculated as the action of the Kohn–Sham Hamiltonian on the orbitals

$$F(\Phi_i) = -f_i H^{\mathrm{KS}} \phi_i \quad . \tag{2.30}$$

The forces with respect to the nuclear positions are

$$F(\mathbf{R}_I) = -\frac{\partial E^{\mathrm{KS}}}{\partial \mathbf{R}_I} \quad . \tag{2.31}$$

These are the same forces as in BOMD (the constraint force will be considered later), but there we derived the forces under the condition that the wavefunctions were optimized

and therefore they are only correct up to the accuracy achieved in the wavefunction optimization. In CPMD these are the correct forces and calculated from analytic energy expressions are correct to machine precision.
Constraint forces are

$$F_c(\Phi_i) = \sum_j \Lambda_{ij} \mid \Phi_j\rangle \tag{2.32}$$

$$F_c(\mathbf{R}_I) = \sum_{ij} \Lambda_{ij} \frac{\partial}{\partial \mathbf{R}_I} \langle \Phi_i \mid \Phi_j \rangle \ , \tag{2.33}$$

where the second force only appears for basis sets (or metrics) with a nuclear position dependent overlap of wavefunctions.

2.2.3 Velocity Verlet Equations for CPMD

The appearance of the constraint terms complicates the velocity Verlet method slightly for CPMD. The Lagrange parameters Λ_{ij} have to be calculated to be consistent with the discretization method employed. How to include constraints in the velocity Verlet algorithm has been explained by Andersen [15]. In the following we will assume that the overlap is not position dependent, as it is the case for plane wave basis sets. The more general case will be explained when needed in a later lecture. These basic equations and generalizations thereof can be found in a series of papers by Tuckerman et al. [22].
For the case of overlap matrices that are not position dependent the constraint term only appears in the equations for the orbitals.

$$\mu \mid \ddot{\Phi}_i(t)\rangle = \mid \varphi_i(t)\rangle + \sum_j \Lambda_{ij} \mid \Phi_j(t)\rangle \tag{2.34}$$

where the definition

$$\mid \varphi_i(t)\rangle = -f_i H^{\mathrm{KS}} \mid \Phi_i(t)\rangle \tag{2.35}$$

has been used. The velocity Verlet scheme for the wavefunctions has to incorporate the constraints by using the RATTLE algorithm. The explicit formulas will be derived in the framework of plane waves in a later lecture. The structure of the algorithm for the wavefunctions is given below

```
CV(:) := CV(:) + dt/(2m)*CF(:)
CRP(:) := CR(:) + dt*CV(:)
Calculte Lagrange multiplier L
CR(:) := CRP(:) + L*CR(:)
Calculate forces CF(:) = HKS*CR(:)
CV(:) := CV(:) + dt/(2m)*CF(:)
Calculte Lagrange multiplier L
CV(:) := CV(:) + L*CR(:)
```

Figure 2.2: Conserved energy $E_{\rm cons}$ from Car–Parrinello (CP) and Born–Oppenheimer (BO) molecular dynamics simulations of a model system for various time steps and convergence criteria; see text for further details and Table 2.1 for the corresponding timings. Top: solid line: CP, 5 a.u.; open circles: CP, 10 a.u.; filled squares: BO, 10 a.u., 10^{-6}. Middle: open circles: CP, 10 a.u.; filled squares: BO, 10 a.u., 10^{-6}; filled triangles: BO, 100 a.u., 10^{-6}; open diamonds: BO, 100 a.u., 10^{-5}. Bottom: open circles: CP, 10 a.u.; open diamonds: BO, 100 a.u., 10^{-5}; dashed line: BO, 100 a.u., 10^{-4}.

2.3 Comparing BOMD and CPMD

The comparison of the overall performance of Car–Parrinello and Born–Oppenheimer molecular dynamics in terms of computer time is a delicate issue. For instance it depends crucially on the choice made concerning the accuracy of the conservation of the energy $E_{\rm cons}$. Thus, this is to some extend subject of "personal taste" as to what is considered to be a "sufficiently accurate" energy conservation. In addition, this comparison might lead to different conclusions as a function of type and size of the system investigated. Nevertheless, in order to shed light on this point, microcanonical simulations of 8 silicon atoms were performed with various parameters using Car–Parrinello and Born–Oppenheimer molecular dynamics. This large–gap system was initially extremely well equilibrated and the runs were extended to 8 ps (and a few to 12 ps with no noticeable difference) at a temperature of about 360–370 K (with ±80 K root–mean–square fluctuations). The wavefunction was expanded up to $E_{\rm cut} = 10$ Ry at the Γ–point of a simple cubic supercell and LDA was used to describe the interactions. In both cases the velocity Verlet scheme was used to integrate the equations of motion. In Car–Parrinello molecular dynamics two different time steps were used, 5 a.u. and 10 a.u. (corresponding to about 0.24 fs), in conjunction with a fictitious electron mass of $\mu = 400$ a.u.. Within Born–Oppenheimer molecular dynamics the minimization of the energy functional was done using the highly efficient DIIS (direct inversion in the iterative subspace) scheme [31]. In this case, the time step was either 10 a.u. or 100 a.u. and three convergence criteria were used; note that the large time step corresponding to 2.4 fs is already at the limit to be used to investigate typical molecular systems (with frequencies up to 4000 $\rm cm^{-1}$). The convergence criterion is based on the largest element of the wavefunction gradient which was required to be smaller than 10^{-6}, 10^{-5} or 10^{-4} a.u..

The outcome of this comparison is shown in Fig. 2.2 in terms of the time evolution of the conserved energy $E_{\rm cons}$ on scales that cover more than three orders of magnitude in absolute accuracy. Within the present comparison ultimate energy stability was obtained using Car–Parrinello molecular dynamics with the shortest time step of 5 a.u., which conserves the energy of the total system to about 6×10^{-8} a.u. per picosecond, see solid line in Fig. 2.2(top). Increasing the time step to 10 a.u. leads to an energy conservation of about 3×10^{-7} a.u./ps and much larger energy fluctuations, see open circles in Fig. 2.2(top). The

Table 2.1: Timings in CPU seconds and energy conservation in a.u. / ps for Car–Parrinello (CP) and Born–Oppenheimer (BO) molecular dynamics simulations of a model system for 1 ps of trajectory on an IBM RS6000 / model 390 (Power2) workstation using the `CPMD` package [32]; see Fig. 2.2 for corresponding energy plots.

Method	Time step (a.u.)	Convergence (a.u.)	Conservation (a.u./ps)	Time (s)
CP	5	—	6×10^{-8}	3230
CP	7	—	1×10^{-7}	2310
CP	10	—	3×10^{-7}	1610
BO	10	10^{-6}	1×10^{-6}	16590
BO	50	10^{-6}	1×10^{-6}	4130
BO	100	10^{-6}	6×10^{-6}	2250
BO	100	10^{-5}	1×10^{-5}	1660
BO	100	10^{-4}	1×10^{-3}	1060

computer time needed in order to generate one picosecond of Car–Parrinello trajectory increases linearly with the time step, see Table 2.1. The most stable Born–Oppenheimer run was performed with a time step of 10 a.u. and a convergence of 10^{-6}. This leads to an energy conservation of about 1×10^{-6} a.u./ps, see filled squares in Fig. 2.2(top).

As the maximum time step in Born–Oppenheimer dynamics is only related to the time scale associated to nuclear motion it could be increased from 10 to 100 a.u. while keeping the convergence at the same tight limit of 10^{-6}. This worsens the energy conservation slightly (to about 6×10^{-6} a.u./ps), whereas the energy *fluctuations* increase dramatically, see filled triangles in Fig. 2.2(middle) and note the change of scale compared to Fig. 2.2(top). The overall gain is an acceleration of the Born–Oppenheimer simulation by a factor of about seven to eight, see Table 2.1. In the Born–Oppenheimer scheme, the computer time needed for a fixed amount of simulated physical time decreases only sub linearly with increasing time step since the initial guess for the iterative minimization degrades in quality as the time step is made larger. Further savings of computer time can be easily achieved by decreasing the quality of the wavefunction convergence from 10^{-6} to 10^{-5} and finally to 10^{-4}, see Table 2.1. This is unfortunately tied to a significant decrease of the energy conservation from 6×10^{-6} a.u./ps at 10^{-6} (filled triangles) to about 1×10^{-3} a.u./ps at 10^{-4} (dashed line) using the same 100 a.u. time step, see Fig. 2.2(bottom) but note the change of scale compared to Fig. 2.2(middle).

In conclusion, Born–Oppenheimer molecular dynamics can be made as fast as (or even faster than) Car–Parrinello molecular dynamics (as measured by the amount of CPU time spent per picosecond) at the expense of sacrificing accuracy in terms of energy conservation.

Lecture 3

Plane Waves

This lecture covers the fundamentals of the plane wave–pseudopotential approach to the Kohn–Sham method. There are many reviews on the pseudopotential plane wave method alone or in connection with the Car–Parrinello algorithm. Older articles [33, 34] as well as the book by Singh [35] concentrate on the electronic structure part. Other reviews [36, 37, 38, 39] present the plane wave method in connection with the molecular dynamics technique.

3.1 Unit Cell and Plane Wave Basis

The unit cell of a periodically repeated system is defined by the lattice vectors $\mathbf{a}_1$, $\mathbf{a}_2$, and $\mathbf{a}_3$. The lattice vectors can be combined into a three by three matrix $\mathbf{h} = [\mathbf{a}_1, \mathbf{a}_2, \mathbf{a}_3]$. The volume Ω of the cell is calculated as the determinant of $\mathbf{h}$

$$\Omega = \det\mathbf{h} \ . \tag{3.1}$$

Further, scaled coordinates $\mathbf{s}$ are introduced that are related to $\mathbf{r}$ via $\mathbf{h}$

$$\mathbf{r} = \mathbf{h}\mathbf{s} \ . \tag{3.2}$$

Periodic boundary conditions can be enforced by using

$$\mathbf{r}_{\mathrm{pbc}} = \mathbf{r} - \mathbf{h}\Big[\mathbf{h}^{-1}\mathbf{r}\Big]_{\mathrm{NINT}} \ , \tag{3.3}$$

where $[\cdots]_{\mathrm{NINT}}$ denotes the nearest integer value. The coordinates $\mathbf{r}_{\mathrm{pbc}}$ will be always within the box centered around the origin of the coordinate system. Reciprocal lattice vectors $\mathbf{b}_i$ are defined as

$$\mathbf{b}_i \cdot \mathbf{a}_j = 2\pi\,\delta_{ij} \tag{3.4}$$

and can also be arranged to a three by three matrix

$$[\mathbf{b}_1, \mathbf{b}_2, \mathbf{b}_3] = 2\pi(\mathbf{h}^{\mathrm{t}})^{-1} \ . \tag{3.5}$$

Plane waves build a complete and orthonormal basis with the above periodicity

$$f_{\mathbf{G}}^{\mathrm{PW}}(\mathbf{r}) = \frac{1}{\sqrt{\Omega}} \exp[i\mathbf{G}\cdot\mathbf{r}] = \frac{1}{\sqrt{\Omega}} \exp[2\pi\, i\, \mathbf{g}\cdot\mathbf{s}] \quad , \tag{3.6}$$

with the reciprocal space vectors

$$\mathbf{G} = 2\pi(\mathbf{h}^{\mathrm{t}})^{-1}\mathbf{g} \ , \tag{3.7}$$

where $\mathbf{g} = [i, j, k]$ is a triple of integer values. A periodic function can be expanded in this basis

$$\psi(\mathbf{r}) = \psi(\mathbf{r}+\mathbf{L}) = \frac{1}{\sqrt{\Omega}} \sum_{\mathbf{G}} \psi(\mathbf{G}) \exp[i\,\mathbf{G}\cdot\mathbf{r}] \quad , \tag{3.8}$$

where $\psi(\mathbf{r})$ and $\psi(\mathbf{G})$ are related by a three-dimensional Fourier transform. The direct lattice vectors $\mathbf{L}$ connect equivalent points in different cells.
The Kohn–Sham potential of a periodic system exhibits the same periodicity as the direct lattice

$$V^{\mathrm{KS}}(\mathbf{r}) = V^{\mathrm{KS}}(\mathbf{r}+\mathbf{L}) \ , \tag{3.9}$$

and the Kohn–Sham orbitals can be written in Bloch form (see e.g. Ref. [40])

$$\Phi(\mathbf{r}) = \Phi_i(\mathbf{r},\mathbf{k}) = \exp[i\,\mathbf{k}\cdot\mathbf{r}]\ u_i(\mathbf{r},\mathbf{k}) \ , \tag{3.10}$$

where $\mathbf{k}$ is a vector in the first Brillouin zone. The functions $u_i(\mathbf{r},\mathbf{k})$ have the periodicity of the direct lattice

$$u_i(\mathbf{r},\mathbf{k}) = u_i(\mathbf{r}+\mathbf{L},\mathbf{k}) \ . \tag{3.11}$$

The index i runs over all states and the states have an occupation $f_i(\mathbf{k})$ associated with them. The periodic functions $u_i(\mathbf{r},\mathbf{k})$ are now expanded in the plane wave basis

$$u_i(\mathbf{r},\mathbf{k}) = \frac{1}{\sqrt{\Omega}} \sum_{\mathbf{G}} c_i(\mathbf{G},\mathbf{k}) \exp[i\mathbf{G}\cdot\mathbf{r}] \quad , \tag{3.12}$$

and the Kohn–Sham orbitals are

$$\Phi_i(\mathbf{r},\mathbf{k}) = \frac{1}{\sqrt{\Omega}} \sum_{\mathbf{G}} c_i(\mathbf{G},\mathbf{k}) \exp[i(\mathbf{G}+\mathbf{k})\cdot\mathbf{r}] \quad , \tag{3.13}$$

where $c_i(\mathbf{G},\mathbf{k})$ are complex numbers. With this expansion the density can also be expanded into a plane wave basis

$$\begin{aligned} n(\mathbf{r}) &= \frac{1}{\Omega}\sum_i \int d\mathbf{k}\ f_i(\mathbf{k}) \sum_{\mathbf{G},\mathbf{G}'} c_i^\star(\mathbf{G}',\mathbf{k}) c_i(\mathbf{G},\mathbf{k}) \exp[i(\mathbf{G}+\mathbf{k})\cdot\mathbf{r}] && (3.14)\\ &= \sum_{\mathbf{G}} n(\mathbf{G}) \exp[i\,\mathbf{G}\cdot\mathbf{r}] \quad , && (3.15) \end{aligned}$$

where the sum over $\mathbf{G}$ vectors in Eq. (3.15) expands over double the range given by the wavefunction expansion. This is one of the main advantages of the plane wave basis. Whereas for atomic orbital basis sets the number of functions needed to describe the density grows quadratically with the size of the system, there is only a linear dependence for plane waves.
In actual calculations the infinite sums over $\mathbf{G}$ vectors and cells has to be truncated. Furthermore, we have to approximate the integral over the Brillouin zone by a finite sum over special $\mathbf{k}$–points

$$\int d\mathbf{k} \rightarrow \sum_{\mathbf{k}} w_{\mathrm{k}} \ , \tag{3.16}$$

where w_k are the weights of the integration points. From now on we will assume that the Brillouin zone integration can be done efficiently by a single point at $k = 0$, the so called Γ–point.
The truncation of the plane wave basis rests on the fact that the Kohn–Sham potential $V^{\mathrm{KS}}(\mathbf{G})$ converges rapidly with increasing modulus of $\mathbf{G}$. For this reason only $\mathbf{G}$ vectors with a kinetic energy lower than a given maximum cutoff

$$\frac{1}{2} |\mathbf{G}|^2 \leq E_{\mathrm{cut}} \tag{3.17}$$

are included in the basis. With this choice of the basis the precision of the calculation within the approximations of density functional theory is controlled by one parameter E_{cut} only.
The number of plane waves for a given cutoff depends on the unit cell. A good estimate for the size of the basis is

$$N_{\mathrm{PW}} = \frac{1}{2\pi^2} \ \Omega \ E_{\mathrm{cut}}^{3/2} \ , \tag{3.18}$$

where E_{cut} is in Hartree units. The basis set needed to describe the density calculated from the Kohn-Sham orbitals has a corresponding cutoff that is four times the cutoff of the orbitals. The number of plane waves needed at a given density cutoff is therefore eight times the number of plane waves needed for the orbitals.

3.2 Kinetic Energy and Local Potentials

Plane waves are eigenfunctions of the kinetic energy operator

$$\frac{1}{2}\nabla^2 \ e^{i\mathbf{G}\cdot\mathbf{r}} = -\frac{1}{2} \mid \mathbf{G} \mid^2 \ e^{i\mathbf{G}\cdot\mathbf{r}} \ . \tag{3.19}$$

The kinetic energy is therefore easily calculated in Fourier space

$$E_{\mathrm{kin}} = \sum_i \sum_{\mathbf{G}} \frac{1}{2} f_i \, |\mathbf{G}|^2 \, |c_i(\mathbf{G})|^2, \ \ , \tag{3.20}$$

and the same is true for the wavefunction forces

$$F_{\rm kin} = \frac{1}{2}\,|\mathbf{G}|^2\,c_i(\mathbf{G}) \ . \tag{3.21}$$

The plane waves do not depend on the atomic positions, therefore there are no Pulay forces and no contribution of the kinetic energy to the forces on the nuclei.
Local operators act multiplicatively on wavefunctions in real space

$$\int d\mathbf{r}'\ V(\mathbf{r},\mathbf{r}')\Phi(\mathbf{r}') = V_{\rm loc}(\mathbf{r})\Phi(\mathbf{r}) \ . \tag{3.22}$$

The matrix elements of local operators can be calculated from the plane wave expansion of the operator in real space

$$\begin{aligned}
\langle \mathbf{G}_1 \mid V_{\rm loc}(\mathbf{r}) \mid \mathbf{G}_2 \rangle &= \frac{1}{\Omega}\sum_{\mathbf{G}} V_{\rm loc}(\mathbf{G}) \int d\mathbf{r}\ e^{-i\mathbf{G}_1\cdot\mathbf{r}} e^{i\mathbf{G}\cdot\mathbf{r}} e^{i\mathbf{G}_2\cdot\mathbf{r}} && (3.23)\\
&= \frac{1}{\Omega}\sum_{\mathbf{G}} V_{\rm loc}(\mathbf{G}) \int d\mathbf{r}\ e^{i(\mathbf{G}-\mathbf{G}_1+\mathbf{G}_2)\cdot\mathbf{r}} && (3.24)\\
&= \frac{1}{\Omega} V_{\rm loc}(\mathbf{G}_1-\mathbf{G}_2) \ . && (3.25)
\end{aligned}$$

The expectation value only depends on the density

$$\begin{aligned}
E_{\rm loc} &= \sum_i f_i \langle \Phi_i \mid V_{\rm loc} \mid \Phi_i \rangle && (3.26)\\
&= \int d\mathbf{r}\ V_{\rm loc}(\mathbf{r})\ n(\mathbf{r}) && (3.27)\\
&= \frac{1}{\Omega}\sum_{\mathbf{G}} V^{\star}_{\rm loc}(\mathbf{G})\ n(\mathbf{G}) \ . && (3.28)
\end{aligned}$$

Expectation values are calculated in Fourier space as a sum over G–vectors. The local potential is multiplied by the density and therefore only those components of the local potential that are non–zero in the density have to be calculated. Forces are calculated in real space by multiplying the wavefunctions with the potential on the real space grid.

3.3 Electrostatic Energy

The electrostatic energy of a system of nuclear charges Z_I at positions $\mathbf{R}_I$ and an electronic charge distribution $n(\mathbf{r})$ consists of three parts: the Hartree energy of the electrons, the interaction energy of the electrons with the nuclei and the internuclear interactions

$$\begin{aligned}
E_{\rm ES} &= \frac{1}{2}\iint d\mathbf{r}\,d\mathbf{r}'\,\frac{n(\mathbf{r})n(\mathbf{r}')}{|\mathbf{r}-\mathbf{r}'|}\\
&\quad + \sum_I \int d\mathbf{r}\,V^I_{\rm core}(\mathbf{r})n(\mathbf{r}) + \frac{1}{2}\sum_{I\neq J}\frac{Z_I Z_J}{|\mathbf{R}_I-\mathbf{R}_J|} \ . && (3.29)
\end{aligned}$$

The Ewald method (see e.g. Ref. [2]) can be used to avoid singularities in the individual terms when the system size is infinite. In order to achieve this a Gaussian core charge distribution associated with each nuclei is defined

$$n_{\rm c}^I(\mathbf{r}) = -\frac{Z_I}{\left(\mathrm{R}_I^{\rm c}\right)^3}\pi^{-3/2}\exp\left[-\left(\frac{\mathbf{r}-\mathbf{R}_I}{\mathrm{R}_I^{\rm c}}\right)^2\right] \quad . \tag{3.30}$$

It is convenient at this point to use a special definition for the core potential and define it to be the potential of the Gaussian charge distribution of Eq. (3.30)

$$V_{\rm core}^I(\mathbf{r}) = \int d\mathbf{r}'\frac{n_{\rm c}^I(\mathbf{r}')}{|\mathbf{r}-\mathbf{r}'|} = -\frac{Z_I}{|\mathbf{r}-\mathbf{R}_I|}\mathrm{erf}\left[\frac{|\mathbf{r}-\mathbf{R}_I|}{\mathrm{R}_I^{\rm c}}\right] \quad , \tag{3.31}$$

where erf is the error function. This potential has the correct long range behavior but we will have to add a correction potential for the short range part. The interaction energy of this Gaussian charge distributions is now added and subtracted from the total electrostatic energy

$$\begin{aligned} E_{\rm ES} &= \frac{1}{2}\iint d\mathbf{r}\,d\mathbf{r}'\,\frac{n(\mathbf{r})n(\mathbf{r}')}{|\mathbf{r}-\mathbf{r}'|} + \frac{1}{2}\iint d\mathbf{r}\,d\mathbf{r}'\,\frac{n_{\rm c}(\mathbf{r})n_{\rm c}(\mathbf{r}')}{|\mathbf{r}-\mathbf{r}'|} \\ &\quad + \iint d\mathbf{r}\,d\mathbf{r}'\,\frac{n_{\rm c}(\mathbf{r})n(\mathbf{r}')}{|\mathbf{r}-\mathbf{r}'|} + \frac{1}{2}\sum_{I\neq J}\frac{Z_I Z_J}{|\mathbf{R}_I-\mathbf{R}_J|} - \frac{1}{2}\iint d\mathbf{r}\,d\mathbf{r}'\,\frac{n_{\rm c}(\mathbf{r})n_{\rm c}(\mathbf{r}')}{|\mathbf{r}-\mathbf{r}'|} \quad , \end{aligned} \tag{3.32}$$

where $n_{\rm c}(\mathbf{r}) = \sum_I n_{\rm c}^I(\mathbf{r})$. The first three terms can be combined to the electrostatic energy of a total charge distribution $n_{\rm tot}(\mathbf{r}) = n(\mathbf{r}) + n_{\rm c}(\mathbf{r})$. The remaining terms are rewritten as a double sum over nuclei and a sum over self–energy terms of the Gaussian charge distributions

$$\begin{aligned} E_{\rm ES} &= \frac{1}{2}\iint d\mathbf{r}\,d\mathbf{r}'\,\frac{n_{\rm tot}(\mathbf{r})n_{\rm tot}(\mathbf{r}')}{|\mathbf{r}-\mathbf{r}'|} \\ &\quad + \frac{1}{2}\sum_{I\neq J}\frac{Z_I Z_J}{|\mathbf{R}_I-\mathbf{R}_J|}\mathrm{erfc}\left[\frac{|\mathbf{R}_I-\mathbf{R}_J|}{\sqrt{\mathrm{R}_I^{\rm c\,2}+\mathrm{R}_J^{\rm c\,2}}}\right] - \sum_I\frac{1}{\sqrt{2\pi}}\frac{Z_I^2}{R_I^{\rm c}} \quad , \end{aligned} \tag{3.33}$$

where erfc denotes the complementary error function.
For a periodically repeated system the total energy per unit cell is derived from the above expression by using the solution to Poisson's equation in Fourier space for the first term and make use of the rapid convergence of the second term in real space. The total charge is expanded in plane waves with expansion coefficients

$$n_{\rm tot}(\mathbf{G}) = n(\mathbf{G}) + \sum_I n_{\rm c}^I(\mathbf{G})S_I(\mathbf{G}) \tag{3.34}$$

$$= n(\mathbf{G}) - \frac{1}{\Omega}\sum_I\frac{Z_I}{\sqrt{4\pi}}\exp\left[-\frac{1}{2}G^2R_I^{\rm c\,2}\right]S_I(\mathbf{G}) \quad . \tag{3.35}$$

The structure factor of an atom is defined by

$$S_I(\mathbf{G}) = \exp[-i\mathbf{G}\cdot\mathbf{R}_I] \ . \tag{3.36}$$

This leads to the electrostatic energy for a periodic system

$$E_{\rm ES} = 2\pi\,\Omega \sum_{\mathbf{G}\neq 0} \frac{|n_{\rm tot}(\mathbf{G})|^2}{G^2} + E_{\rm ovrl} - E_{\rm self} \ , \tag{3.37}$$

where

$$E_{\rm ovrl} = \sum_{I,J}{}' \sum_{\mathbf{L}} \frac{Z_I Z_J}{|\mathbf{R}_I - \mathbf{R}_J - \mathbf{L}|} {\rm erfc}\left[\frac{|\mathbf{R}_I - \mathbf{R}_J - \mathbf{L}|}{\sqrt{{\rm R}_I^{\rm c\,2} + {\rm R}_J^{\rm c\,2}}}\right] \tag{3.38}$$

and

$$E_{\rm self} = \sum_I \frac{1}{\sqrt{2\pi}} \frac{Z_I^2}{R_I^{\rm c}} \ . \tag{3.39}$$

Here, the sums expand over all atoms in the simulation cell, all direct lattice vectors $\mathbf{L}$, and the prime in the first sum indicates that $I < J$ is imposed for $\mathbf{L} = \mathbf{0}$.

3.4 Exchange and Correlation Energy

Exchange and correlation functionals almost exclusively used in plane wave calculations are of the local type with gradient corrections. These type of functionals can be written as

$$E_{\rm xc} = \int d\mathbf{r}\, \varepsilon_{\rm xc}(n, \nabla n)\, n(\mathbf{r}) = \Omega \sum_{\mathbf{G}} \varepsilon_{\rm xc}(\mathbf{G}) n^\star(\mathbf{G}) \tag{3.40}$$

with the corresponding potential

$$V_{\rm xc}(\mathbf{r}) = \frac{\partial F_{\rm xc}}{\partial n} - \sum_s \frac{\partial}{\partial \mathbf{r}_s}\left[\frac{\partial F_{\rm xc}}{\partial(\partial_s n)}\right] \ , \tag{3.41}$$

where $F_{\rm xc} = \varepsilon_{\rm xc}(n, \nabla n) n$ and $\partial_s n$ is the s-component of the density gradient. Exchange and correlation functionals have complicated analytical forms that can give rise to high frequency components in $\varepsilon_{\rm xc}(\mathbf{G})$. Although these high frequency components do not enter the sum in Eq. (3.40) due to the filter effect of the density, they affect the calculation of $\varepsilon_{\rm xc}$. As the functionals are only local in real space, not in Fourier space, they have to be evaluated on a real space grid. The function $\varepsilon_{\rm xc}(\mathbf{G})$ can then be calculated by a Fourier transform. Therefore, the exact calculation of $E_{\rm xc}$ would require a grid with a very high resolution. However, the high frequency components are usually very small and even a moderate grid gives accurate results. The use of a finite grid results in an effective redefinition of the exchange and correlation energy

$$E_{\rm xc} = \frac{\Omega}{N_{\rm x} N_{\rm y} N_{\rm z}} \sum_{\mathbf{R}} \varepsilon_{\rm xc}(n, \nabla n)(\mathbf{R}) n(\mathbf{R}) = \Omega \sum_{\mathbf{G}} \tilde{\varepsilon}_{\rm xc}(\mathbf{G}) n(\mathbf{G}) \ , \tag{3.42}$$

where $\tilde{\varepsilon}_{\rm xc}(\mathbf{G})$ is the finite Fourier transform of $\varepsilon_{\rm xc}(\mathbf{R})$. This definition of $E_{\rm xc}$ allows the calculation of all gradients analytically. In most applications the real space grid used in the calculation of the density and the potentials is also used for the exchange and correlation energy.
The above redefinition has an undesired side effect. The new exchange and correlation energy is no longer translationally invariant. Only translations by a multiple of the grid spacing do not change the total energy. This introduces a small modulation of the energy hypersurface, known as "ripples". Highly accurate optimizations of structures and the calculation of harmonic frequencies can be affected by the ripples. Using a denser grid for the calculation of $E_{\rm xc}$ is the only solution to avoid these problems.

3.5 Car–Parrinello Equations

The Car–Parrinello Lagrangian and its derived equations of motions were introduced before. Here the equations are specialized to the case of a plane wave basis within Kohn–Sham density functional theory using norm–conserving pseudopotentials. Specifically, the functions Φ_i are replaced by the expansion coefficients $c_i(\mathbf{G})$ and the orthonormality constraint only depends on the wavefunctions, not the nuclear positions. The equations of motion for the Car–Parrinello method are derived from this specific extended Lagrangian

$$\begin{aligned}\mathcal{L} = \mu \sum_i \sum_{\mathbf{G}} |\dot{c}_i(\mathbf{G})|^2 + \frac{1}{2}\sum_I M_I \dot{\mathbf{R}}_I^2 - E_{\rm KS}\left[\{\mathbf{G}\},\{\mathbf{R_I}\}\right] \\ + \sum_{ij} \Lambda_{ij}\left(\sum_{\mathbf{G}} c_i^\star(\mathbf{G}) c_j(\mathbf{G}) - \delta_{ij}\right) \quad , \end{aligned} \tag{3.43}$$

where μ is the ficticious electron mass, and M_I are the masses of the nuclei. Because of the expansion of the Kohn–Sham orbitals in plane waves, the orthonormality constraint does not depend on the nuclear positions. The Euler–Lagrange equations derived from Eq.(3.43) are

$$\mu \ddot{c}_i(\mathbf{G}) = -\frac{\partial E}{\partial c_i^\star(\mathbf{G})} + \sum_j \Lambda_{ij} c_j(\mathbf{G}) \tag{3.44}$$

$$M_I \ddot{\mathbf{R}}_I = -\frac{\partial E}{\partial \mathbf{R}_I}. \tag{3.45}$$

The two sets of equations are coupled through the Kohn–Sham energy functional and special care has to be taken for the integration because of the orthonormality constraint. The velocity Verlet integration algorithm for the Car–Parrinello equations is defined as follows

$$\dot{\tilde{\mathbf{R}}}_I(t+\delta t) = \dot{\mathbf{R}}_I(t) + \frac{\delta t}{2M_I}\mathbf{F}_I(t)$$

$$
\begin{aligned}
\mathbf{R}_I(t+\delta t) &= \mathbf{R}_I(t) + \delta t\, \dot{\tilde{\mathbf{R}}}_I(t+\delta t) \\
\dot{\tilde{\mathbf{c}}}_I(t+\delta t) &= \dot{\mathbf{c}}_I(t) + \frac{\delta t}{2\mu}\mathbf{f}_i(t) \\
\tilde{\mathbf{c}}_i(t+\delta t) &= \mathbf{c}_i(t) + \delta t\, \dot{\tilde{\mathbf{c}}}_i(t+\delta t) \\
\mathbf{c}_i(t+\delta t) &= \tilde{\mathbf{c}}_i(t+\delta t) + \sum_j \mathbf{X}_{ij}\, \mathbf{c}_j(t) \\
\text{calculate} & \quad \mathbf{F}_I(t+\delta t) \\
\text{calculate} & \quad \mathbf{f}_i(t+\delta t) \\
\dot{\mathbf{R}}_I(t+\delta t) &= \dot{\tilde{\mathbf{R}}}_I(t+\delta t) + \frac{\delta t}{2M_I}\mathbf{F}_I(t+\delta t) \\
\dot{\mathbf{c}'}_i(t+\delta t) &= \dot{\tilde{\mathbf{c}}}_i(t+\delta t) + \frac{\delta t}{2\mu}\mathbf{f}_i(t+\delta t) \\
\dot{\mathbf{c}}_i(t+\delta t) &= \dot{\mathbf{c}'}_i(t+\delta t) + \sum_j \mathbf{Y}_{ij}\, \mathbf{c}_j(t+\delta t) \ ,
\end{aligned}
$$

where $\mathbf{R}_I(t)$ and $\mathbf{c}_i(t)$ are the atomic positions of particle I and the Kohn–Sham orbital i at time t respectively. Here, $\mathbf{F}_I$ are the forces on atom I, and $\mathbf{f}_i$ are the forces on Kohn–Sham orbital i. The matrices $\mathbf{X}$ and $\mathbf{Y}$ are directly related to the Lagrange multipliers by

$$
\mathbf{X}_{ij} = \frac{\delta t^2}{2\mu}\Lambda^{\mathrm{p}}_{ij} \tag{3.46}
$$

$$
\mathbf{Y}_{ij} = \frac{\delta t}{2\mu}\Lambda^{\mathrm{v}}_{ij} \ . \tag{3.47}
$$

Notice that in the RATTLE algorithm the Lagrange multipliers to enforce the orthonormality for the positions Λ^{p} and velocities Λ^{v} are treated as independent variables. Denoting with $\mathbf{C}$ the matrix of wavefunction coefficients $c_i(\mathbf{G})$, the orthonormality constraint can be written as

$$
\begin{aligned}
\mathbf{C}^\dagger(t+\delta t)\mathbf{C}(t+\delta t) - \mathbf{I} &= 0 && (3.48)\\
\left[\tilde{\mathbf{C}} + \mathbf{X}\mathbf{C}\right]^\dagger \left[\tilde{\mathbf{C}} + \mathbf{X}\mathbf{C}\right] - \mathbf{I} &= 0 && (3.49)\\
\tilde{\mathbf{C}}^\dagger\tilde{\mathbf{C}} + \mathbf{X}\tilde{\mathbf{C}}^\dagger\mathbf{C} + \mathbf{C}^\dagger\tilde{\mathbf{C}}\mathbf{X}^\dagger + \mathbf{X}\mathbf{X}^\dagger - \mathbf{I} &= 0 && (3.50)\\
\mathbf{X}\mathbf{X}^\dagger + \mathbf{X}\mathbf{B} + \mathbf{B}^\dagger\mathbf{X}^\dagger &= \mathbf{I} - \mathbf{A} \ , && (3.51)
\end{aligned}
$$

where the new matrices $\mathbf{A}_{ij} = \tilde{\mathbf{c}}_i^\dagger(t+\delta t)\tilde{\mathbf{c}}_j(t+\delta t)$ and $\mathbf{B}_{ij} = \mathbf{c}_i^\dagger(t)\tilde{\mathbf{c}}_j(t+\delta t)$ have been introduced in Eq. (3.51). The unit matrix is denoted by the symbol $\mathbf{I}$. By noting that $\mathbf{A} = \mathbf{I} + \mathcal{O}(\delta t^2)$ and $\mathbf{B} = \mathbf{I} + \mathcal{O}(\delta t)$, Eq. (3.51) can be solved iteratively using

$$
\begin{aligned}
\mathbf{X}^{(n+1)} &= \frac{1}{2}\Big[\mathbf{I} - \mathbf{A} + \mathbf{X}^{(n)}\,(\mathbf{I} - \mathbf{B}) \\
&\quad + (\mathbf{I} - \mathbf{B})\,\mathbf{X}^{(n)} - \left(\mathbf{X}^{(n)}\right)^2\Big]
\end{aligned} \tag{3.52}
$$

and starting from the initial guess

$$\mathbf{X}^{(0)} = \frac{1}{2}(\mathbf{I} - \mathbf{A}) \ . \tag{3.53}$$

In Eq. (3.52) it has been made use of the fact that the matrices $\mathbf{X}$ and $\mathbf{B}$ are real and symmetric, which follows directly from their definitions. Eq. (3.52) can usually be iterated to a tolerance of 10^{-6} within a few iterations.
The rotation matrix $\mathbf{Y}$ is calculated from the orthogonality condition on the orbital velocities

$$\dot{\mathbf{c}}_i^\dagger(t+\delta t)\mathbf{c}_j(t+\delta t) + \mathbf{c}_i^\dagger(t+\delta t)\dot{\mathbf{c}}_j(t+\delta t) = 0. \tag{3.54}$$

Applying Eq. (3.54) to the trial states $\dot{\mathbf{C}}' + \mathbf{YC}$ yields a simple equation for $\mathbf{Y}$

$$\mathbf{Y} = -\frac{1}{2}(\mathbf{Q} + \mathbf{Q}^\dagger), \tag{3.55}$$

where $\mathbf{Q}_{ij} = \mathbf{c}_i^\dagger(t+\delta t)\dot{\mathbf{c}'}_i^\dagger(t+\delta t)$. The fact that $\mathbf{Y}$ can be obtained without iteration means that the velocity constraint condition Eq. (3.54) is satisfied exactly at each time step.

Lecture 4

Pseudopotentials

The norm–conserving pseudopotential approach provides an effective and reliable means for performing calculations on complex molecular, liquid and solid state systems using plane wave basis sets. In this approach only the chemically active valence electrons are dealt with explicitely. The inert core electrons are eliminated within the frozen–core approximation, being considered together with the nuclei as rigid non–polarizable ion cores. In turn, all electrostatic and quantum–mechanical interactions of the valence electrons with the cores, as the nuclear Coulomb attraction screened by the core electrons, Pauli repulsion and exchange and correlation between core and valence electrons, are accounted for by angular momentum dependent pseudopotentials. These reproduce the true potential and valence orbitals outside a chosen core region but remain much weaker and smoother inside. The valence electrons are described by smooth pseudo orbitals which play the same role as the true orbitals, but avoid the nodal structure near the nuclei that keeps the core and valence states orthogonal in an all–electron framework. The respective Pauli repulsion largely cancels the attractive parts of the true potential in the core region, and is built into the therefore rather weak pseudopotential. This pseudoization of the valence wavefunctions along with the removal of the core states eminently facilitates a numerically accurate solution of the Kohn–Sham equations and the Poisson equation, and enables the use of plane waves as an expedient basis set in electronic structure calculations. By virtue of the norm–conservation property and when constructed carefully pseudopotentials present a rather marginal approximation, and indeed allow for an adequate description of the valence electrons over the entire chemically relevant range of systems.

4.1 Why Pseudopotentials ?

- Pseudopotentials should be additive and transferable. Additivity can most easily be achieved by building pseudopotentials for atoms in reference states. Transferability means that one and the same pseudopotential should be adequate for an atom in

Atom	Z	Cutoff	Plane Waves
H	1	1	1
Li	3	4	8
C	6	9	27
Si	14	27	140
Ge	32	76	663
Sn	50	133	1534

Table 4.1: Relative cutoffs (in energy units) and number of plane waves for several atoms.

all possible chemical environments. This is especially important when a change of the environment is expected during a simulation, like in chemical reactions or for phase transitions.

- Pseudopotentials replace electronic degrees of freedom in the Hamiltonian by an effective potential. They lead to a reduction of the number of electrons in the system and thereby allow for faster calculation or the treatment of bigger systems.

- Pseudopotentials allow for a considerable reduction of the basis set size. Valence states are smoother than core states and need therefore less basis functions for an accurate description. The pseudized valence wavefunctions are nodeless (in the here considered type of pseudopotentials) functions and allow for an additional reduction of the basis. This is especially important for plane waves.
  Consider the 1s function of an atom

$$\varphi_{1s}(\mathbf{r}) \sim e^{-Z^\star r}$$

  with $Z^\star \approx Z$, the nuclear charge. The Fourier transform of the orbital is

$$\varphi_{1s}(\mathbf{G}) \sim 16\pi \frac{Z^{5/2}}{\mathbf{G}^2 + Z^2} \ .$$

  From this formula we can estimate the relative cutoffs needed for different elements in the periodic table (see table 4.1).

- Most relativistic effects are connected to core electrons. These effects can be incorporated in the pseudopotentials without complicating the calculations of the final system.

4.2 Norm–Conserving Pseudopotentials

4.2.1 Hamann–Schlüter–Chiang Conditions

Norm–conserving pseudopotentials are derived from atomic reference states, calculated from the atomic Schrödinger equation

$$(T + V_{\mathrm{AE}})\,|\Psi_l\rangle = \epsilon_l |\Psi_l\rangle \ ,$$

where T is the kinetic energy operator and V_{AE} the all–electron potential derived from Kohn–Sham theory. This equation is replaced by a valence electron only equation of the same form

$$(T + V_{\mathrm{val}})\,|\Phi_l\rangle = \hat{\epsilon}_l |\Phi_l\rangle \ .$$

Hamann, Schlüter, and Chiang [42] proposed a set of requirements for the pseudo wavefunction and pseudopotential.
The pseudopotential should have the following properties

1. Real and pseudo valence eigenvalues agree for a chosen prototype atomic configuration. $\epsilon_l = \hat{\epsilon}_l$

2. Real and pseudo atomic wave functions agree beyond a chosen core radius r_c.

$$\Psi_l(r) = \Phi_l(r) \quad \text{for } r \geq r_c$$

3. The integrals from 0 to R of the real and pseudo charge densities agree for $\mathrm{R} \geq \mathrm{r}_c$ for each valence state (norm conservation).

$$\langle \Phi_l | \Phi_l \rangle_R = \langle \Psi_l | \Psi_l \rangle_R \quad \text{for } R \geq r_c$$

   where

$$\langle \Phi | \Phi \rangle_R = \int_0^R r^2 |\phi(r)|^2 dr$$

4. The logarithmic derivatives of the real and pseudo wave function and their first energy derivatives agree for $\mathrm{r} \geq \mathrm{r}_c$.

Property 3) and 4) are related through the identity

$$-\frac{1}{2}\left[(r\Phi)^2 \frac{d}{d\epsilon}\frac{d}{dr} ln\Phi\right]_R = \int_0^R r^2 |\Phi|^2 dr$$

They also gave a recipe that allows to generate pseudopotentials with the above properties.

1.
$$V_l^{(1)}(r) = V_{AE}(r)[1 - f_1\left(\frac{r}{r_{cl}}\right)]$$
r_{cl} : core radius $\approx$ 0.4 - 0.6 R_{max}, where R_{max} is the outermost maximum of the real wave function.

2.
$$V_l^{(2)}(r) = V_l^{(1)}(r) + c_l f_2\left(\frac{r}{r_{cl}}\right)$$
determine c_l so that $\hat{\epsilon}_l = \epsilon_l$ in
$$(T + V_l^{(2)}(r))w_l^{(2)}(r) = \hat{\epsilon}_l w_l^{(2)}(r)$$

3.
$$\Phi_l(r) = \gamma_l \left[w_l^{(2)}(r) + \delta_l r^{l+1} f_3\left(\frac{r}{r_{cl}}\right)\right]$$
where γ_l and δ_l are chosen such that
$$\Phi_l(r) \rightarrow \Psi_l(r) \quad \text{for } r \geq r_{cl}$$
and
$$\gamma_l^2 \int |w_l^{(2)}(r) + \delta_l r^{l+1} f_3\left(\frac{r}{r_{cl}}\right)|^2 dr = 1$$

4. Invert the Schrödinger equation for $\hat{\epsilon}_l$ and $\Phi_l(r)$ to get V_{val}^l(r).

5. Unscreen V_{val}^l(r) to get V_{ps}^l(r).
$$V_{ps}^l(r) = V_{val}^l(r) - V_H(n_v) - V_{xc}(n_v)$$
where $V_H(\rho_v)$ and $V_{xc}(\rho_v)$ are the Hartree and exchange and correlation potentials of the pseudo valence density.

Hamann, Schlüter and Chiang chose the following cutoff functions $f_1(x) = f_2(x) = f_3(x) = \exp(-x^4)$.
These pseudopotentials are angular momentum dependent. Each angular momentum state has its own potential that can be determined independently from the other potentials. It is therefore possible to have a different reference configuration for each angular momentum. This allows it for example to use excited or ionic states to construct the pseudopotential for l states that are not occupied in the atomic ground state.
The total pseudopotential in a solid state calculation then takes the form
$$V_{ps}(r) = \sum_L V_{ps}^L(r)\mathbf{P}_L$$
where L is a combined index {l,m} and $\mathbf{P}_L$ is the projector on the angular momentum state {l,m}.

4.2.2 Bachelet-Hamann-Schlüter (BHS) form

Bachelet et al. [43] proposed an analytic fit to the pseudopotentials generated by the HSC recipe of the following form

$$\begin{aligned} V_{ps}(r) &= V_{core}(r) + \sum_L \Delta V_L^{ion}(r) \\ V_{core}(r) &= -\frac{Z_v}{r}\left[\sum_{i=1}^{2} c_i^{core}\mathrm{erf}\left(\sqrt{\alpha_i^{core}}r\right)\right] \\ \Delta V_L^{ion}(r) &= \sum_{i=1}^{3}\left(A_i + r^2 A_{i+3}\right)\exp(-\alpha_i r^2) \end{aligned}$$

The cutoff functions were slightly modified to be $f_1(x) = f_2(x) = f_3(x) = \exp(-x^{3.5})$. They generated pseudopotentials for almost the entire periodic table (for the local density approximation), where generalizations of the original scheme to include spin–orbit effects for heavy atoms were made. Useful is also their list of atomic reference states.
BHS did not tabulate the A_i coefficients as they are often very big numbers but another set of numbers C_i, where

$$C_i = -\sum_{l=1}^{6} A_l Q_{il}$$

and

$$A_i = -\sum_{l=1}^{6} C_l Q_{il}^{-1}$$

with

$$Q_{il} = \begin{cases} 0 & \text{for } i > l \\ \left[S_{il} - \sum_{k=1}^{i-1} Q_{ki}^2\right]^{1/2} & \text{for } i = l \\ \frac{1}{Q_{ii}}\left[S_{il} - \sum_{k=1}^{i-1} Q_{ki}Q_{kl}\right]^{1/2} & \text{for } i < l \end{cases}$$

where $S_{il} = \int_0^\infty r^2 \varphi_i(r)\varphi_l(r)dr$, and

$$\varphi_i(r) = \begin{cases} e^{-\alpha_i r^2} & \text{for } i = 1,2,3 \\ r^2 e^{-\alpha_i r^2} & \text{for } i = 4,5,6 \end{cases} .$$

4.2.3 Kerker Pseudopotentials

Also in this approach [44] pseudopotentials with the HSC properties are constructed. But instead of using cutoff functions (f_1, f_2, f_3) the pseudo wavefunctions are directly constructed from the all–electron wavefunctions by replacing the all–electron wavefunction inside some cutoff radius by a smooth analytic function that is matched to the all–electron wavefunction at the cutoff radius. The HSC properties then translate into a set of equations for the parameters of the analytic form. After having determined the pseudo

wavefunction the Schrödinger equation is inverted and the resulting potential unscreened. Note that the cutoff radius of this type of pseudopotential construction scheme is considerably larger than the one used in the HSC scheme. Typically the cutoff radius is chosen slightly smaller than $R_{\max}$, the outermost maximum of the all–electron wavefunction. The analytic form proposed by Kerker is

$$\Phi_l(r) = r^{l+1} e^{p(r)}$$

with

$$p(r) = \alpha r^4 + \beta r^3 + \gamma r^2 + \delta \ .$$

The term linear in r is missing to avoid a singularity of the potential at $r = 0$. The HSC conditions can be translated into a set of equations for the parameters $\alpha, \beta, \gamma, \delta$.

4.2.4 Trouiller–Martins Pseudopotentials

The Kerker method was generalized by Trouiller and Martins [45] to polynomials of higher order. The rational behind this was to use the additional parameters (the coefficients of the higher terms in the polynomial) to construct smoother pseudopotentials. The Trouiller–Martins wavefunctions has the following form

$$\Phi_l(r) = r^{l+1} e^{p(r)}$$

with

$$p(r) = c_0 + c_2 r^2 + c_4 r^4 + c_6 r^6 + c_8 r^8 + c_{10} r^{10} + c_{12} r^{12}$$

and the coefficients c_n are determined from

- norm–conservation
- For $n = 0 \ldots 4$

$$\left.\frac{d^n \Phi}{dr^n}\right|_{r=r_c} = \left.\frac{d^n \Psi}{dr^n}\right|_{r=r_c}$$

-

$$\left.\frac{d\Phi}{dr}\right|_{r=0} = 0$$

4.2.5 Kinetic Energy Optimized Pseudopotentials

This scheme is based on the observation that the total energy and the kinetic energy have similar convergence properties when expanded in plane waves. Therefore, the kinetic

energy expansion is used as an optimization criteria in the construction of the pseudopotentials. Also this type [46] uses an analytic representation of the pseudo wavefunction within r_c

$$\Phi_l(r) = \sum_{i=1}^{n} a_i j_l(q_i r)$$

where $j_l(qr)$ are spherical Bessel functions with $i-1$ zeros at positions smaller than r_c. The values of q_i are fixed such that

$$\frac{j'(q_i r_c)}{j(q_i r_c)} = \frac{\Psi_l'(r_c)}{\Psi_l(r_c)} \ .$$

The conditions that are used to determine the values of a_i are:

- Φ_l is normalized
- First and second derivatives of Φ_l are continuous at r_c
- $\Delta E_{\mathrm{K}}(\{a_i\}, q_c)$ is minimal

$$\Delta E_{\mathrm{K}} = -\int d^3 r \Phi_l^\star \nabla^2 \Phi_l - \int_0^{q_c} dq q^2 \mid \Phi_l(q) \mid^2$$

ΔE_{K} is the kinetic energy contribution above a target cutoff value q_c. The value of q_c is an additional parameter (as for example r_c) that has to be chosen at a reasonable value. In practice q_c is changed until it is possible to minimize ΔE_{K} to a small enough value.

4.3 Pseudopotentials in the Plane Wave Basis

With the methods described in the last section we are able to construct pseudopotentials for states $l = s, p, d, f$ by using reference configurations that are either the ground state of the atom or of an ion, or excited states. In principle higher angular momentum states could also be generated but there physical significance is questionable. In a solid or molecular environment there will be wavefunction components of all angular momentum character at each atom. The general form of a pseudopotential is

$$V_{\mathrm{pp}}(\mathbf{r}, \mathbf{r\prime}) = \sum_{l=0}^{\infty} \sum_{m=-l}^{l} V^l(r) P^{lm}(\omega) \ , \tag{4.1}$$

where $P^{lm}(\omega)$ is a projector on angular momentum functions. A good approximation is to use

$$V^l(r) = V^c(r) \quad \text{for } l > l_{\max} \ . \tag{4.2}$$

With this approximation one can rewrite

$$\begin{aligned} V_{\mathrm{pp}}(\mathbf{r},\mathbf{r\prime}) &= \sum_{L}^{\infty} V^c(r)P^{lm}(\omega) + \sum_{L}^{\infty}\left[V^l(r) - V^c(r)\right]P^{lm}(\omega) \\ &= V^c(r)\sum_{L}^{\infty} P^{lm}(\omega) + \sum_{L}^{\infty}\delta V^l(r)P^{lm}(\omega) \\ &= V^c(r) + \sum_{L}^{\infty}\delta V^l(r)P^{lm}(\omega) \ , \end{aligned} \tag{4.3}$$

where the combined index $L = \{l, m\}$ has been used. The pseudopotential is now separated into two parts; the local or core pseudopotential $V^c(r)$ and the non–local pseudopotentials $\delta V^l(r)P^{lm}(\omega)$. The pseudopotentials of this type are also called semilocal, as they are local in the radial coordinate and the nonlocality is restricted to the angular part.
The contribution of the local pseudopotential to the total energy in a Kohn–Sham calculation is of the form

$$E_{\mathrm{local}} = \int V^c(\mathbf{r})n(\mathbf{r})d\mathbf{r} \ . \tag{4.4}$$

It can easily be calculated together with the other local potentials. The non–local part needs special consideration as the operator in the plane wave basis has no simple structure in real or reciprocal space. There are two approximations that can be used to calculate this contribution to the energy. One is based on numerical integration and the other on a projection on a local basis set.

4.3.1 Gauss–Hermit Integration

The matrix element of the non–local pseudopotential

$$V^{\mathrm{nl}}(\mathbf{G},\mathbf{G}') = \sum_{L}\frac{1}{\Omega}\int d\mathbf{r}e^{-i\mathbf{G}\cdot\mathbf{r}}\Delta V^L(\mathbf{r})e^{i\mathbf{G}'\cdot\mathbf{r}} \tag{4.5}$$

$$= \sum_{L}\int_0^{\infty} dr\langle\mathbf{G} \mid Y_{\mathrm{L}}\rangle_\omega r^2\Delta V^L(r)\langle Y_{\mathrm{L}} \mid \mathbf{G}'\rangle_\omega \ , \tag{4.6}$$

where $\langle\cdot \mid \cdot\rangle_\omega$ stands for an integration over the unit sphere. These integrals still depend on r. The integration over the radial coordinate is replaced by a numerical approximation

$$\int_0^{\infty} r^2 f(r)dr \approx \sum_i w_i f(r_i) \ . \tag{4.7}$$

The integration weights w_i and integration points r_i are calculated using the Gauss–Hermit scheme. The non–local pseudopotential is in this approximation

$$V^{\mathrm{nl}}(\mathbf{G},\mathbf{G}') = \sum_{L}\frac{1}{\Omega}\sum_i w_i\Delta V^L(r_i)\langle\mathbf{G} \mid Y_{\mathrm{L}}\rangle_\omega^{r_i}\langle Y_{\mathrm{L}} \mid \mathbf{G}'\rangle_\omega^{r_i} \tag{4.8}$$

$$= \sum_L \frac{1}{\Omega} \sum_i w_i \Delta V^L(r_i) P_i^{L\star}(\mathbf{G}) P_i^L(\mathbf{G}') \ , \tag{4.9}$$

where the definition for the projectors P

$$P_i^L(\mathbf{G}) = \langle Y_{\rm L} \mid \mathbf{G} \rangle_\omega^{r_i} \tag{4.10}$$

has been introduced. The number of projectors per atom is the number of integration points (5 - 20 for low to high accuracy) multiplied by the number of angular momenta. For the case of s and p non–local components and 15 integration points this accounts to 60 projectors per atom.
The integration of the projectors can be done analytically

$$\begin{aligned} P_i^L(\mathbf{G}) &= \int_\omega Y_L^\star(\omega) e^{iGr_i} d\omega & (4.11)\\ &= \int_\omega Y_L^\star(\omega) 4\pi \sum_{l=0}^{\infty} i^l j_l(Gr_i) \sum_{m\prime=-l}^{l} Y_{lm\prime}^\star(\omega) Y_{lm\prime}(\mathbf{G}) \mathbf{d}\omega & (4.12)\\ &= 4\pi i^l j_l(Gr_i) Y_L(\hat{G}) \ , & (4.13) \end{aligned}$$

where the expansion of a plane wave in spherical harmonics has been used. j_l are the spherical Bessel functions and $\hat{G}$ the angular components of the Fourier vector $\mathbf{G}$.

4.3.2 Kleinman–Bylander Scheme

The other method is based on the resolution of the identity in a local basis set

$$\sum_\alpha \mid \chi_\alpha \rangle \langle \chi_\alpha \mid = 1 \ , \tag{4.14}$$

where $\{\chi_\alpha\}$ are orthonormal functions. This identity can now be introduced in the integrals for the non–local part

$$\begin{aligned} V^{\rm nl}(\mathbf{G}, \mathbf{G}') &= \sum_L \int_0^\infty dr \langle \mathbf{G} \mid Y_{\rm L} \rangle_\omega r^2 \Delta V^L(r) \langle Y_{\rm L} \mid \mathbf{G}' \rangle_\omega \\ &= \sum_{\alpha,\beta} \sum_L \int_0^\infty dr \langle \mathbf{G} \mid \chi_\alpha \rangle \langle \chi_\alpha \mid Y_{\rm L} \rangle_\omega r^2 \Delta V^L(r) \langle Y_{\rm L} \mid \chi_\beta \rangle_\omega \langle \chi_\beta \mid \mathbf{G}' \rangle & (4.15) \end{aligned}$$

and the angular integrations are easily performed using the decomposition of the basis in spherical harmonics

$$\chi_\alpha(\mathbf{r}) = \chi_\alpha^{lm}(r) Y_{lm}(\omega) \ . \tag{4.16}$$

This leads to

$$\begin{aligned} V^{\rm nl}(\mathbf{G}, \mathbf{G}') &= \sum_{\alpha,\beta} \sum_L \langle \mathbf{G} \mid \chi_\alpha \rangle \int_0^\infty dr \chi_\alpha^{lm}(r) r^2 \Delta V^L(r) \chi_\beta^{lm}(r) \langle \chi_\beta \mid \mathbf{G}' \rangle & (4.17)\\ &= \sum_{\alpha,\beta} \sum_L \langle \mathbf{G} \mid \chi_\alpha \rangle \Delta V_{\alpha\beta}^l \langle \chi_\beta \mid \mathbf{G}' \rangle & (4.18) \end{aligned}$$

which is the non–local pseudopotential in fully separable form. The coupling elements of the pseudopotential

$$\Delta V^l_{\alpha\beta} = \int_0^\infty dr \chi^{lm}_\alpha(r) r^2 \Delta V^L(r) \chi^{lm}_\beta(r) \tag{4.19}$$

are independent of the plane wave basis and can be calculated for each type of pseudopotential once the expansion functions χ are known.
The final question is now what is an optimal set of basis function χ. Kleinman and Bylander[47] proposed to use the eigenfunctions of the pseudo atom, i.e. the solutions to the calculations of the atomic reference state using the pseudopotential Hamiltonian. This choice of a single reference function per angular momenta guarantees nevertheless the correct result for the reference state. Now assuming that in the molecular environment only small perturbations of the wavefunctions close to the atoms occur, this minimal basis should still be adequate. The Kleinman–Bylander form of the projectors is

$$\sum_L \frac{\mid \chi_L \rangle \langle \Delta V^L \chi_L \mid}{\langle \chi_L \Delta V^L \chi_L \rangle} = 1 \ , \tag{4.20}$$

where χ_L are the atomic pseudo wavefunctions. The plane wave matrix elements of the non–local pseudopotential in Kleinman–Bylander form is

$$V^{\mathrm{KB}}(\mathbf{G}, \mathbf{G}') = \frac{\langle \mathbf{G} \mid \Delta V^L \chi_L \rangle \langle \Delta V^L \chi_L \mid \mathbf{G}' \rangle}{\langle \chi_L \Delta V^L \chi_L \rangle} \ . \tag{4.21}$$

Generalizations of the Kleinman–Bylander scheme to more than one reference function were introduced by Blöchl [48] and Vanderbilt [49]. They make use of several reference functions, calculated at a set of reference energies.
In transforming a semilocal to the corresponding Kleinman–Bylander(KB) pseudopotential one needs to make sure that the KB–form does not lead to unphysical "ghost" states at energies below or near those of the physical valence states as these would undermine its transferability. Such spurious states can occur for specific (unfavorable) choices of the underlying semilocal and local pseudopotentials. They are an artefact of the KB–form nonlocality by which the nodeless reference pseudo wavefunctions need to be the lowest eigenstate, unlike for the semilocal form [50]. Ghost states can be avoided by using more than one reference state or by a proper choice of the local component and the cutoff radii in the basic semilocal pseudopotentials. The appearance of ghost states can be analyzed by investigating the following properties:

- Deviations of the logarithmic derivatives of the energy of the KB–pseudopotential from those of the respective semilocal pseudopotential or all–electron potential.
- Comparison of the atomic bound state spectra for the semilocal and KB–pseudopotentials.
- Ghost states below the valence states are identified by a rigorous criteria by Gonze et al. [50].

4.4 Dual–Space Gaussian Pseudopotentials

Pseudopotentials in the Kleinman–Bylander form have the advantage of requiring minimal amount of work in a plane wave calculation by still keeping most of the transferability and general accuracy of the underlying semilocal pseudopotential. However, one wonders if it would not be possible to generate directly pseudopotentials in the separable form fulfilling the Hamann–Schlüter–Chiang conditions. It was found [51] that indeed it is possible to optimize a small set of parameters defining an analytical form for the local and non–local form of a pseudopotential that fulfills those conditions and reproduces even additional properties leading to highly transferable pseudopotentials.
The local part of the pseudopotential is given by

$$V_{\rm loc}(r) \;=\; \frac{-Z_{\rm ion}}{r}{\rm erf}\left(\bar{r}/\sqrt{2}+\exp\left[-\frac{1}{2}\bar{r}^2\right]\right)\times\left[C_1+C_2\bar{r}^2+C_3\bar{r}^4+C_6\bar{r}^6\right] \;\;, \quad (4.22)$$

where erf denotes the error function and $\bar{r}=r/r_{\rm loc}$. $Z_{\rm ion}$ is the ionic charge of the atomic core, i.e. the total charge minus the charge of the valence electrons. The non–local contribution to the pseudopotential is a sum of separable terms

$$V_l(\mathbf{r},\mathbf{r}')=\sum_{i=1}^{3}\sum_{j=1}^{3}\sum_{m=-l}^{l} Y_{lm}(\hat{r})p_i^l(r)\;h_{ij}^l\;p_j^l(r)Y_{lm}^{\star}(\hat{r}') \;\;, \quad (4.23)$$

where the projectors $p_i^l(r)$ are Gaussians of the form

$$p_i^l(r)=\frac{\sqrt{2}r^{l+2(i-1)}\exp\left[-\frac{r^2}{2r_l^2}\right]}{r_l^{l+(4i-1)/2}\sqrt{\Gamma\left[l+\frac{4i-1}{2}\right]}} \;\;, \quad (4.24)$$

where Γ is the gamma function. The projectors are normalized

$$\int_0^\infty r^2 p_i^l(r)p_i^l(r)dr=1 \;\;. \quad (4.25)$$

This pseudopotential also has an analytical form in Fourier space. In both real and Fourier space, the projectors have the form of a Gaussian multiplied by a polynomial. Due to this property the dual–space Gaussian pseudopotential is the optimal compromise between good convergence properties in real and Fourier space. The multiplication of the wavefunction with the non–local pseudopotential arising from an atom can be limited to a small region around the atom as the radial projectors asymptotically tend to zero outside the covalent radius of the atom. In addition, a very dense integration grid is not required, as the projector is reasonably smooth because of its good decay properties in Fourier space.
The parameters of the pseudopotential are found by minimizing a target function. This function is build up as the sum of the differences of properties calculated from the all–electron atom and the pseudo–atom. Properties included are the integrated charge and the eigenvalues of occupied and the lowest unoccupied states.

Figure 4.1: Trouiller–Martins pseudopotential for Oxygen. Core radius was set to 1.05 bohr for s and p angular momentum. Top left graph shows the core and valence density of the reference state. Top right graph shows all–electron and pseudo wavefunction of s and p type. The lower graph show the pseudopotential (semilocal) in screened and unscreened form

Figure 4.2: Convergence of the bond length of the O_2 molecule for different types of pseudopotentials. See text for details.

4.5 Example: Pseudopotentials for Oxygen

It is very important that pseudopotentials are tested before used in large scale applications. We will show here some important points that should be considered whenever a new pseudopotential was created. Our test example are pseudopotentials for oxygen. We will compare pseudopotentials generated according the recipe by Trouiller and Martins [45] with cutoff radii of 1.05 and 1.40 Bohr. The pseudopotentials are used within the Kleinman–Bylander approximation using the p potential as local part (TM105p, TM140p) or the d potential as local part (TM140d). In addition we will also compare to a dual–space pseudopotential (HGH) [51] that uses a single s–type nonlocal projector.

- The first property to check is if the pseudo wavefunctions overlap with the all–electron wavefunction outside the cutoff region. See top left plot in figure 4.1 for the TM105 case. From this plot we immediately see that this pseudopotential will need a rather high cutoff as the p function was almost not pseudized.

- The oxygen pseudopotentials will be used without nonlinear core corrections. We have to see if there is considerable overlap between the valence density and the core density. This is not the case and the approximation though justified (see upper left plot in figure 4.1).

- The lower plots show the s and p potentials in the screened and unscreened form. We see that both potentials are rather smooth. There is the danger that for too large values of the core radius the potential will exhibit oscillations.

- As a further test we compare bond length is of the oxygen molecule (triplet state using LSD) as a function of the plane wave cutoff. As can be seen in figure 4.2 the calculations with the TM140 pseudopotentials need the smallest cutoff (about 60 Rydberg). However, a cutoff of 1.4 Bohr means that the core regions will overlap for the oxygen molecule and special care is needed. It can be seen that the converged

bond length of the TM140p potential has an error of about 2 %. Including also the p potential as a nonlocal function improves the result considerably, at the cost of four projector functions compared to one in the other case. The HGH and TM105p potentials have converged bond lengths close to the all–electron value using a single projector of s type. However, convergence is only achieved at about 100 to 125 Rydberg.

Lecture 5

Implementation

5.1 Total Energy and Gradients

5.1.1 Plane Wave Expansion

The plane wave expansions introduced in the last lecture were for local potentials

$$V^{\text{local}}(\mathbf{r}) = \sum_{\mathbf{G}} V^{\text{local}}(\mathbf{G}) \exp[i\mathbf{G}\cdot\mathbf{r}] \quad , \tag{5.1}$$

Kohn–Sham orbitals

$$\Phi(\mathbf{r}) = \frac{1}{\sqrt{\Omega}} \sum_{\mathbf{G}} c_i(\mathbf{G}) \exp[i\mathbf{G}\cdot\mathbf{r}] \quad , \tag{5.2}$$

and the electron density

$$n(\mathbf{r}) \quad = \quad \sum_{\mathbf{G}} n(\mathbf{G}) \exp[i\,\mathbf{G}\cdot\mathbf{r}] \quad . \tag{5.3}$$

5.1.2 Total Energy

Molecular dynamics calculations with interaction potentials derived from density functional theory require the evaluation of the total energy and derivatives with respect to the parameters of the Lagrangian.
The total energy can be calculated as a sum of kinetic, external (local and non-local pseudopotential), exchange and correlation, and electrostatic energy

$$E_{\text{total}} = E_{\text{kin}} + E^{\text{PP}}_{\text{local}} + E^{\text{PP}}_{\text{nonlocal}} + E_{\text{xc}} + E_{\text{ES}} \quad . \tag{5.4}$$

The individual terms are defined by

$$E_{\text{kin}} \quad = \quad \sum_i \sum_{\mathbf{G}} \frac{1}{2} f_i \, |\mathbf{G}|^2 \, |c_i(\mathbf{G})|^2 \tag{5.5}$$

$$E^{\rm PP}_{\rm local} = \sum_I \sum_{\mathbf{G}} \Delta V^I_{\rm local}(\mathbf{G})\, S_I(\mathbf{G}) n^\star(\mathbf{G}) \tag{5.6}$$

$$E^{\rm PP}_{\rm nonlocal} = \sum_i f_i \sum_I \sum_{\alpha,\beta\in I} \left(F^\alpha_{I,i}\right)^\star h^I_{\alpha\beta} F^\beta_{I,i} \tag{5.7}$$

$$E_{\rm xc} = \Omega \sum_{\mathbf{G}} \epsilon_{\rm xc}(\mathbf{G}) n^\star(\mathbf{G}) \tag{5.8}$$

$$E_{\rm ES} = 2\pi\,\Omega \sum_{\mathbf{G}\neq 0} \frac{|n_{\rm tot}(\mathbf{G})|^2}{G^2} + E_{\rm ovrl} - E_{\rm self}. \tag{5.9}$$

The overlap between the projectors of the non-local pseudopotential and the Kohn–Sham orbitals has been introduced in the equation above

$$F^\alpha_{I,i} = \frac{1}{\sqrt{\Omega}} \sum_{\mathbf{G}} P^I_\alpha(\mathbf{G})\, S_I(\mathbf{G})\, c^\star_i(\mathbf{G}) \ . \tag{5.10}$$

5.1.3 Wavefunction Gradient

Analytic derivatives of the total energy with respect to the parameters of the calculation are needed for stable molecular dynamics calculations. All derivatives needed are easily accessible in the plane wave pseudopotential approach. In the following Fourier space formulas are presented

$$\begin{aligned} \frac{1}{f_i}\frac{\partial E_{\rm total}}{\partial c^\star_i(\mathbf{G})} &= \frac{1}{2} G^2\, c_i(\mathbf{G}) \\ &\quad + \sum_{\mathbf{G}'} V^\star_{\rm loc}(\mathbf{G}-\mathbf{G}') c_i(\mathbf{G}') \\ &\quad + \sum_I \sum_{\alpha,\beta} \left(F^\alpha_{I,i}\right)^\star h^I_{\alpha\beta} P^I_\beta(\mathbf{G}) S_I(\mathbf{G}) \ , \end{aligned} \tag{5.11}$$

where $V_{\rm loc}$ is the total local potential

$$V_{\rm loc}(\mathbf{G}) = \sum_I \Delta V^I_{\rm local}(\mathbf{G}) S_I(\mathbf{G}) + V_{\rm xc}(\mathbf{G}) + 4\pi \frac{n_{\rm tot}(\mathbf{G})}{G^2} \ . \tag{5.12}$$

Wavefunction gradients are needed in optimization calculations and in the Car-Parrinello molecular dynamics approach.

5.1.4 Nuclear Gradient

The derivative of the total energy with respect to nuclear positions is needed for structure optimization and in molecular dynamics, that is

$$\frac{\partial E_{\rm total}}{\partial \mathbf{R}_{I,s}} = \frac{\partial E^{\rm PP}_{\rm local}}{\partial \mathbf{R}_{I,s}} + \frac{\partial E^{\rm PP}_{\rm nonlocal}}{\partial \mathbf{R}_{I,s}} + \frac{\partial E_{\rm ES}}{\partial \mathbf{R}_{I,s}} \ , \tag{5.13}$$

as the kinetic energy $E_{\rm kin}$ and the exchange and correlation energy $E_{\rm xc}$ do not depend directly on the atomic positions, the relevant parts are

$$\frac{\partial E^{\rm PP}_{\rm local}}{\partial \mathbf{R}_{I,s}} = -\Omega \sum_{\mathbf{G}} i\mathbf{G}_s \, \Delta V^I_{\rm local}(\mathbf{G}) \, S_I(\mathbf{G}) \, n^\star(\mathbf{G}) \tag{5.14}$$

$$\frac{\partial E^{\rm PP}_{\rm nonlocal}}{\partial \mathbf{R}_{I,s}} = \sum_i f_i \sum_{\alpha,\beta\in I} \left\{ \left(F^\alpha_{I,i}\right)^\star h^I_{\alpha\beta} \left(\frac{\partial F^\beta_{I,i}}{\partial \mathbf{R}_{I,s}}\right) + \left(\frac{\partial F^\alpha_{I,i}}{\partial \mathbf{R}_{I,s}}\right)^\star h^I_{\alpha,\beta} F^\beta_{I,i} \right\} \tag{5.15}$$

$$\frac{\partial E_{\rm ES}}{\partial \mathbf{R}_{I,s}} = -\Omega \sum_{\mathbf{G}\neq 0} i\mathbf{G}_s \, \frac{n^\star_{\rm tot}(\mathbf{G})}{G^2} \, n^I_{\rm c}(\mathbf{G}) \, S_I(\mathbf{G}) + \frac{\partial E_{\rm ovrl}}{\partial \mathbf{R}_{I,s}} \ . \tag{5.16}$$

The contribution of the projectors of the non-local pseudopotentials is calculated from

$$\frac{\partial F^\alpha_{I,i}}{\partial \mathbf{R}_{I,s}} = -\frac{1}{\sqrt{\Omega}} \sum_{\mathbf{G}} i\mathbf{G}_s \, P^I_\alpha(\mathbf{G}) \, S_I(\mathbf{G}) \, c^\star_i(\mathbf{G},\mathbf{k}) \ . \tag{5.17}$$

Finally, the real space part contribution of the Ewald sum is

$$\begin{aligned} \frac{\partial E_{\rm ovrl}}{\partial \mathbf{R}_{I,s}} = {} & \sum_J{}' \sum_{\mathbf{L}} \left\{ \frac{Z_I Z_J}{|\mathbf{R}_I - \mathbf{R}_J - \mathbf{L}|^3} {\rm erfc}\left[\frac{|\mathbf{R}_I - \mathbf{R}_J - \mathbf{L}|}{\sqrt{{\rm R}^{\rm c\,2}_I + {\rm R}^{\rm c\,2}_J}}\right] \right. \\ & \left. + \frac{2}{\sqrt{\pi}} \frac{1}{\sqrt{{\rm R}^{\rm c\,2}_I + {\rm R}^{\rm c\,2}_J}} \frac{Z_I Z_J}{|\mathbf{R}_I - \mathbf{R}_J - \mathbf{L}|^2} \exp\left[-\frac{|\mathbf{R}_I - \mathbf{R}_J - \mathbf{L}|^2}{\sqrt{{\rm R}^{\rm c\,2}_I + {\rm R}^{\rm c\,2}_J}}\right] \right\} \\ & \times (\mathbf{R}_{I,s} - \mathbf{R}_{J,s} - \mathbf{L}_s) \ . \end{aligned} \tag{5.18}$$

The self energy $E_{\rm self}$ is independent of the atomic positions and does not contribute to the forces.

5.2 Fast Fourier Transforms

A function given as a finite linear combination of plane waves can also be defined as a set of functional values on a equally spaced grid in real space. The sampling theorem (see e.g. Ref. [13]) gives the maximal grid spacing that still allows to hold the same information as the expansion coefficients of the plane waves. The real space sampling points $\mathbf{R}$ are defined

$$\mathbf{R} = \mathbf{h}\,\mathbf{N}\mathbf{q} \ , \tag{5.19}$$

where $\mathbf{N}$ is a diagonal matrix with the entries $1/N_s$ and $\mathbf{q}$ is a vector of integers ranging from 0 to $N_s - 1$ (s = x, y, z). To fulfill the sampling theorem N_s has to be bigger than $2\max(\mathbf{g}_s) + 1$. To be able to use fast Fourier techniques, N_s must be decomposable into small prime numbers (typically 2, 3, and 5). In applications the smallest number N_s that fulfills the above requirements is chosen.

A periodic function can be calculated at the real space grid points

$$
\begin{aligned}
f(\mathbf{R}) &= \sum_{\mathbf{G}} f(\mathbf{G}) \exp[i\,\mathbf{G}\cdot\mathbf{R}] && (5.20)\\
&= \sum_{\mathbf{g}} f(\mathbf{G}) \exp\Big[2\pi\, i\,\Big((\mathbf{h}^{\mathrm{t}})^{-1}\mathbf{g}\Big)\cdot(\mathbf{hNq})\Big] && (5.21)\\
&= \sum_{\mathbf{g}} f(\mathbf{G}) \exp\Big[\frac{2\pi}{N_{\mathrm{x}}} i g_{\mathrm{x}} q_{\mathrm{x}}\Big] \exp\Big[\frac{2\pi}{N_{\mathrm{y}}} i g_{\mathrm{y}} q_{\mathrm{y}}\Big] \exp\Big[\frac{2\pi}{N_{\mathrm{z}}} i g_{\mathrm{z}} q_{\mathrm{z}}\Big] \quad . && (5.22)
\end{aligned}
$$

The function $f(\mathbf{G})$ is zero outside the cutoff region and the sum over $\mathbf{g}$ can be extended over all indices in the cube $-\mathbf{g}_{\mathrm{s}}^{\max}\ldots\mathbf{g}_{\mathrm{s}}^{\max}$. The functions $f(\mathbf{R})$ and $f(\mathbf{G})$ are related by three–dimensional Fourier transforms

$$
\begin{aligned}
f(\mathbf{R}) &= \mathrm{FT}^{-1}\left[f(\mathbf{G})\right] && (5.23)\\
f(\mathbf{G}) &= \mathrm{FT}\left[f(\mathbf{R})\right] \quad . && (5.24)
\end{aligned}
$$

The Fourier transforms are defined by

$$
\begin{aligned}
\Big[\mathrm{FT}^{-1}\left[f(\mathbf{G})\right]\Big]_{uvw} &= \sum_{j=0}^{N_{\mathrm{x}}-1}\sum_{k=0}^{N_{\mathrm{y}}-1}\sum_{l=0}^{N_{\mathrm{z}}-1} f_{jkl}^{\mathbf{G}} \\
&\quad \exp\Big[i\frac{2\pi}{N_{\mathrm{x}}}\,j\,u\Big]\exp\Big[i\frac{2\pi}{N_{\mathrm{y}}}\,k\,v\Big]\exp\Big[i\frac{2\pi}{N_{\mathrm{z}}}\,l\,w\Big] && (5.25)\\
\left[\mathrm{FT}\left[f(\mathbf{R})\right]\right]_{jkl} &= \sum_{u=0}^{N_{\mathrm{x}}-1}\sum_{v=0}^{N_{\mathrm{y}}-1}\sum_{w=0}^{N_{\mathrm{z}}-1} f_{uvw}^{\mathbf{R}} \\
&\quad \exp\Big[-i\frac{2\pi}{N_{\mathrm{x}}}\,j\,u\Big]\exp\Big[-i\frac{2\pi}{N_{\mathrm{y}}}\,k\,v\Big]\exp\Big[-i\frac{2\pi}{N_{\mathrm{z}}}\,l\,w\Big] \quad , && (5.26)
\end{aligned}
$$

where the appropriate mappings of $\mathbf{q}$ and $\mathbf{g}$ to the indices

$$
\begin{aligned}
[u,v,w] &= \mathbf{q} && (5.27)\\
\{j,k,l\} &= \mathbf{g}_s \quad \text{if} \;\; \mathbf{g}_s \geq 0 && (5.28)\\
\{j,k,l\} &= N_s + \mathbf{g}_s \quad \text{if} \;\; \mathbf{g}_s < 0 && (5.29)
\end{aligned}
$$

have to be used. From Eqs. (5.25) and (5.26) it can be seen, that the calculation of the three–dimensional Fourier transforms can be performed by a series of one dimensional Fourier transforms. The number of transforms in each direction is $N_{\mathrm{x}}N_{\mathrm{y}}$, $N_{\mathrm{x}}N_{\mathrm{z}}$, and $N_{\mathrm{y}}N_{\mathrm{z}}$ respectively. Assuming that the one-dimensional transforms are performed within the fast Fourier transform framework, the number of operations per transform of length n is approximately $5n\log n$. This leads to an estimate for the number of operations for the full three-dimensional transform of $5N\log N$, where $N = N_{\mathrm{x}}N_{\mathrm{y}}N_{\mathrm{z}}$.

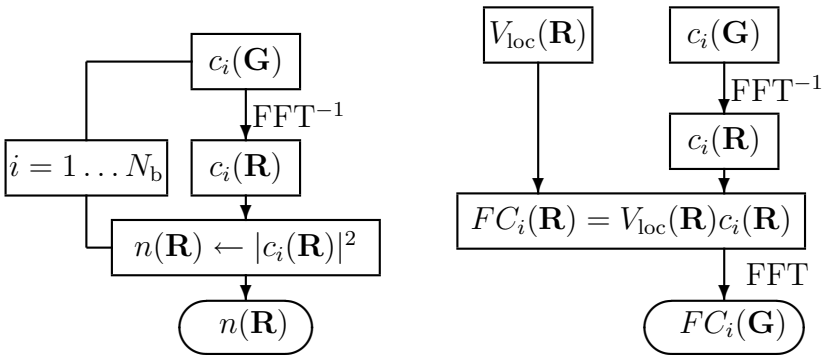

Figure 5.1: Flow chart for the calculation of the charge density (on the left) and the force on the wavefunction from the local potential (on the right). The charge density calculation requires N_b (number of states) three dimensional Fourier transforms. For the application of the local potential two Fourier transforms per state are needed. If enough memory is available the first transform can be avoided if the wavefunction on the real space grid are stored during the density calculation.

5.3 Density and Force Calculations in Practice

Above formulas for the total energy and forces were given in their Fourier space representation. Many terms are in fact calculated most easily in this form, but some terms would require double sums over plane waves. In particular, the calculation of the charge density and the wavefunction gradient originating from the local potential

$$\sum_{\mathbf{G}'} V^\star_\mathrm{loc}(\mathbf{G} - \mathbf{G}')c_i(\mathbf{G}') \ . \tag{5.30}$$

The expression in Eq. (5.30) is a convolution and can be calculated efficiently by a series of Fourier transforms. The flow charts of this calculations are presented in Fig. 5.1. Both of these modules contain a Fourier transform of the wavefunctions from $\mathbf{G}$ space to the real space grid. In addition, the calculation of the wavefunction forces requires a back transform of the product of the local potential with the wavefunctions, performed on the real space grid, to Fourier space. This leads to a number of Fourier transforms that is three times the number of states in the system. If enough memory is available on the computer the second transform of the wavefunctions to the grid can be avoided if the wavefunctions are stored in real space during the computation of the density.

5.4 Saving Computer Time

In an implementation of the plane wave/pseudopotential method it is possible to use the special structure of the wavefunctions to save computer time. If the Kohn–Sham

orbitals are only calculated at the Γ–point then the wavefunctions can be taken as real quantities. The plane wave expansion coefficients of real functions have to following symmetry property

$$c(-\mathbf{G}) = c^{\star}(\mathbf{G}) \ , \tag{5.31}$$

and $c(\mathbf{0})$ is real. Therefore it is possible to store only half of the coefficients and recalculate the others whenever needed. In addition the symmetry can be used in calculating overlap integrals

$$\langle \Phi_i \mid \Phi_j \rangle = \sum_{\mathbf{G}} c_i^{\star}(\mathbf{G}) c_j(\mathbf{G}) \ . \tag{5.32}$$

The sum can be restricted to half of the G–vectors

$$\langle \Phi_i \mid \Phi_j \rangle = c_i(\mathbf{0}) c_j(\mathbf{0}) + \sum_{\mathbf{G}} 2 \ \mathrm{Re}(c_i^{\star}(\mathbf{G}) c_j(\mathbf{G})) \ . \tag{5.33}$$

This sum can be implemented efficiently using real arithmetic avoiding multiplication of complex numbers.
Another direct use of the symmetry of the wavefunctions can be made when using Fourier transforms. The Fourier transform pair is defined by

$$\begin{aligned} F(\omega) &= \int_{-\infty}^{\infty} f(t) e^{i\omega t} dt \\ f(t) &= \frac{1}{2\pi} \int_{-\infty}^{\infty} F(\omega) e^{-i\omega t} d\omega \ , \end{aligned}$$

where in our case t is the direct (real) space and ω is reciprocal space (G - space). We want to make use of the special structure of our wavefunctions

$$f(t) is real \Rightarrow F(\omega) = F(-\omega)^* \ , \tag{5.34}$$

that allows to perform two transforms together. First we investigate a real to complex transform. We define a new function

$$g(t) = f_1(t) + i f_2(t)$$

then we get for the transformed function

$$\begin{aligned} G(\omega) &= F_1(\omega) + i F_2(\omega) \\ G(-\omega) &= F_1(-\omega) + i F_2(-\omega) \\ &= F_1(\omega)^* + i F_2(\omega)^* \end{aligned}$$

We can calculate the two new functions $G(\omega) + G(-\omega)$ and $G(\omega) - G(-\omega)$.

$$\begin{aligned} G(\omega) + G(-\omega) &= F_1(\omega) + F_1(\omega)^* + i \left(F_2(\omega) + F_2(\omega)^* \right) \\ &= 2\mathrm{Re}\left[F_1(\omega) \right] + 2i\mathrm{Re}\left[F_2(\omega) \right] \\ G(\omega) - G(-\omega) &= 2i\mathrm{Im}\left[F_1(\omega) \right] - 2\mathrm{Im}\left[F_2(\omega) \right] \end{aligned}$$

Table 5.1: Comparison of number of one dimensional FFT's needed in a full transform and a transform making use of the sparsity of the data set in reciprocal space

Reciprocal space to direct space transform		Direct space to reciprocal space transform	
full transform	sparse transform	full transform	sparse transform
N^2	$\frac{\pi}{16}\ N^2$	N^2	N^2
N^2	$\frac{1}{2}\ N^2$	N^2	$\frac{1}{2}\ N^2$
N^2	N^2	N^2	$\frac{\pi}{16}\ N^2$
$3\ N^2$	$\left(\frac{3}{2}+\frac{\pi}{16}\right)\ N^2$	$3\ N^2$	$\left(\frac{3}{2}+\frac{\pi}{16}\right)\ N^2$

and we find

$$\begin{aligned} F_1(\omega) &= \frac{1}{2}\left(\mathrm{Re}\left[G(\omega)+G(-\omega)\right]+i\mathrm{Im}\left[G(\omega)-G(-\omega)\right]\right) \\ F_2(\omega) &= \frac{1}{2}\left(\mathrm{Im}\left[G(\omega)+G(-\omega)\right]+i\mathrm{Re}\left[G(\omega)-G(-\omega)\right]\right) \end{aligned}$$

For the complex to real transform we define

$$G(\omega) = F_1(\omega) + iF_2(\omega)$$

then we get for the functions in direct (time) space

$$\begin{aligned} g(t) &= f_1(t) + f_2(t) \\ f_1(t) &= \mathrm{Re}\left[g(t)\right] \\ f_2(t) &= \mathrm{Im}\left[g(t)\right] \end{aligned}$$

Finally, we can take advantage of the fact that the wavefunction cutoff is only 1/4 of the density cutoff. Therefore in reciprocal space only the values of grid points inside a sphere of radius N/4 are non-zero, where for simplicity we assume a simple cubic box with N^3 grid points. In a three dimensional FFT there will be many one dimensional transforms that can be avoided. In table 5.4 the amount of work for a full transform and a transform that makes use of the sparsity of the data set are compared. In both transforms the savings amount to about a factor of two.

5.5 Exchange and Correlation Functionals

Gradient corrected exchange and correlation functionals and their potentials are defined as

$$E_{xc} = \int F(n, \nabla n) d\mathbf{r} \tag{5.35}$$

$$
\begin{aligned}
V_{xc} &= \frac{\delta E_{xc}}{\delta n} = \frac{\partial F}{\partial n} - \sum_{\alpha=1}^{3} \frac{d}{dr_\alpha}\left[\frac{\partial F}{\partial(\nabla_\alpha n)}\right] \\
&= \frac{\partial F}{\partial n} - \sum_{\alpha=1}^{3} \frac{\partial}{\partial r_\alpha}\left[\frac{1}{|\nabla n|}\frac{\partial F}{\partial|\nabla n|}\frac{\partial n}{\partial r_\alpha}\right]
\end{aligned} \tag{5.36}
$$

The function F and its derivatives with respect to n and $|\nabla n|$ have to be calculated in real space. The derivatives with respect to r can be calculated most easily in reciprocal space. The following scheme outlines the steps necessary to perform the calculation

1. $$n(R) \stackrel{FFT}{\longrightarrow} n(G)$$
2. $$\frac{\partial n}{\partial r_\alpha} = iG_\alpha n(G)$$
3. $$iG_\alpha n(G) \stackrel{INVFFT}{\longrightarrow} \frac{\partial n}{\partial r_\alpha}(R)$$
4. $$|\nabla n(R)|$$
5. $$F(n(R), \nabla n(R))$$
6. $$\frac{\partial F(R)}{\partial n}$$
7. $$\frac{1}{|\nabla n(R)|}\frac{\partial F(R)}{\partial|\nabla n(R)|}$$
8. $$
\begin{aligned}
H^1(R) &= \frac{\partial F(R)}{\partial n} \stackrel{FFT}{\longrightarrow} H^1(G) \\
H^2_\alpha(R) &= \frac{1}{|\nabla n(R)|}\frac{\partial F(R)}{\partial|\nabla n(R)|}\frac{\partial n}{\partial r_\alpha}(R) \stackrel{FFT}{\longrightarrow} H^2_\alpha(G)
\end{aligned}
$$
9. $$V_{xc}(G) = H^1(G) - \sum_{\alpha=1}^{3} iG_\alpha H^2_\alpha(G)$$
10. $$V_{xc}(G) \stackrel{INVFFT}{\longrightarrow} V_{xc}(R)$$

Lecture 6

Extensions to the Original Method

6.1 Non-linear Core Correction

The success of pseudopotentials in density functional calculations relies on two assumptions. The transferability of the core electrons to different environments and the linearization of the exchange and correlation energy. The second assumption is only valid if the frozen core electrons and the valence state do not overlap. However, if there is significant overlap between core and valence densities, the linearization will lead to reduced transferability and systematic errors. The most straightforward remedy is to include "semi–core states" in addition to the valence shell, i.e. one more inner shell (which is from a chemical viewpoint an inert "core level") is treated explicitely. This approach, however, leads to quite hard pseudopotentials which call for high plane wave cutoffs. Alternatively, it was proposed to treat the non–linear parts of the exchange and correlation energy $E_{\rm xc}$ explicitely [52]. This idea does not lead to an increase of the cutoff but ameliorates the above–mentioned problems quite a bit. To achieve this, $E_{\rm xc}$ is calculated not from the valence density $n(\mathbf{R})$ alone, but from a modified density

$$\tilde{n}(\mathbf{R}) = n(\mathbf{R}) + \tilde{n}_{\rm core}(\mathbf{R}) \ , \tag{6.1}$$

where $\tilde{n}_{core}(\mathbf{R})$ denotes a density that is equal to the core density of the atomic reference state in the region of overlap with the valence density

$$\tilde{n}_{\rm core}(r) = n_{\rm core}(r) \quad \text{if } r > r_0 \ ; \tag{6.2}$$

with the vanishing valence density inside r_0. Close to the nuclei a model density is chosen in order to reduce the cutoff for the plane wave expansion. Finally, the two densities and their derivatives are matched at r_0. This procedure leads to a modified total energy, where $E_{\rm xc}$ is replace by

$$E_{\rm xc} = E_{\rm xc}(n + \tilde{n}_{\rm core}) \ , \tag{6.3}$$

and the corresponding potential is

$$V_{\rm xc} = V_{\rm xc}(n + \tilde{n}_{\rm core}) \ . \tag{6.4}$$

The sum of all modified core densities

$$\tilde{n}_{core}(\mathbf{G}) = \sum_I \tilde{n}^I_{core}(\mathbf{G}) S_I(\mathbf{G}) \tag{6.5}$$

depends on the nuclear positions, leading to a new contribution to the forces

$$\frac{\partial E_{\rm xc}}{\partial \mathbf{R}_{I,s}} = -\Omega \sum_{\mathbf{G}} i\mathbf{G}_s V^\star_{\rm xc}(\mathbf{G}) \tilde{n}^I_{\rm core}(\mathbf{G}) S_I(\mathbf{G}) \ . \tag{6.6}$$

The method of the non-linear core correction dramatically improves results on systems with alkali and transition metal atoms. For practical applications, one should keep in mind that the non-linear core correction should only be applied together with pseudopotentials that were generated using the same energy expression.

6.2 Ultrasoft Pseudopotentials and the Projector Augmented–Wave Method

For norm–conserving pseudopotentials the all–electron (AE) wavefunction is inside some core radius replaced by a soft nodeless pseudo (PS) wavefunction, with the crucial restriction that the PS wavefunction must have the same norm as the AE wavefunction within the chosen core radius; outside the core radius the PS and AE wavefunction are identical. It is well established that good transferability requires a core radius around the outermost maximum of the AE wavefunction, because only then the charge distribution and moments of the AE wavefunction are well reproduced by the PS wavefunctions. Therefore, for elements with strongly localized orbitals (like first–row, 3d, and rare–earth elements) the resulting pseudopotentials require large plane wave basis sets. To work around this problem, compromises are often made by increasing the core radius significantly beyond the outermost maximum of the AE wavefunction. But this is usually not a satisfactory solution because the transferability is always adversely affected when the core radius is increased, and for any new chemical environment, additional tests are required to establish the reliability of such soft PP's.
An elegant solution to this problem was proposed by Vanderbilt [53]. In his method, the norm–conservation constraint is relaxed and to make up for the resulting charge deficit, localized atom–centered augmentation charges are introduced. These augmentation charges are defined as the charge difference between the AE and PS wavefunctions, but for convenience they are pseudized to allow an efficient treatment of the augmentation charges on a regular grid. The core radius of the pseudopotential can now be chosen around

the nearest neighbor distance; independent of the position of the maximum of the AE wavefunction. Only for the augmentation charges a small cutoff radius must be used to restore the moments and the charge distribution of the AE wavefunction accurately. The pseudized augmentation charges are usually treated on a regular grid in real space, which is not necessarily the same as the one used for the representation of the wavefunctions. The relation between the ultrasoft pseudopotential method and other plane wave based methods was discussed by Singh [35].
A closely related method to Vanderbilts ultrasoft pseudopotentials was introduced by Blöchl [112]. In the projector augmented–wave method (PAW) a linear transformation is defined that connects the PS and AE wavefunctions. Already Blöchl did mention the similarities of his approach to the ultrasoft pseudopotentials. A formal derivation of the ultrasoft pseudopotentials from the PAW equations was done by Kresse and Joubert [54].

6.2.1 The PAW Transformation

We start the derivation of the ultrasoft pseudopotentials and the PAW method by introducing a linear transformation [112, 55]. The PAW method is based on a formal division of the whole space Ω in distinct regions: a collection of non overlapping spherical regions around each atom: atomic spheres region $\bigcup_a \Omega_a$, and the remainder, the interstitial region Ω_{I}:

$$\Omega = \Omega_{\mathrm{I}} + \bigcup_a \Omega_a \quad . \tag{6.7}$$

It is clear that the plane wave basis, being the ideal choice in the interstitial region Ω_{I} will have great difficulties describing the wavefunctions in the atomic spheres region. In the PAW method this problem is circumvented by introducing auxiliary wavefunctions which satisfies the following requirements. First, the auxiliary wavefunction $\tilde{\Phi}_i(\mathbf{r})$ can be obtained from the AE wavefunction $\Phi_i(\mathbf{r})$ via a invertible linear transformation $\mathcal{T}$

$$| \tilde{\Phi}_i\rangle = \mathcal{T} \mid \Phi_i\rangle \tag{6.8}$$
$$| \Phi_i\rangle = \mathcal{T}^{-1} \mid \tilde{\Phi}_i\rangle \tag{6.9}$$

Second, $\tilde{\Phi}_i(\mathbf{r})$ is smooth, i.e. can be represented by plane wave basis set of a practicle size, everywhere, including the atomic spheres region

$$\tilde{\Phi}_i(\mathbf{r}) = \frac{1}{\sqrt{\Omega}} \sum_{\mathbf{G}} c_i(\mathbf{G}) e^{i\mathbf{G}\cdot\mathbf{r}} \quad . \tag{6.10}$$

The first requirement ensures that the task of solving the Kohn–Sham equations can be equivalently reformulated in terms of $\tilde{\Phi}_i(\mathbf{r})$, whereas the second requirement allows the entire process to be performed using the plane wave basis set.
The actual construction of $\tilde{\Phi}_i(\mathbf{r})$ from a given $\Phi_i(\mathbf{r})$ proceeds as follows. For each atom, we define a finite set of local basis functions $\{\chi^a_\alpha\}$ that is expected to accurately describe the

oscillating behavior of the relevant wavefunction $\Phi_i(\mathbf{r})$ within the corresponding atomic sphere. Associated with $\{\chi^a_\alpha\}$ we introduce a set of localized projector functions $\{p^a_\alpha\}$ such that

$$\begin{aligned} \langle p^a_\beta \mid \chi^a_\alpha \rangle &= \delta_{\alpha\beta} && (6.11) \\ p^a_\alpha(\mathbf{r}) &= 0 \ , \quad \forall \mathbf{r} \subset \Omega_{\rm I} \ . && (6.12) \end{aligned}$$

Using $\{\chi^a_\alpha\}$ and $\{p^a_\alpha\}$, the wavefunction $\Phi_i(\mathbf{r})$ in the atomic sphere region can be represented as

$$\Phi_i(\mathbf{r}) = \sum_\alpha c^a_{i,\alpha} \chi^a_\alpha(\mathbf{r}) + \Delta^a_i(\mathbf{r}) \ , \quad \forall \mathbf{r} \subset \Omega_a \ . \tag{6.13}$$

The coefficients $c^a_{i,\alpha}$ in the expansion (6.13) are given by

$$c^a_{i,\alpha} = \langle p^a_\alpha \mid \Phi_i \rangle \ . \tag{6.14}$$

The correction

$$\mid \Delta^a_i \rangle = (1 - \sum_\alpha \mid \chi^a_\alpha \rangle \langle p^a_\alpha \mid) \mid \Phi_i \rangle \ , \tag{6.15}$$

reflects the incompleteness of the set $\{\chi^a_\alpha\}$. As the size of the basis $\{\chi^a_\alpha\}$ gets larger, the local basis representation of $\Phi_i(\mathbf{r})$ becomes more accurate, and $\Delta^a_i(\mathbf{r})$ goes to zero. To define a mapping into $\tilde{\Phi}_i(\mathbf{r})$ an auxiliary smooth basis set $\{\tilde{\chi}^a_\alpha\}$ is formed, subject to the following conditions. First, the basis functions $\tilde{\chi}^a_\alpha(\mathbf{r})$ are smooth, i.e. expandable in terms of the plane wave basis of a practical size, everywhere including the atomic sphere region. Second, $\tilde{\chi}^a_\alpha(\mathbf{r})$ merges differentiable into $\chi^a_\alpha(\mathbf{r})$ outside the atomic sphere:

$$\tilde{\chi}^a_\alpha(\mathbf{r}) = \chi^a_\alpha(\mathbf{r}) \ , \quad \forall \mathbf{r} \subset \Omega_{\rm I} \ . \tag{6.16}$$

Third, both $\tilde{\chi}^a_\alpha(\mathbf{r})$ and differences $\tilde{\chi}^a_\alpha(\mathbf{r}) - \chi^a_\alpha(\mathbf{r})$ form linearly independent sets. The smooth wavefunction $\tilde{\Phi}_i(\mathbf{r})$ can be obtained based on the following prescription. Inside the atomic sphere region it is generated by replacing each occurrence of $\chi^a_\alpha(\mathbf{r})$ with $\tilde{\chi}^a_\alpha(\mathbf{r})$ in the expansion (6.13)

$$\tilde{\Phi}_i(\mathbf{r}) = \sum_\alpha c^a_{i,\alpha} \chi^a_\alpha(\mathbf{r}) + \Delta^a_i(\mathbf{r}) \ , \quad \forall \mathbf{r} \subset \Omega_a \ , \tag{6.17}$$

whereas in the interstitial region it simply coincides with $\Phi_i(\mathbf{r})$:

$$\tilde{\Phi}_i(\mathbf{r}) = \Phi_i(\mathbf{r}) \quad \forall \mathbf{r} \subset \Omega_{\rm I} \ . \tag{6.18}$$

The transformation can therefore be expressed as

$$\mathcal{T} = 1 + \sum_a \sum_\alpha (\mid \tilde{\chi}^a_\alpha \rangle - \mid \chi^a_\alpha \rangle) \langle p^a_\alpha \mid \ . \tag{6.19}$$

Its inverse can be obtained as

$$\mathcal{T}^{-1} = 1 + \sum_a \sum_\alpha (\mid \chi^a_\alpha\rangle - \mid \tilde{\chi}^a_\alpha\rangle)\langle \tilde{p}^a_\alpha \mid \ , \tag{6.20}$$

where a set of smooth projector functions $\{\tilde{p}^a_\alpha\}$ is defined as

$$\langle \tilde{p}^a_\alpha \mid = \sum_\beta (p^a \mid \tilde{\chi}^a\rangle)^{-1}_{\alpha\beta} \langle p^a_\beta \mid \ . \tag{6.21}$$

It can be shown that similar to $\{p^a_\alpha\}$, the smooth projector functions $\{\tilde{p}^a_\alpha\}$ have the following properties

$$\langle \tilde{p}^a_\beta \mid \tilde{\chi}^a_\alpha\rangle = \delta_{\alpha\beta} \tag{6.22}$$

$$\tilde{p}^a_\alpha(\mathbf{r}) = 0 \ , \quad \forall \mathbf{r} \subset \Omega_{\mathrm{I}} \ . \tag{6.23}$$

Furthermore, it is straightforward to prove that

$$\langle \tilde{p}^a_\alpha \mid = \langle p^a_\alpha \mid \mathcal{T}^{-1} \tag{6.24}$$

and therefore the local basis expansion coefficients and the remainder can be alternatively represented as

$$c^a_{i,\alpha} = \langle \tilde{p}^a_\alpha \mid \tilde{\Phi}_i\rangle \ . \mid \Delta^a_i\rangle = (1 - \sum_\alpha \mid \tilde{\chi}^a_\alpha\rangle\langle \tilde{p}^a_\alpha \mid) \mid \tilde{\Phi}_i\rangle \ . \tag{6.25}$$

The above two expressions show that if the basis $\{\chi^a_\alpha\}$ provides an accurate local representation for $\Phi_i(\mathbf{r})$, then the smooth basis $\{\tilde{\chi}^a_\alpha\}$ provides an accurate local representation for $\tilde{\Phi}_i(\mathbf{r})$ and vice versa. This is an important observation, since it is our objective to completely eliminate $\Phi_i(\mathbf{r})$and seek for $\tilde{\Phi}_i(\mathbf{r})$ directly.
From a practical point of view, it is the inverse transformation $\mathcal{T}^{-1}$ that plays a major role in all the applications. The expression for $\mathcal{T}^{-1}$ involves basis sets $\Phi_i(\mathbf{r})$ and $\tilde{\Phi}_i(\mathbf{r})$ and smooth projector functions $\{\tilde{p}^a_\alpha\}$. If desired the projector functions $\{p^a_\alpha\}$ can be found from

$$\langle p^a_\alpha \mid = \sum_\beta (\langle \tilde{p}^a \mid \chi^a\rangle)^{-1}_{\alpha\beta} \langle \tilde{p}^a_\beta \mid \ . \tag{6.26}$$

In the following we will make the approximation that the local expansions are accurate and the remainder terms can be neglected.

6.2.2 Expectation Values

Consider the expectation value of the general local or quasilocal operator $\mathcal{O}$ with respect to the Kohn–Sham orbital Φ

$$\langle O\rangle = \langle \Phi \mid \mathcal{O} \mid \Phi\rangle \ . \tag{6.27}$$

This can be rewritten in terms of the smooth wavefunction

$$\begin{aligned}\langle O\rangle &= \langle \mathcal{T}^{-1}\tilde{\Phi} \mid \mathcal{O} \mid \mathcal{T}^{-1}\tilde{\Phi}\rangle \\ &= \langle \tilde{\Phi} \mid \mathcal{O} \mid \tilde{\Phi}\rangle + \\ &\quad \sum_a \sum_{\alpha\beta} \langle \tilde{\Phi} \mid \tilde{p}^a_\alpha\rangle \left(\langle \chi^a_\alpha \mid \mathcal{O} \mid \chi^a_\beta\rangle - \langle \tilde{\chi}^a_\alpha \mid \mathcal{O} \mid \tilde{\chi}^a_\beta\rangle\right) \langle \tilde{p}^a_\beta \mid \tilde{\Phi}\rangle \ . \end{aligned} \tag{6.28}$$

Note that the last expression can not be directly derived using the explicit form of the transformation, but is in fact an equivalence that is based on the properties of the expansion basis. The original expression for the expectation value splits into several parts. The first part is a simple expectation value over the smooth wave function which can be accurately calculated using plane wave basis. The second term is one–center and restricted to atomic spheres region. This second term already has the same structure as the nonlocal part in a fully separable pseudopotential.
Setting the operator $\mathcal{O}$ to the identity,

$$\langle \mathbf{r} \mid \mathcal{O} \mid \mathbf{r}'\rangle = \delta(\mathbf{r}-\mathbf{r}') \tag{6.29}$$

reveals that the orthogonality properties of smooth wavefunctions $\{\tilde{\Phi}_i\}$ are different from those of $\{\Phi_i\}$. Namely, if

$$\langle \Phi_i \mid \Phi_j\rangle = \delta_{ij} \tag{6.30}$$

then

$$\langle \tilde{\Phi}_i \mid \mathcal{S} \mid \tilde{\Phi}_j\rangle = \delta_{ij} \ . \tag{6.31}$$

Here the overlap operator is given by

$$\mathcal{S} = 1 + \sum_a \sum_{\alpha\beta} \mid \tilde{p}^a_\alpha\rangle \left(\langle \chi^a_\alpha \mid \chi^a_\beta\rangle - \langle \tilde{\chi}^a_\alpha \mid \tilde{\chi}^a_\beta\rangle\right) \langle \tilde{p}^a_\beta \mid \ . \tag{6.32}$$

The relationship between the electron density

$$n(\mathbf{r}) = \sum_i f_i \mid \Phi_i(\mathbf{r}) \mid^2 \tag{6.33}$$

and its smooth image

$$\tilde{n}(\mathbf{r}) = \sum_i f_i \mid \tilde{\Phi}_i(\mathbf{r}) \mid^2 \tag{6.34}$$

can be obtained by setting

$$\mathcal{O} = \mid \mathbf{r}\rangle\langle \mathbf{r} \mid \ . \tag{6.35}$$

We obtain

$$n(\mathbf{r}) = \tilde{n}(\mathbf{r}) + \sum_a \left[n^a(\mathbf{r}-\mathbf{R}_a) - \tilde{n}^a(\mathbf{r}-\mathbf{R}_a)\right] \ , \tag{6.36}$$

where one–center atomic densities $n^a(\mathbf{r})$ and $\tilde{n}^a(\mathbf{r})$ are given by

$$n^a(\mathbf{r}) = \sum_i f_i \left| \sum_\alpha c^a_{i\alpha} \chi^a_\alpha(\mathbf{r}) \right|^2 \tag{6.37}$$

$$\tilde{n}^a(\mathbf{r}) = \sum_i f_i \left| \sum_\alpha c^a_{i\alpha} \tilde{\chi}^a_\alpha(\mathbf{r}) \right|^2 \quad , \tag{6.38}$$

and we get the following relationships

$$n^a(\mathbf{r}) = n(\mathbf{r}) \quad , \quad \forall \mathbf{r} \subset \Omega_a \tag{6.39}$$

$$\tilde{n}^a(\mathbf{r}) = \tilde{n}(\mathbf{r}) \quad , \quad \forall \mathbf{r} \subset \Omega_a \quad . \tag{6.40}$$

6.2.3 Ultrasoft Pseudopotentials

We are now in the position to derive the energy expression for the ultrasoft pseudopotentials. To do so we write the energy of a system of atoms using the results from the last section within the Kohn–Sham approach

$$\tilde{n}(\mathbf{r}) = \sum_i f_i \mid \tilde{\Phi}_i(\mathbf{r}) \mid^2 \tag{6.41}$$

$$n^a(\mathbf{r}) - \tilde{n}^a(\mathbf{r}) = \sum_i f_i \sum_{\alpha\beta} \langle \tilde{\Phi}_i \mid \tilde{p}^a_\alpha \rangle \left(\chi^a_\alpha(\mathbf{r}) \chi^a_\beta(\mathbf{r}) - \tilde{\chi}^a_\alpha(\mathbf{r}) \tilde{\chi}^a_\beta(\mathbf{r}) \right) \langle \tilde{p}^a_\beta \mid \tilde{\Phi}_i \rangle \tag{6.42}$$

$$n(\mathbf{r}) = \tilde{n}(\mathbf{r}) + \sum_a \left[n^a(\mathbf{r} - \mathbf{R}_a) - \tilde{n}^a(\mathbf{r} - \mathbf{R}_a) \right] \tag{6.43}$$

$$\langle \tilde{\Phi}_i \mid \mathcal{S} \mid \tilde{\Phi}_j \rangle = \delta_{ij} \tag{6.44}$$

$$\begin{aligned} E_{\mathrm{KS}} = & \sum_i f_i \langle \tilde{\Phi}_i \mid \mathcal{T} + \mathcal{V}_{\mathrm{ext}} \mid \tilde{\Phi}_i \rangle + \sum_i f_i \sum_a \sum_{\alpha\beta} \langle \tilde{\Phi}_i \mid \tilde{p}^a_\alpha \rangle \\ & \times \left(\langle \chi^a_\alpha \mid \mathcal{T} + \mathcal{V}_{\mathrm{ext}} \mid \chi^a_\beta \rangle - \langle \tilde{\chi}^a_\alpha \mid \mathcal{T} + \mathcal{V}_{\mathrm{ext}} \mid \tilde{\chi}^a_\beta \rangle \right) \langle \tilde{p}^a_\beta \mid \tilde{\Phi}_i \rangle \\ & + E_{\mathrm{Hxc}}[n(\mathbf{r})] + E_{\mathrm{ion}} \quad , \end{aligned} \tag{6.45}$$

where E_{Hxc} is the combined energy of the Hartree potential and the exchange and correlation energy. We now introduce the new quantities

$$Q^a_{\alpha\beta}(\mathbf{r}) = \chi^a_\alpha(\mathbf{r}) \chi^a_\beta(\mathbf{r}) - \tilde{\chi}^a_\alpha(\mathbf{r}) \tilde{\chi}^a_\beta(\mathbf{r}) \tag{6.46}$$

$$q^a_{\alpha\beta} = \int d\mathbf{r} \; Q^a_{\alpha\beta}(\mathbf{r}) \tag{6.47}$$

$$\mathcal{V}^a_{\mathrm{ext}}(\mathbf{r}) = \mathcal{V}^a_{\mathrm{loc}}(\mathbf{r}) + \Delta\mathcal{V}^a_{\mathrm{ext}}(\mathbf{r}) \tag{6.48}$$

$$D^a_{\alpha\beta} = \langle \chi^a_\alpha \mid \mathcal{T} + \Delta\mathcal{V}_{\mathrm{ext}} \mid \chi^a_\beta \rangle - \langle \tilde{\chi}^a_\alpha \mid \mathcal{T} + \Delta\mathcal{V}_{\mathrm{ext}} \mid \tilde{\chi}^a_\beta \rangle \quad , \tag{6.49}$$

where $\mathcal{V}^a_{\mathrm{loc}}(\mathbf{r})$ is a local smooth potential and $\Delta\mathcal{V}^a_{\mathrm{ext}}(\mathbf{r})$ is localized within the atomic sphere regions. Using these quantities the basic equations can be written

$$n(\mathbf{r}) = \sum_i f_i \left[\mid \tilde{\Phi}_i(\mathbf{r}) \mid^2 + \sum_a \sum_{\alpha\beta} Q^a_{\alpha\beta}(\mathbf{r}) \langle \tilde{\Phi}_i \mid \tilde{p}^a_\alpha \rangle \langle \tilde{p}^a_\beta \mid \tilde{\Phi}_i \rangle \right] \tag{6.50}$$

$$\langle \tilde{\Phi}_i \mid \mathcal{S} \mid \tilde{\Phi}_j \rangle = \delta_{ij} \tag{6.51}$$

$$\mathcal{S} = 1 + \sum_a \sum_{\alpha\beta} q^a_{\alpha\beta} \mid \tilde{p}^a_\alpha \rangle \langle \tilde{p}^a_\beta \mid \tag{6.52}$$

$$\begin{aligned} E_{\rm KS} = & \sum_i f_i \langle \tilde{\Phi}_i \mid -\frac{1}{2}\nabla^2 \mid \tilde{\Phi}_i \rangle + \int d\mathbf{r}\ \mathcal{V}_{\rm loc}(\mathbf{r}) \tilde{n}(\mathbf{r}) + \\ & \sum_i f_i \sum_a \sum_{\alpha\beta} \langle \tilde{\Phi}_i \mid \tilde{p}^a_\alpha \rangle \left(D^a_{\alpha\beta} + \int d\mathbf{r}\ \mathcal{V}_{\rm loc}(\mathbf{r}) Q^a_{\alpha\beta}(\mathbf{r}) \right) \langle \tilde{p}^a_\beta \mid \tilde{\Phi}_i \rangle \\ & + E_{\rm Hxc}[n(\mathbf{r})] + E_{\rm ion}\ . \end{aligned} \tag{6.53}$$

These are the working equations for the Kohn–Sham method using ultrasoft pseudopotentials. The pseudopotentials are specified through the functions $\mathcal{V}_{\rm loc}(\mathbf{r})$, the local pseudopotential; the augmentation charges $Q^a_{\alpha\beta}(\mathbf{r})$ and their integrated values $q^a_{\alpha\beta}$; the nonlocal matrix elements $D^a_{\alpha\beta}$ and the projector functions $\{\tilde{p}^a_\alpha(\mathbf{r})\}$. Note that we made the transition from a formally all–electron method to a pseudopotential treatment by assuming that the external potential is given as a norm–conserving pseudopotential. By doing so we of course also introduced the approximations coming with pseudopotentials, e.g. the frozen core approximation and the linearization of the exchange and correlation functional. Methods to calculate the parameters and functions needed for an ultrasoft pseudopotential are described in the literature [49, 56, 57].
The only difference in the energy expression to the form with fully nonlocal pseudopotentials is that the total charge density includes the augmentation charges $Q^a_{\alpha\beta}(\mathbf{r})$. However, for the calculation of derivatives the special form of the metric $\mathcal{S}$ introduces many new terms. Starting from the extended energy functional

$$\mathcal{E}_{\rm uspp}(\{\Phi_i\}, \Lambda, \mathbf{R}^N) = E_{\rm KS}(\{\Phi_i\}, \mathbf{R}^N) + \sum_{ij} \Lambda_{ij} \left(\langle \tilde{\Phi}_i \mid \mathcal{S} \mid \tilde{\Phi}_j \rangle - \delta_{ij} \right)\ , \tag{6.54}$$

one arrives at the force expressions

$$\frac{\delta \mathcal{E}_{\rm uspp}}{\delta \langle \Phi_i \mid} = f_i\ \mathcal{H} \mid \Phi_i \rangle + \sum_j \Lambda_{ij}\ \mathcal{S} \mid \tilde{\Phi}_j \rangle \tag{6.55}$$

$$\mathcal{H} = -\frac{1}{2}\nabla^2 + \mathcal{V}_{\rm eff}(\mathbf{r}) + \sum_a \sum_{\alpha\beta} \bar{D}^a_{\alpha\beta} \mid \tilde{p}^a_\alpha \rangle \langle \tilde{p}^a_\beta \mid \tag{6.56}$$

$$\mathcal{V}_{\rm eff}(\mathbf{r}) = \frac{\delta E_{\rm KS}}{\delta n(\mathbf{r})} = \mathcal{V}_{\rm loc}(\mathbf{r}) + \int d\mathbf{r}'\ \frac{n(\mathbf{r}')}{\mid \mathbf{r} - \mathbf{r}' \mid} + V_{\rm xc}(\mathbf{r}')\ , \tag{6.57}$$

where $V_{\rm xc}(\mathbf{r}') = \delta E_{\rm xc}[n]/\delta n(\mathbf{r})$ and all the terms arising from the augmentation part of the electron density have been grouped together with the nonlocal part of the pseudopotential, by defining new coefficients

$$\bar{D}^a_{\alpha\beta} = D^a_{\alpha\beta} + \int d\mathbf{r}\ \mathcal{V}_{\rm eff}(\mathbf{r})\ Q^a_{\alpha\beta}(\mathbf{r})\ . \tag{6.58}$$

The forces on the ions are calculated from the derivative of $\mathcal{E}_{\text{uspp}}$ wrt. the nuclei positions

$$\frac{\partial \mathcal{E}_{\text{uspp}}}{\partial \mathbf{R}_I} = \frac{\partial E_{\text{KS}}}{\partial \mathbf{R}_I} + \sum_{ij} \Lambda_{ij} \langle \tilde{\Phi}_i \mid \frac{\partial \mathcal{S}}{\partial \mathbf{R}_I} \mid \tilde{\Phi}_j \rangle \tag{6.59}$$

$$\frac{\partial \mathcal{S}}{\partial \mathbf{R}_I} = \sum_{\alpha\beta} q^I_{\alpha\beta} \left\{ \left| \frac{\partial \tilde{p}^I_\alpha}{\partial \mathbf{R}_I} \right\rangle \langle \tilde{p}^I_\beta \mid + \mid \tilde{p}^I_\alpha \rangle \left\langle \frac{\partial \tilde{p}^I_\beta}{\partial \mathbf{R}_I} \right| \right\} \tag{6.60}$$

$$\begin{aligned} \frac{\partial E_{\text{KS}}}{\partial \mathbf{R}_I} &= \frac{\partial E_{\text{ion}}}{\partial \mathbf{R}_I} + \int d\mathbf{r}\, \frac{\partial \mathcal{V}_{\text{loc}}(\mathbf{r})}{\partial \mathbf{R}_I} \tilde{n}(\mathbf{r}) \\ &\quad + \int d\mathbf{r}\, \mathcal{V}_{\text{eff}}(\mathbf{r}) \sum_{\alpha\beta} \frac{\partial Q^I_{\alpha\beta}(\mathbf{r})}{\partial \mathbf{R}_I} \left[\sum_i \langle \tilde{\Phi}_i \mid \tilde{p}^I_\alpha \rangle \langle \tilde{p}^I_\beta \mid \tilde{\Phi}_i \rangle \right] \\ &\quad + \sum_{\alpha\beta} \bar{D}^I_{\alpha\beta} \sum_i \left[\langle \tilde{\Phi}_i \left| \frac{\partial \tilde{p}^I_\alpha}{\partial \mathbf{R}_I} \right\rangle \langle \tilde{p}^I_\beta \mid \tilde{\Phi}_i \rangle + \langle \tilde{\Phi}_i \mid \tilde{p}^I_\alpha \rangle \left\langle \frac{\partial \tilde{p}^I_\beta}{\partial \mathbf{R}_I} \right| \tilde{\Phi}_i \rangle \right] \end{aligned} \tag{6.61}$$

6.2.4 PAW Energy Expression

In contrast to the ultrasoft pseudopotential derivation the PAW approach avoids the introduction of a pseudopotential but rather works in the frozen core approximation directly. The sum over states is therfore restricted to valence electrons but the electronic densities always include contributions from the core electrons. In addition, the expansion functions $\chi^a_\alpha(\mathbf{r})$ have to be orthogonal to the core state on the atom (see Refs. ([112, 54, 55]) for details). In the following we will assume a all–electron treatment although this is in practice never done.
The PAW method works directly with the three sets of functions $\{\chi^a_i\}$, $\{\tilde{\chi}^a_i\}$, and $\{\tilde{p}^a_i\}$. These functions together with a local potential $\mathcal{V}_{\text{loc}}$ fully define the PAW energy expression.
Similar to the expectation values the total energy is divided into individual terms

$$E_{\text{KS}} = \tilde{E} + \sum_a E^a - \sum_a \tilde{E}^a \ . \tag{6.62}$$

The smooth part $\tilde{E}$, which is evaluated on regular grids in Fourier or real space, and the one–center contributions E^a and $\tilde{E}^a$, which are evaluated on radial grids in an angular momentum representation. The three contributions to E_{KS} are

$$\tilde{E} = \sum_i f_i \langle \tilde{\Phi}_i \mid -\frac{1}{2}\nabla^2 \mid \tilde{\Phi}_i \rangle + \int d\mathbf{r}\, \mathcal{V}_{\text{loc}}(\mathbf{r})\, \tilde{n}(\mathbf{r}) + E_{\text{H}}[\tilde{n} + \hat{n}] + E_{\text{xc}}[\tilde{n}] \tag{6.63}$$

$$\begin{aligned} E^a &= \sum_i f_i \sum_{\alpha\beta} \langle \tilde{\Phi}_i \mid \tilde{p}^a_\alpha \rangle \langle \chi_\alpha \mid -\frac{1}{2}\nabla^2 \mid \chi_\beta \rangle \langle \tilde{p}^a_\beta \mid \tilde{\Phi}_i \rangle + \\ &\quad E_{\text{H}}[n^a + n^{Za}] + E_{\text{xc}}[n^a] \end{aligned} \tag{6.64}$$

$$E^a = \sum_i f_i \sum_{\alpha\beta} \langle \tilde{\Phi}_i \mid \tilde{p}^a_\alpha \rangle \langle \tilde{\chi}_\alpha \mid -\frac{1}{2}\nabla^2 \mid \tilde{\chi}_\beta \rangle \langle \tilde{p}^a_\beta \mid \tilde{\Phi}_i \rangle + \int d\mathbf{r}\ \mathcal{V}_{\rm loc}(\mathbf{r})\ \tilde{n}^a(\mathbf{r}) + E_{\rm H}[\tilde{n}^a + \hat{n}] + E_{\rm xc}[\tilde{n}^a]\ . \tag{6.65}$$

The potential $\mathcal{V}_{\rm loc}$ is an arbitrary potential localized in the augmentation regions. Its contribution to the total energy vanishes exactly because $\tilde{n}(\mathbf{r}) = \tilde{n}^a(\mathbf{r})$ within the atomic spheres. Since the potential contributes only if the partial wave expansion is not complete, it is used to minimize truncation errors. In addition the point charge density n^{Za} of the nuclei and a compensation charge density $\hat{n}$ was introduced. The compensation charge density has the same multipole moments as the density $n^a + n^{Za} - \tilde{n}^a$ and is localized within the atomic regions. Whereas the division of the kinetic energy and the exchange–correlation energy are straightforward from the formulas derived for the expectation value of local operators, the derivation of the electrostatic terms is rather involved [112, 54, 55] and will be omitted here. In fact, another compensation charge [112] is needed in order to be able to calculate the electrostatic term in the first energy contribution solely within an energy cutoff dictated by $\tilde{\Phi}_i(\mathbf{r})$.

6.2.5 Integrating the CP Equations

We will now derive the velocity Verlet equations for the Car–Parrinello molecular dynamics method using ultrasoft pseudopotentials are the PAW method. The equations of motion are

$$\begin{aligned} \mu|\ddot{\phi}_i\rangle &= |\varphi_i\rangle + \sum_j \Lambda_{ij}\mathcal{S}(\{\mathbf{R}_I\})|\phi_j\rangle \\ M_I\ddot{\mathbf{R}}_I &= \mathbf{F}_I + \sum_{i,j}\Lambda_{ij}\langle\phi_i|\nabla_I\mathcal{S}(\{\mathbf{R}_I\})|\phi_j\rangle \end{aligned} \tag{6.66}$$

where the electronic equation is cast in the abstract Dirac notation, and the forces are defined to be

$$\begin{aligned} \varphi_i(\mathbf{r}) &= -\frac{\delta E}{\delta\phi_i^*(\mathbf{r})} \\ \mathbf{F}_I &= -\frac{\partial E}{\partial \mathbf{R}_I} \end{aligned} \tag{6.67}$$

The electronic force is often written in the form

$$|\varphi_i\rangle = -f_i\mathcal{H}|\phi_i\rangle \tag{6.68}$$

where $\mathcal{H}$ was defined before. In the velocity Verlet scheme, the positions and velocities are treated explicitly. That is, one carries the information $\{\mathbf{R}_I(t), \dot{\mathbf{R}}_I(t)\}$ and

$\{\phi_i(\mathbf{r},t), \dot{\phi}_i(\mathbf{r},t)\}$ at each time step. A prediction of the orbital positions and velocities is then made according to

$$\begin{aligned} |\dot{\bar{\phi}}_i\rangle &= |\dot{\phi}_i(t)\rangle + \frac{\Delta t}{2\mu}|\varphi_i(t)\rangle \\ |\bar{\phi}_i\rangle &= |\phi_i(t)\rangle + \Delta t|\dot{\bar{\phi}}_i\rangle \end{aligned} \tag{6.69}$$

and similarly for the ionic positions and velocities

$$\begin{aligned} \dot{\bar{\mathbf{R}}}_I &= \dot{\mathbf{R}}_I(t) + \frac{\Delta t}{2M_I}\mathbf{F}_I(t) \\ \bar{\mathbf{R}}_I &= \mathbf{R}_I(t) + \Delta t\dot{\bar{\mathbf{R}}}_I \end{aligned} \tag{6.70}$$

The new orbital and ionic positions are then obtained from

$$|\phi_i(t+\Delta t)\rangle = |\bar{\phi}_i\rangle + \frac{\Delta t^2}{2\mu}\sum_j \Lambda_{ij}\mathcal{S}(t)|\phi_j(t)\rangle \tag{6.71}$$

$$\mathbf{R}_I(t+\Delta t) = \bar{\mathbf{R}}_I + \frac{\Delta t^2}{2M_I}\sum_{i,j}\Lambda_{ij}\langle\phi_i(t)|\nabla_I\mathcal{S}(t)|\phi_j(t)\rangle \tag{6.72}$$

The Lagrange multipliers are determined by imposing the constraint condition

$$\langle\phi_i(t+\Delta t)|\mathcal{S}(t+\Delta t)|\phi_j(t+\Delta t)\rangle = \delta_{ij} \ , \tag{6.73}$$

so that the substitution of Eq.(6.71) into Eq.(6.73) gives the matrix equation

$$\mathrm{A} + \mathrm{XB} + \mathrm{B}^\dagger\mathrm{X}^\dagger + \mathrm{XCX}^\dagger = \mathrm{I} \tag{6.74}$$

where $X_{ij} = (\Delta t^2/2\mu)\Lambda_{ij}$ and the matrices are given by

$$\begin{aligned} A_{ij} &= \langle\bar{\phi}_i|\mathcal{S}(t+\Delta t)|\bar{\phi}_j\rangle \\ B_{ij} &= \langle\mathcal{S}(t)\phi_i(t)|\mathcal{S}(t+\Delta t)|\bar{\phi}_j\rangle \\ C_{ij} &= \langle\mathcal{S}(t)\phi_i(t)|\mathcal{S}(t+\Delta t)|\mathcal{S}(t)\phi_j(t)\rangle \end{aligned} \tag{6.75}$$

From the solution of this equation for the Lagrange multipliers, the new orbitals and ionic positions are obtained from Eqs.(6.71) and (6.72). However, we immediately see that this procedure poses a self-consistency problem because the matrices B and C appearing in Eq.(6.74) and therefore the solution for X (or Λ) depend on the new ionic positions $\mathbf{R}_I(t+\Delta t)$ through $\mathcal{S}(t+\Delta t)$, which in turn cannot be determined until the matrix $\Lambda(t+\Delta t)$ is known. Thus, Eq.(6.74) and Eq.(6.72) must be solved self-consistently via iteration. This is accomplished first by guessing a solution to Eq.(6.74) using the solution from two previous time steps:

$$X_{ij}^{(0)}(t+\Delta t) = 2X_{ij}(t) - X_{ij}(t-\Delta t) \tag{6.76}$$

This guess is substituted into Eq.(6.72) to obtain a guess of the new ionic positions which are then used to determine the matrices in Eq.(6.74), and the procedure is iterated until a self-consistent solution is obtained. The matrix equation Eq.(6.74) must itself be solved iteratively, being quadratic in the unknown matrix $\mathbf{X}$. The details of the solution of this equation are given in Ref.[56] and will therefore be omitted here. Despite the rapid convergence of the iterative procedure, the determination of the matrix X in Eq.(6.74) is one of the most time consuming parts of the calculation. Thus, each time X must be determined anew adds considerably to the total time per step.
Once the self-consistent solution has been obtained, the new orbitals and ionic positions are calculated from Eqs.(6.71) and (6.72), and the prediction of the velocities is completed according to

$$\begin{aligned} |\dot{\tilde{\phi}}_i\rangle &= |\dot{\bar{\phi}}_i\rangle + \frac{\Delta t}{2\mu}\sum_j \Lambda_{ij}|\phi_j(t)\rangle + \frac{\Delta t}{2\mu}|\varphi_i(t+\Delta t)\rangle \\ \dot{\tilde{\mathbf{R}}}_I &= \dot{\bar{\mathbf{R}}}_I + \frac{\Delta t}{2M_I}\sum_{i,j}\Lambda_{ij}\langle\phi_i(t)|\nabla_I\mathcal{S}(t)|\phi_j(t)\rangle + \frac{\Delta t}{2M_I}\mathbf{F}_I(t+\Delta t) \end{aligned} \tag{6.77}$$

The final correction step for the velocities consists of writing the new orbital and ionic velocities as

$$\begin{aligned} |\dot{\phi}_i(t+\Delta t)\rangle &= |\dot{\tilde{\phi}}_i\rangle + \sum_j Y_{ij}|\phi_j(t+\Delta t)\rangle \\ \dot{\mathbf{R}}_I(t+\Delta t) &= \dot{\tilde{\mathbf{R}}}_I + \frac{\mu}{M_I}\sum_{i,j}Y_{ij}\langle\phi_i(t+\Delta t)|\nabla_I\mathcal{S}(t+\Delta t)|\phi_j(t+\Delta t)\rangle \end{aligned} \tag{6.78}$$

The Lagrange multipliers Y_{ij} are determined by requiring that the first time derivative of the constraint condition

$$\langle\dot{\phi}_i(t)|\mathcal{S}(t)|\phi_j(t)\rangle + \langle\phi_i(t)|\mathcal{S}(t)|\dot{\phi}_j(t)\rangle + \sum_I\langle\phi_i(t)|\nabla_I\mathcal{S}(t)|\phi_j(t)\rangle\cdot\dot{\mathbf{R}}_I(t) = 0 \tag{6.79}$$

be satisfied at $t+\Delta t$: Eqs.(6.78) are substituted into Eq.(6.79), and the following matrix equation for $\mathbf{Y}$ is obtained:

$$\mathrm{YP} + \mathrm{Y}^\dagger\mathrm{P}^\dagger + \mathrm{Q} + \mathrm{Q}^\dagger + \sum_I \boldsymbol{\Delta}^I(t)\cdot\left[\dot{\tilde{\mathbf{R}}}_I + \frac{\mu}{M_I}\mathrm{Tr}\left(\mathrm{Y}^\dagger\boldsymbol{\Delta}^I(t)\right)\right] = 0 \tag{6.80}$$

where the 3-component vector-matrix $\boldsymbol{\Delta}^I$ is given by

$$\boldsymbol{\Delta}^I_{ij} = \langle\phi_i|\nabla_I\mathcal{S}(\{\mathbf{R}_I\})|\phi_j\rangle \ . \tag{6.81}$$

The matrices P and Q are defined by

$$\begin{aligned} P_{ij} &= \langle\mathcal{S}(t+\Delta t)\phi_i(t+\Delta t)|\mathcal{S}(t+\Delta t)|\phi_j(t+\Delta t)\rangle \\ Q_{ij} &= \langle\dot{\tilde{\phi}}_i(t+\Delta t)|\mathcal{S}(t+\Delta t)|\phi_j(t+\Delta t)\rangle \end{aligned} \tag{6.82}$$

Note that Eq.(6.80), although linear in Y is most easily solved iteratively. However, because the ionic velocities in Eq.(6.78) have been used explicitly in Eq.(6.79), there is no self-consistency problem. Once Eq.(6.80) has been solved, then the new velocities can be determined via Eq.(6.78) straightforwardly. The solution for $\mathrm{Y}(=\mathrm{Y}(t+\Delta t))$ can be used to obtain an initial guess for the matrix X in the next step via

$$\mathrm{X}^{(0)}(t+\Delta t) = \mathrm{X}(t) + \Delta t \mathrm{Y}(t+\Delta t) \ . \tag{6.83}$$

In the velocity Verlet algorithms, the iteration of the position step requires several applications of the matrix $\mathbf{\Delta}^I$. This matrix can either be stored or recalculated as needed. However, due to the size of this matrix ($3 \times N_A \times N_s^2$, where N_A is the number of atoms and N_s is the number of electronic states in the system), storing it for large systems is often not possible and recalculating it is expensive. To circumvent these problems the constraint nonorthogonal orbital method has been devised [22].

6.3 Metals; Free Energy Functional

In the free energy approach [58], the excited states are populated according to the Fermi–Dirac (finite–temperature equilibrium) distribution which is based on the assumption that the electrons "equilibrate" more rapidly than the timescale of the nuclear motion. This means that the set of electronic states evolves at a given temperature "isothermally" (rather than adiabatically) under the inclusion of *incoherent* electronic transitions at the nuclei move. Thus, instead of computing the force acting on the nuclei from the electronic ground–state energy it is obtained from the electronic *free* energy as defined in the canonical ensemble. By allowing such electronic transitions to occur the free energy approach transcends the usual Born–Oppenheimer approximation. However, the approximation of an instantaneous equilibration of the electronic subsystem implies that the electronic structure at a given nuclear configuration $\{\mathbf{R}_I\}$ is completely independent from previous configurations along a molecular dynamics trajectory. Due to this assumption the notion "free energy Born–Oppenheimer approximation" was coined in Ref. [59] in a similar context. Certain non–equilibrium situations can also be modeled within the free energy approach by starting off with an initial orbital occupation pattern that does not correspond to any temperature in its thermodynamic meaning, see e.g. Refs. [60] for such applications.
The free energy functional as defined in Refs. [58] is introduced most elegantly by starting the discussion for the special case of *non*–interacting Fermions

$$H_{\mathrm{s}} = -\frac{1}{2}\nabla^2 - \sum_I \frac{Z_I}{|\mathbf{R}_I - \mathbf{r}|} \tag{6.84}$$

in a *fixed* external potential due to a collection of nuclei at positions $\{\mathbf{R}_I\}$. The associated grand partition function and its thermodynamic potential ("grand free energy") are given

by

$$\Xi_{\rm s}(\mu VT) = \det{}^2\left(1+\exp\left[-\beta\left(H_{\rm s}-\mu\right)\right]\right) \tag{6.85}$$

$$\Omega_{\rm s}(\mu VT) = -k_{\rm B}T\ln\Xi_{\rm s}(\mu VT)\ , \tag{6.86}$$

where μ is the chemical potential acting on the electrons and the square of the determinant stems from considering the spin–unpolarized special case only. This reduces to the well–known grand potential expression

$$\begin{aligned}\Omega_{\rm s}(\mu VT) &= -2k_{\rm B}T\ln\det\left(1+\exp\left[-\beta\left(H_{\rm s}-\mu\right)\right]\right)\\ &= -2k_{\rm B}T\sum_i\ln\left(1+\exp\left[-\beta\left(\epsilon_{\rm s}^{(i)}-\mu\right)\right]\right)\end{aligned} \tag{6.87}$$

for non–interacting spin–1/2 Fermions where $\{\epsilon_{\rm s}^{(i)}\}$ are the eigenvalues of a one–particle Hamiltonian such as Eq. (6.84); here the standard identity $\ln\det\mathbf{M}=\mathrm{Tr}\ln\mathbf{M}$ was invoked for positive definite $\mathbf{M}$.

According to thermodynamics the Helmholtz free energy $\mathcal{F}(NVT)$ associated to Eq. (6.86) can be obtained from a Legendre transformation of the grand free energy $\Omega(\mu VT)$

$$\mathcal{F}_{\rm s}(NVT)=\Omega_{\rm s}(\mu VT)+\mu N+\sum_{I<J}\frac{Z_IZ_J}{|\mathbf{R}_I-\mathbf{R}_J|} \tag{6.88}$$

by fixing the average number of electrons N and determining μ from the conventional thermodynamic condition

$$N=-\left(\frac{\partial\Omega}{\partial\mu}\right)_{VT}\ . \tag{6.89}$$

In addition, the internuclear Coulomb interactions between the classical nuclei were included at this stage in Eq. (6.88). Thus, derivatives of the free energy Eq. (6.88) with respect to ionic positions $-\nabla_I\mathcal{F}_{\rm s}$ define forces on the nuclei that could be used in a (hypothetical) molecular dynamics scheme using non–interacting electrons.
The interactions between the electrons can be "switched on" by resorting to Kohn–Sham density functional theory and the concept of a non–interacting reference system. Thus, instead of using the simple one–particle Hamiltonian Eq. (6.84) the effective Kohn–Sham Hamiltonian Eq. (2.9) has to be utilized. As a result, the grand free energy Eq. (6.85) can be written as

$$\Omega^{\rm KS}(\mu VT) = -2k_{\rm B}T\ln\left[\det\left(1+\exp\left[-\beta\left(H^{\rm KS}-\mu\right)\right]\right)\right] \tag{6.90}$$

$$H^{\rm KS} = -\frac{1}{2}\nabla^2-\sum_I\frac{Z_I}{|\mathbf{R}_I-\mathbf{r}|}+V_{\rm H}(\mathbf{r})+\frac{\delta\Omega_{\rm xc}[n]}{\delta n(\mathbf{r})} \tag{6.91}$$

$$H^{\rm KS}\phi_i = \epsilon_i\phi_i \tag{6.92}$$

where $\Omega_{\rm xc}$ is the exchange–correlation functional at finite temperature. By virtue of Eq. (6.87) one can immediately see that $\Omega^{\rm KS}$ is nothing else than the "Fermi–Dirac weighted sum" of the bare Kohn–Sham eigenvalues $\{\epsilon_i\}$. Whence, this term is the extension to finite temperatures of the "band–structure energy" contribution to the total electronic energy.
In order to obtain the correct total electronic free energy of the interacting electrons the corresponding extra terms (properly generalized to finite temperatures) have to be included in $\Omega^{\rm KS}$. This finally allows one to write down the generalization of the Helmholtz free energy of the interacting many–electron case

$$\begin{aligned} \mathcal{F}^{\rm KS}(NVT) &= \Omega^{\rm KS}(\mu VT) + \mu \int d\mathbf{r}\ n(\mathbf{r}) + \sum_{I<J} \frac{Z_I Z_J}{|\mathbf{R}_I - \mathbf{R}_J|} \\ &\quad -\frac{1}{2}\int d\mathbf{r}\ V_{\rm H}(\mathbf{r})\, n(\mathbf{r}) + \Omega_{\rm xc} - \int d\mathbf{r}\ \frac{\delta\Omega_{\rm xc}[n]}{\delta n(\mathbf{r})}\, n(\mathbf{r}) \end{aligned} \tag{6.93}$$

in the framework of a Kohn–Sham–like formulation. The corresponding one–particle density at the Γ–point is given by

$$n(\mathbf{r}) = \sum_i f_i(\beta)\ |\phi_i(\mathbf{r})|^2 \tag{6.94}$$

$$f_i(\beta) = \left(1 + \exp\left[\beta\left(\epsilon_i - \mu\right)\right]\right)^{-1}\ , \tag{6.95}$$

where the fractional occupation numbers $\{f_i\}$ are obtained from the Fermi–Dirac distribution at temperature T in terms of the Kohn–Sham eigenvalues $\{\epsilon_i\}$. Finally, *ab initio* forces can be obtained as usual from the nuclear gradient of $\mathcal{F}^{\rm KS}$, which makes molecular dynamics possible.

By construction, the total free energy Eq. (6.93) reduces to that of the non–interacting toy model Eq. (6.88) once the electron–electron interaction is switched off. Another useful limit is the ground–state limit $\beta \to \infty$ where the free energy $\mathcal{F}^{\rm KS}(NVT)$ yields the standard Kohn–Sham total energy expression $E^{\rm KS}$ after invoking the appropriate limit $\Omega_{\rm xc} \to E_{\rm xc}$ as $T \to 0$. Most importantly, stability analysis [58] of Eq. (6.93) shows that this functional shares the same stationary point as the exact finite–temperature functional due to Mermin [62], see e.g. the textbooks [23, 24] for introductions to density functional formalisms at finite temperatures. This implies that the self–consistent density, which defines the stationary point of $\mathcal{F}^{\rm KS}$, is identical to the exact one. This analysis reveals furthermore that, unfortunately, this stationary point is not an extremum but a saddle point so that no variational principle and, numerically speaking, no direct minimization algorithms can be applied. For the same reason a Car–Parrinello fictitious dynamics approach to molecular dynamics is not a straightforward option, whereas Born–Oppenheimer dynamics based on diagonalization can be used directly.

The band–structure energy term can be evaluated by diagonalizing the Kohn–Sham Hamiltonian after a suitable "preconditioning" [58]. Specifically, a second–order Trotter

approximation is used

$$\begin{aligned}
\mathrm{Tr}\ \exp\left[-\beta H^{\mathrm{KS}}\right] &= \sum_i \exp\left[-\beta\epsilon_i\right] = \sum_i \rho_{ii}(\beta) && (6.96)\\
&= \mathrm{Tr}\left(\left\{\exp\left[-\frac{\Delta\tau}{2}\left(-\frac{1}{2}\nabla^2\right)\right]\exp\left[-\Delta\tau V^{\mathrm{KS}}[n]\right]\right.\right.\\
&\quad \left.\left.\exp\left[-\frac{\Delta\tau}{2}\left(-\frac{1}{2}\nabla^2\right)\right]\right\} + \mathcal{O}\left(\Delta\tau^3\right)\right)^P && (6.97)\\
&\approx \sum_i \left\{\rho_{ii}(\Delta\tau)\right\}^P = \sum_i \left\{\exp\left[-\Delta\tau\epsilon_i\right]\right\}^P && (6.98)
\end{aligned}$$

in order to compute first the diagonal elements $\rho_{ii}(\Delta\tau)$ of the "high–temperature" Boltzmann operator $\rho(\Delta\tau)$; here $\Delta\tau = \beta/P$ and P is the Trotter "time slice". To this end, the kinetic and potential energies can be conveniently evaluated in reciprocal and real space, respectively, by using the split–operator / FFT technique [61]. The Kohn–Sham eigenvalues ϵ_i are finally obtained from the density matrix via $\epsilon_i = -(1/\Delta\tau)\ln\rho_{ii}(\Delta\tau)$. They are used in order to compute the occupation numbers $\{f_i\}$, the density $n(\mathbf{r})$, the band–structure energy Ω^{KS}, and thus the free energy Eq. (6.93).

In practice a diagonalization / density–mixing scheme is employed in order to compute the self–consistent density $n(\mathbf{r})$. A suitably constructed trial input density n_{in} is used in order to compute the potential $V^{\mathrm{KS}}[n_{\mathrm{in}}]$. Then the lowest–order approximant to the Boltzmann operator Eq. (6.98) is diagonalized using an iterative Lanczos–type method. This yields an output density n_{out} and the corresponding free energy $\mathcal{F}^{\mathrm{KS}}[n_{\mathrm{out}}]$. Finally, the densities are mixed and the former steps are iterated until a stationary solution n_{scf} of $\mathcal{F}^{\mathrm{KS}}[n_{\mathrm{scf}}]$ is achieved. Of course the most time–consuming part of the calculation is in the iterative diagonalization. In principle this is not required, and it should be possible to compute the output density directly from the Fermi–Dirac density matrix even in a linear scaling scheme [63], thus circumventing the explicit calculation of the Kohn–Sham eigenstates.

As a method, molecular dynamics with the free energy functional is most appropriate to use when the excitation gap is either small, or in cases where the gap might close during a chemical transformation. In the latter case no instabilities are encountered with this approach, which is not true for ground–state *ab initio* molecular dynamics methods. The price to pay is the quite demanding iterative computation of well–converged forces. Besides allowing such applications with physically relevant excitations this method can also be straightforwardly combined with **k**–point sampling and applied to metals at "zero" temperature. In this case, the electronic "temperature" is only used as a smearing parameter of the Fermi edge by introducing fractional occupation numbers, which is known to improve greatly the convergence of these ground–state electronic structure calculations [63, 64, 65, 66, 67, 68, 69].

Finite–temperature expressions for the exchange–correlation functional Ω_{xc} are available in the literature. However, for most temperatures of interest the corrections to the ground–

state expression are small and it seems justified to use one of the various well–established parameterizations of the exchange–correlation energy $E_{\rm xc}$ at zero temperature.

6.4 Charged Systems

The possibility to use fast Fourier transforms to calculate the electrostatic energy is one of the reasons for the high performance of plane wave calculations. However, plane wave based calculations imply periodic boundary conditions. This is appropriate for crystal calculations but very unnatural for molecule or slab calculations. For neutral systems this problem is circumvented by use of the supercell method. Namely, the molecule is periodically repeated but the distance between each molecule and its periodic images is so large that their interaction is negligible. This procedure is somewhat wasteful but can lead to satisfactory results.
Handling charged molecular systems is, however, considerably more difficult, due to the long range Coulomb forces. A charged periodic system has infinite energy and the interaction between images cannot really be completely eliminated. In order to circumvent this problem several solutions have been proposed. The simplest fix-up is to add to the system a neutralizing background charge. This is achieved trivially as the $\mathbf{G} = \mathbf{0}$ term in the electrostatic energy is already eliminated. This leads to finite energies but does not eliminate the interaction between the images and makes the calculation of absolute energies difficult. Other solutions involve performing a set of different calculations on the system such that extrapolation to the limit of infinitely separated images is possible. This procedure is lengthy and one cannot use it easily in molecular dynamics applications. It has been shown, that it is possible to estimate the correction to the total energy for the removal of the image charges [70]. Still it seems not easy to incorporate this scheme into the frameworks of molecular dynamics. Another method [71, 72, 73] works with the separation of the long and short range parts of the Coulomb forces. In this method the low–order multipole moments of the charge distribution are separated out and handled analytically. This method was used in the context of coupling *ab initio* and classical molecular dynamics [74].
The long-range forces in the electrostatic energy are contained in the first term. This term can be written

$$\frac{1}{2}\iint d\mathbf{r}\, d\mathbf{r}'\, \frac{n_{\rm tot}(\mathbf{r}) n_{\rm tot}(\mathbf{r}')}{|\mathbf{r}-\mathbf{r}'|} = \frac{1}{2}\int d\mathbf{r}\, V_{\rm H}(\mathbf{r}) n_{\rm tot}(\mathbf{r}) \ , \tag{6.99}$$

where the electrostatic potential $V_{\rm H}(\mathbf{r})$ is the solution of Poisson's equation. We will discuss two approaches to solve Poisson's equation subject to the boundary conditions $V_{\rm H}(\mathbf{r}) \to 0$ for $\mathbf{r} \to \infty$. Both of them rely on fast Fourier transforms, thus keeping the same framework as for the periodic case.
The first method is due to Hockney [75] and was first applied to density functional plane wave calculations in Ref. [76]. In the following outline, for the sake of simplicity, a one-

Figure 6.1: Schematic view of the Hockney method to decouple images in the electrostatic energy. The first line shows the artificially replicated system consisting of the original computational cell and an empty duplicated cell. The Green's function of this new periodic system is shown in the lower part of the figure.

dimensional case is presented. The charge density is assumed to be non-zero only within an interval L and sampled on N equidistant points. These points are denoted by x_p. The potential can then be written

$$V_{\mathrm{H}}(x_p) = \frac{L}{N} \sum_{p'=-\infty}^{\infty} G(x_p - x_{p'}) n(x_{p'}) \tag{6.100}$$

$$= \frac{L}{N} \sum_{p'=0}^{N} G(x_p - x_{p'}) n(x_{p'}) \tag{6.101}$$

for $p = 0, 1, 2, \ldots N$, where $G(x_p - x_{p'})$ is the corresponding Green's function. In Hockney's algorithm this equation is replaced by the cyclic convolution

$$\tilde{V}_{\mathrm{H}}(x_p) = \frac{L}{N} \sum_{p'=0}^{2N+1} \tilde{G}(x_p - x_{p'}) \tilde{n}(x_{p'}) \tag{6.102}$$

where $p = 0, 1, 2, \ldots 2N + 1$, and

$$\tilde{n}(x_p) = \begin{cases} n(x_p) & 0 \leq p \leq N \\ 0 & N \leq p \leq 2N + 1 \end{cases} \tag{6.103}$$

$$\tilde{G}(x_p) = G(x_p) \qquad -(N+1) \leq p \leq N \tag{6.104}$$

$$\tilde{n}(x_p) = \tilde{n}(x_p + L) \tag{6.105}$$

$$\tilde{G}(x_p) = \tilde{G}(x_p + L) \tag{6.106}$$

The solution $\tilde{V}_{\mathrm{H}}(x_p)$ can be obtained by a series of fast Fourier transforms and has the desired property

$$\tilde{V}_{\mathrm{H}}(x_p) = V_{\mathrm{H}}(x_p) \quad \text{for } 0 \leq p \leq N \ . \tag{6.107}$$

To remove the singularity of the Green's function at $x = 0$, $G(x)$ is modified for small x and the error is corrected by using the identity

$$G(x) = \frac{1}{x} \mathrm{erf}\left[\frac{x}{r_{\mathrm{c}}}\right] + \frac{1}{x} \mathrm{erfc}\left[\frac{x}{r_{\mathrm{c}}}\right] \ , \tag{6.108}$$

where r_{c} is chosen such, that the short-ranged part can be accurately described by a plane wave expansion with the density cutoff. In an optimized implementation Hockney's method requires the double amount of memory and two additional fast Fourier transforms

Table 6.1: Fourier space formulas for the Hartree energy, see text for definitions.

Dim.	periodic	$(G^2/4\pi)V_{\rm H}(\mathbf{G})$	$V_{\rm H}(\mathbf{0})$
0	–	$(1-\cos[R\,G])\,n(\mathbf{G})$	$2\pi R^2 n(0)$
1	z	$(1+R\,(G_{\rm xy}J_1(RG_{\rm xy})\,K_0(Rg_{\rm z})$	
		$-g_{\rm z}J_0(RG_{\rm xy})\,K_1(Rg_{\rm z})))\,n(\mathbf{G})$	0
2	x, y	$(1-(-1)^{g_{\rm z}}\exp[-GZ/2])\,n(\mathbf{G})$	0
3	x, y, z	n($\mathbf{G}$)	0

on the box of double size. Hockney's method can be generalized to systems with periodicity in one (wires) and two (slabs) dimensions. It was pointed out [77] that Hockney's method gives the exact solution to Poisson's equation for isolated systems if the boundary condition (zero density at the edges of the box) are fulfilled.
A different, fully reciprocal space based method, that can be seen as an approximation to Hockney's method, was recently proposed [78]. The final expression for the Hartree energy is also based on the splitting of the Green's function in Eq. (6.108)

$$E_{\rm ES} = 2\pi\,\Omega \sum_{\mathbf{G}} V_{\rm H}^{\rm MT}(\mathbf{G}) n^{\star}_{\rm tot}(\mathbf{G}) + E_{\rm ovrl} - E_{\rm self}\ . \tag{6.109}$$

The potential function is calculated from two parts,

$$V_{\rm H}^{\rm MT}(\mathbf{G}) = \bar{V}_{\rm H}(\mathbf{G}) + \tilde{V}_{\rm H}(\mathbf{G})\ , \tag{6.110}$$

where $\tilde{V}_{\rm H}(\mathbf{G})$ is the analytic part, calculated from a Fourier transform of erfc

$$\tilde{V}_{\rm H}(\mathbf{G}) = \frac{4\pi}{G^2}\left(1-\exp\left[-\frac{G^2 r_{\rm c}^2}{4}\right]\right) n(\mathbf{G}) \tag{6.111}$$

and $\bar{V}_{\rm H}(\mathbf{G})$ is calculated from a discrete Fourier transform of the Green's function on an appropriate grid. The calculation of the Green's function can be done at the beginning of the calculation and has not to be repeated again. It is reported [78] that a cutoff of ten to twenty percent higher than the one employed for the charge density gives converged results. The same technique can also be applied for systems that are periodic in one and two dimensions.
If the boundary conditions are appropriately chosen, the discrete Fourier transforms for the calculation of $\bar{V}_{\rm H}(\mathbf{G})$ can be performed analytically [79]. This is possible for the limiting case where $r_{\rm c} = 0$ and the boundary conditions are on a sphere of radius R for the cluster. For a one-dimensional system we choose a torus of radius R and for the two-dimensional system a slab of thickness Z. The electrostatic potential for these systems are listed in Table 6.1, where $G_{\rm xy} = \left[g_{\rm x}^2 + g_{\rm y}^2\right]^{1/2}$ and J_n and K_n are the Bessel functions of the first and second kind of integer order n.

Hockney's method requires a computational box such that the charge density is negligible at the edges. This is equivalent to the supercell approach [80]. Practical experience tells that a minimum distance of about 3 Å of all atoms to the edges of the box is sufficient for most systems. The Green's function is then applied to the charge density in a box double this size. The Green's function has to be calculated only once at the beginning of the calculation. The other methods presented in this chapter require a computational box of double the size of the Hockney method as they are applying the artificially periodic Green's function within the computational box. This can only be equivalent to the exact Hockney method if the box is enlarged to double the size. In plane wave calculations computational costs grow linearly with the volume of the box. Therefore Hockney's method will prevail over the others in accuracy, speed, and memory requirements in the limit of large systems. The direct Fourier space methods have advantages through their easy implementation and for small systems, if not full accuracy is required, i.e. if they are used with smaller computational boxes. In addition, they can be of great use in calculations with classical potentials.

Lecture 7

Properties from CPMD

7.1 Position Operator in Periodic Systems

The problem of the position operator in periodic systems has been analyzed by Resta and others [81]. The position operator within the Schrödinger representation acts multiplying the wave function by the space coordinate. This applies only to the bound eigenstates of a finite system which belong to the class of square–integrable wave functions. However, if one considers a large system within periodic boundary conditions (PBC) the position operator becomes meaningless. Let's take the Hilbert space of the single–particle wave functions defined by the condition $\Psi(x + L) = \Psi(x)$ (for the sake of simplicity a one–dimensional system is assumed), where L is the imposed periodicity, chosen to be large with respect to atomic dimensions. An operator maps any vector of the given space into another vector belonging to the same space: the multiplicative position operator x is not a legitimate operator when PBC are adopted for the state vectors, since $x\Psi(x)$ is not a periodic function whenever $\Psi(x)$ is such. Since the position operator is ill defined, so is its expectation value, whose observable effects in condensed matter are related to macroscopic polarization. For the crystalline case, the problem of the dielectric polarization has been solved [82]: polarization is a manifestation of the Berry phase [83], i.e. it is an observable which cannot be cast as the expectation value of any operator, being instead a gauge–invariant phase of the wave function. The most relevant features are that the expectation value is defined modulo L, and the operator is no longer one body; it acts as a genuine many–body operator on the periodic wave function of N electrons.
The position expectation value of a wavefunction using PBC is

$$\langle X \rangle = \frac{L}{2\pi} \mathrm{Im} \ln \langle \Psi \mid e^{i\frac{2\pi}{L}\hat{X}} \mid \Psi \rangle \ . \tag{7.1}$$

The expectation value $\langle X \rangle$ is thus defined only modulo L. The right–hand side of Eq.(7.1) is not simply the expectation value of an operator: the given form, as the imaginary part of a logarithm, is indeed essential. Furthermore, its main ingredient is the expectation

value of the multiplicative operator $e^{i\frac{2\pi}{L}\hat{X}}$, a genuine many–body operator. In general, one defines an operator to be one body whenever it is the sum of N identical operators, acting on each electronic coordinate separately.

7.2 Dipole Moments and IR Spectra

Suppose we have a one dimensional system of lattice constant a, where we impose PBC over M cells: there are M equally spaced Bloch vectors in the reciprocal cell $[0, 2\pi/a)$

$$q_s = \frac{2\pi}{Ma}s, \qquad s = 0, 1, \ldots, M-1 \ . \tag{7.2}$$

The size of the periodically repeated system is $L = Ma$. The orbitals can be chosen to have the Bloch form

$$\Phi_{q_s,m}(x+\tau) = e^{iq_s\tau}\Phi_{q_s,m}(x) \ , \tag{7.3}$$

where $\tau = la$ is a lattice translation, and m is a band index. There are N/M occupied bands in the Slater determinant wave function, which we write as

$$\mid \Psi\rangle = \mathrm{A} \prod_{m=1}^{N/M} \prod_{s=0}^{M-1} \Phi_{q_s,m} \ , \tag{7.4}$$

where A is the antisymmetrizer. A new set of Bloch orbitals can be defined

$$\tilde{\Phi}_{q_s,m}(x) = e^{-i\frac{2\pi}{L}x}\Phi_{q_s,m}(x) \ . \tag{7.5}$$

The position expectation value can now be written as

$$\langle X\rangle = -\frac{L}{2\pi}\ \mathrm{Im}\ \ln\langle\Psi \mid \tilde{\Psi}\rangle \ , \tag{7.6}$$

where $\mid\tilde{\Psi}\rangle$ is the Slater determinant of the $\tilde{\Phi}$'s. The overlap among two determinants is equal to the determinant of the overlap matrix of the orbitals:

$$\langle X\rangle = -\frac{L}{2\pi}\ \mathrm{Im}\ \ln\ \mathrm{det}S \ , \tag{7.7}$$

where

$$S_{sm,s'm'} = \int_0^L dx\ \Phi^{\star}_{q_s,m}(x)e^{-i\frac{2\pi}{L}x}\Phi_{q_{s'},m'}(x) \ . \tag{7.8}$$

Because of the orthogonality of the Bloch functions, the overlap matrix elements vanish except for $q_{s'} = q_s + 2\pi/L$, that is $s' = s+1$. The $N \times N$ determinant can then be factorized into M small determinants

$$\mathrm{det}S = \prod_{s=0}^{M-1} \mathrm{det}S(q_s, q_{s+1}) \ , \tag{7.9}$$

where for the small overlap matrix the notation

$$S_{m,m'}(q_s, q_{s+1}) = \int_0^L dx\ \Phi^{\star}_{q_s,m}(x) e^{-i\frac{2\pi}{L}x} \Phi_{q_{s+1},m'}(x)\ , \tag{7.10}$$

and $\Phi_{q_M,m}(x) = \Phi_{q_0,m}(x)$ is implicitly understood. Finally we get for the electric polarization

$$P_{\rm el} = -\frac{e}{2\pi} \lim_{L\to\infty} {\rm Im}\ \ln\ \prod_{s=0}^{M-1} {\rm det} S(q_s, q_{s+1})\ . \tag{7.11}$$

The total dipole of a system is calculated as the sum of nuclear and electronic contributions

$$P_{\rm tot} = P_{\rm nuc} + P_{\rm el}\ . \tag{7.12}$$

Only the total dipole will be independent of the gauge and a proper choice of reference point will be discussed later. First we will give the formulas for the electronic contribution in three dimension and for the case where only the Γ point of the supercell Brillouin zone is used

$$P^{\alpha}_{\rm el} = -\frac{2e}{2\pi \mid \mathbf{G}_{\alpha} \mid} {\rm Im}\ \ln\ {\rm det} S^{\alpha}\ . \tag{7.13}$$

The additional factor of 2 comes from the assumed spin degeneracy. The matrix S is defined as

$$S^{\alpha}_{mn} = \langle \Phi_m \mid e^{-i\mathbf{G}_{\alpha}x} \mid \Phi_n \rangle\ . \tag{7.14}$$

The index $\alpha = 1, 2, 3$ labels the reciprocal–lattice basis vectors $\{\mathbf{G}_{\alpha}\}$, $P^{\alpha}_{\rm el}$ is the projection of the electronic dipole moment along the direction defined by $\mathbf{G}_{\alpha}$, and Φ_m are the Γ point Kohn–Sham orbitals.
The IR absorption coefficient $\alpha(\omega)$ can be calculated from the formula [84]

$$\alpha(\omega) = \frac{4\pi\ \omega\ \tanh(\beta\hbar\omega/2)}{3\hbar n(\omega) c V} \int_{-\infty}^{\infty} dt\ e^{-i\omega t} \langle P(t) \cdot P(0) \rangle\ , \tag{7.15}$$

where V is the volume of the supercell, T the temperature, $\beta = 1/k_{\rm B}T$, $n(\omega)$ is the refractive index, c is the speed of light in vacuum. The angular brackets indicate a statistical average. The correlation function $\langle P(t) \cdot P(0) \rangle$ is calculated classically and quantum effect corrections are taken into account through the factor $\tanh(\beta\hbar\omega/2)$. More sophisticated treatments of quantum effects are also available. They consist of replacing the classical correlation function with a more involved procedure [85].
As mentioned above only the total dipole moment is independent of the reference point. This can cause some problems during a molecular dynamics simulation. The electronic contribution can only be calculated modulo the supercell size and a unfortunate choice of reference might lead to frequent changes of the dipole moment by amounts of the cell size. Therefore it is most convenient to use a dynamic reference calculated from the nuclear

positions and charges. If the reference point is chosen to be the center of charge of the nuclei, the nuclear contribution to the dipole will always be zero

$$\mathbf{Q} = \frac{1}{\sum_I Z_I} \sum_I Z_I \mathbf{R}_I \ . \tag{7.16}$$

Z_I are the nuclear charges and $\mathbf{R}_I$ the nuclear positions within the supercell. The electronic contribution is then

$$\begin{aligned} P_{\rm el} &= -\frac{2e}{2\pi}\mathbf{hd} && (7.17)\\ \mathbf{d} &= \tan^{-1}\left[{\rm Im}D_\alpha/{\rm Re}D_\alpha\right] && (7.18)\\ D_\alpha &= \exp\left[i(\mathbf{h}^T)^{-1}\mathbf{Q}\right] \det\ S^\alpha \ , && (7.19) \end{aligned}$$

where $\mathbf{h}$ is the matrix defining the supercell.

7.3 Localized Orbitals, Wannier Functions

The representation of the electronic ground state in terms of localized Wannier orbitals [86] provides a powerful tool in the study of periodic solids. Recent advances in the formulation of a theory of electronic polarization [81] and the development of linear-scaling methods [63] have rejuvenated the use of Wannier functions as an analysis tool. Namely, Wannier functions afford an insightful picture to the nature of chemical bonding and aid in the understanding of classical chemical concepts (*e.g.* nonbonding electron pairs or valency) in terms of quantum mechanics.
Wannier functions (WF) are defined in terms of a unitary transformation performed on the occupied Bloch orbitals (BO) [86]. One major problem in a practical calculation is their non-uniqueness. This is a result of the indeterminacy of the BO's, which are, in the case of a single band, only determined up to a phase factor, in the multi-band case, up to an arbitrary unitary transformation among all occupied orbitals at every point in the Brillouin zone. As proposed recently by Marzari and Vanderbilt [87], one can resolve this non-uniqueness by requiring that the total spread of the localized function be minimal. This criterion is in close analogy with the Boys-Foster method [88] for finite systems, here one uses the spread defined through the conventional position operator. The new technique has been successfully applied to crystal systems and to small molecules within a general $\mathbf{k}$-point scheme[87, 89]. An extension to disordered systems within the $\mathbf{\Gamma}$-point approximation was recently performed[90]. This is of particular interest when one would like a localized orbital picture within the framework of Car-Parrinello molecular dynamics (CPMD). Here we examine the problem focusing on the $\mathbf{\Gamma}$-point approximation only. Upon minimization of the spread functional the appropriate unitary transformation to the localized orbitals can be calculated. With explicit knowledge of the spread functional

we can derive the complete expressions required to implement the iterative minimization procedure.

We begin by reviewing the work of Resta [93]. In his treatment, the fundamental object for studying localization of an electronic state within Born-Von Karman boundary conditions is the dimensionless complex number,

$$z = \int_L dx \ \exp(i2\pi x/L) \ |\psi(x)|^2 \ . \tag{7.20}$$

Here, L is the linear dimension, and $\psi(x)$ denotes the wavefunction. By considering the definition of the spread of the wavefunction to be $\Omega = \langle x^2 \rangle - \langle x \rangle^2$, where $\langle \cdots \rangle$ denotes an expectation value, Resta has shown that to $O(1/L^2)$ the functional for the spread in one-dimension to be,

$$\Omega = \frac{1}{(2\pi)^2} \ln |z|^2. \tag{7.21}$$

One goal of this study is to generalize Eq. (7.20) to three-dimensions and obtain the appropriate generalization of Eq. (7.21). Thus, we choose to study the following dimensionless complex number within Born-Von Karman boundary conditions,

$$z_I = \int_V d\mathbf{r} \ \exp(i\mathbf{G}_I \cdot \ \mathbf{r}) \ |\psi(\mathbf{r})|^2 \ . \tag{7.22}$$

Here, I labels a general reciprocal lattice vector, $\mathbf{G}_I = l_I\mathbf{b}_1 + m_I\mathbf{b}_2 + n_I\mathbf{b}_3$, where $\mathbf{b}_\alpha$ are the primitive reciprocal lattice vectors, the integers l, m, and n are the Miller indices, V is the volume of the supercell, and $\psi(\mathbf{r})$ denotes the wavefunction. We must find an appropriate function of the z_I's that gives the three dimensional spread in the case of an arbitrary simulation cell. We proceed by noting that in a molecular dynamics simulation the cell parameters (primitive lattice vectors) to describe systems of general symmetry are given by $\mathbf{a}_1$, $\mathbf{a}_2$ and $\mathbf{a}_3$. It is convenient to form a matrix of these cell parameters, $\overleftrightarrow{\mathbf{h}} = (\mathbf{a}_1, \mathbf{a}_2, \mathbf{a}_3)$ where the volume V of the simulation cell is given by the determinant of $\overleftrightarrow{\mathbf{h}}$. It is also very useful to define scaled coordinates, $\mathbf{s} = \overleftrightarrow{\mathbf{h}}^{-1} \cdot \mathbf{r}$ that lie in the unit cube. In molecular dynamics simulations, this allows one to perform periodic boundary conditions for systems with general symmetry by first transforming to the unit cube, performing cubic periodic boundary conditions, and transforming back to the general cell with the action of $\overleftrightarrow{\mathbf{h}}$ One can also compute the reciprocal space vectors for systems of general symmetry with knowledge of the matrix of cell parameters. Thus, the I-th reciprocal lattice vector,

$$\mathbf{G}_I = 2\pi \left(\overleftrightarrow{\mathbf{h}}^{-1}\right)^{\mathrm{T}} \cdot \ \hat{\mathbf{g}}_I \ . \tag{7.23}$$

Here, the superscript T denotes transposition, and $\hat{\mathbf{g}}_I = (l_I, m_I, n_I)$ is the I-th Miller index. We then substitute this expression into Eq. (7.22) and use the definition of $\mathbf{r}$ to obtain,

$$z_I = \det \overleftrightarrow{\mathbf{h}} \int_0^1 d\mathbf{s} \ \exp\left(i2\pi\hat{\mathbf{g}}_I^{\mathrm{T}} \cdot \ \mathbf{s}\right) \ |\psi(\overleftrightarrow{\mathbf{h}} \cdot \mathbf{s})|^2 \ . \tag{7.24}$$

Note that the exponential in Eq. (7.24) is independent of any coordinate system. Following Resta [93] we can write the electron density in terms of a superposition of localized density and its periodic images, $|\psi(\overleftrightarrow{\mathbf{h}} \cdot \mathbf{s})|^2 = \sum_{\hat{\mathbf{m}}=-\infty}^{\infty} n_{\rm loc}(\overleftrightarrow{\mathbf{h}} \cdot \mathbf{s} - \overleftrightarrow{\mathbf{h}} \cdot \mathbf{s}_0 - \overleftrightarrow{\mathbf{h}} \cdot \hat{\mathbf{m}})$. Here $\hat{\mathbf{m}}$ is a vector of integers and $\overleftrightarrow{\mathbf{h}} \cdot \mathbf{s}_0$ is the center of the distribution such that $\int_{-\infty}^{\infty} d\mathbf{s}\ \overleftrightarrow{\mathbf{h}} \cdot \mathbf{s}\ n_{\rm loc}(\overleftrightarrow{\mathbf{h}} \cdot \mathbf{s}) = 0$. Using the Poisson summation formula [94], we rewrite Eq. (7.24),

$$z_I = \exp\left(i2\pi \hat{\mathbf{g}}_I^{\rm T} \cdot\ \mathbf{s}_0\right) \hat{n}_{\rm loc}(-2\pi \hat{\mathbf{g}}_I^{\rm T} \cdot\ \overleftrightarrow{\mathbf{h}}^{-1}) \ , \tag{7.25}$$

where $\hat{n}_{\rm loc}$ denotes the Fourier transform of $n_{\rm loc}$. Furthermore, since we are considering $n_{\rm loc}$ to be localized, its Fourier transform is smooth over reciprocal distances and we can be assured that it is well represented about $\hat{g}_I = 0$. We expand $\hat{n}_{\rm loc}(-2\pi \hat{\mathbf{g}}_I^{\rm T} \cdot\ \overleftrightarrow{\mathbf{h}}^{-1})$ to second order, obtaining,

$$\hat{n}_{\rm loc}(-2\pi \hat{\mathbf{g}}_I^{\rm T} \cdot\ \overleftrightarrow{\mathbf{h}}^{-1}) = 1 + \sum_{\alpha} \hat{g}_{\alpha,I} \frac{\partial \hat{n}_{\rm loc}}{\partial \hat{g}_{\alpha,I}}|_{\hat{g}_I=0} + \frac{1}{2} \sum_{\alpha,\beta} \hat{g}_{\alpha,I} \hat{g}_{\beta,I} \frac{\partial^2 \hat{n}_{\rm loc}}{\partial \hat{g}_{\alpha,I} \partial \hat{g}_{\beta,I}}|_{\hat{g}_I=0} + \dots \ . \tag{7.26}$$

The second term in Eq.(7.26) is zero given our imposed condition $\langle \overleftrightarrow{\mathbf{h}} \cdot \mathbf{s} \rangle = 0$. Thus, we are left with,

$$\hat{n}_{\rm loc}(-2\pi \hat{\mathbf{g}}_I^{\rm T} \cdot\ \overleftrightarrow{\mathbf{h}}^{-1}) = 1 - \frac{(2\pi)^2}{2} V \sum_{\alpha,\beta} \hat{g}_{\alpha,I} \hat{g}_{\beta,I} \int_{-\infty}^{\infty} d\mathbf{s}\ s_\alpha s_\beta\ n_{\rm loc}(\overleftrightarrow{\mathbf{h}} \cdot \mathbf{s}) \ . \tag{7.27}$$

Combining Eq. (7.27) and Eq. (7.25), we obtain,

$$1 - |z_I| = V \frac{(2\pi)^2}{2} \sum_{\alpha,\beta} \hat{g}_{\alpha,I} \hat{g}_{\beta,I} \int_{-\infty}^{\infty} d\mathbf{s}\ s_\alpha s_\beta\ n_{\rm loc}(\overleftrightarrow{\mathbf{h}} \cdot \mathbf{s}) \ . \tag{7.28}$$

Keeping in mind that $\int_{-\infty}^{\infty} d\mathbf{s}\ \ \overleftrightarrow{\mathbf{h}} \cdot \mathbf{s}\ n_{\rm loc}(\overleftrightarrow{\mathbf{h}} \cdot \mathbf{s}) = 0$, one can define the spread of the electronic distribution for the case of a general box through,

$$\langle r^2 \rangle - \langle r \rangle^2 = \langle \left(\overleftrightarrow{\mathbf{h}} \cdot \mathbf{s} \right)^2 \rangle = \sum_{\alpha,\beta} g_{\alpha\beta}\ V \int_{-\infty}^{\infty} d\mathbf{s}\ s_\alpha s_\beta\ n_{\rm loc}(\overleftrightarrow{\mathbf{h}} \cdot \mathbf{s}) \ . \tag{7.29}$$

Here, $g_{\alpha\beta} = \sum_\mu \overleftrightarrow{h}^{\rm T}_{\alpha\mu} \overleftrightarrow{h}_{\mu\beta}$ can be thought of as a metric tensor to describe the corresponding distances in the unit cube. Eq. (7.29) shows us exactly how the length scales are built into the spread through the metric tensor. From direct comparison of Eq. (7.28) and Eq. (7.29) we see that for supercells of general symmetry we need to choose linear combinations of $\hat{g}_{\alpha,I} \hat{g}_{\beta,I}$ that reproduce the metric tensor, $g_{\alpha\beta}$. However, as stated earlier, $\hat{g}_{\alpha,I}$ are dimensionless numbers. Thus, an appropriate generalization takes the form of a sum rule,

$$g_{\alpha\beta} = \sum_I \omega_I \hat{g}_{\alpha,I} \hat{g}_{\beta,I} \ . \tag{7.30}$$

Here, ω_I are the "weights" with the appropriate dimensions to be determined later. Thus, it should also be clear that $g_{\alpha\beta}$ will have at most six independent entries (for triclinic symmetry) and thus a maximum of six weights are needed. It is interesting to note that by multiplying Eq. (7.30) on the left and right hand sides by $\overleftrightarrow{\mathbf{h}}^{-1}$ and using the definition of $\mathbf{G}_I$, one will recover the rule used by Silvestrelli [91] and by Marzari and Vanderbilt [87]. Finally, we generalize to more than one state, $|\psi\rangle \rightarrow |\psi_n\rangle$ and the desired expression for the spread, Ω in a supercell of general symmetry is,

$$\begin{aligned} \Omega &= \frac{2}{(2\pi)^2} \sum_{n}^{\mathrm{N_{states}}} \sum_{I} \omega_I (1 - |z_{I,n}|) + O(2\pi \hat{\mathbf{g}}_I^{\mathrm{T}} \cdot \overleftrightarrow{\mathbf{h}}^{-1})^2 \\ z_{I,n} &= \int_V d\mathbf{r}\ \exp(i\mathbf{G}_I \cdot\ \mathbf{r})\ |\psi_n(\mathbf{r})|^2\ , \end{aligned} \tag{7.31}$$

where Eq. (7.30) determine the $\mathbf{G}_I$.
At this point it is useful to make contact with other spread formulas that are present in the current literature. Following Resta's derivation one finds the formula [93], that in our notation reads,

$$\Omega = -\frac{1}{(2\pi)^2} \sum_{n}^{\mathrm{N_{states}}} \sum_{I} \omega_I \log |z_{I,n}|^2\ , \tag{7.32}$$

with $z_{I,n}$ defined as above. Eq. (7.32) is obtained by inserting Eq. (7.27) into Eq. (7.25), taking the log of the absolute value and expanding to consistent order.
Silvestrelli[91] on the other hand uses (again, in our notation),

$$\Omega = \frac{1}{(2\pi)^2} \sum_{n}^{\mathrm{N_{states}}} \sum_{I} \omega_I (1 - |z_{I,n}|^2)\ , \tag{7.33}$$

with a similar definition for $z_{I,n}$. Obviously Eq. (7.33) is obtained from Eq. (7.32) by an expansion of the log.
At first glance, it seems confusing that there are different definitions for the spread. Admittedly, one has to keep in mind that all formulae are only valid up to the order given in Eq. (7.31). Thus, although different, they are consistent and there is no fundamental reason to choose one definition of the spread over another.
One can also derive a general expression for the expectation value of the periodic position operator for computing the center of the localized function. Recall, that for a cubic simulation supercell the expectation value of the position operator is given as,

$$\begin{aligned} r_{\alpha,n} &= -\frac{L}{2\pi} \mathrm{Im}\ \log z_{\alpha,n} \\ z_{\alpha,n} &= \int_V d\mathbf{r}\ \exp(i\mathbf{g}_\alpha \cdot\ \mathbf{r})\ |\psi_n(\mathbf{r})|^2\ , \end{aligned} \tag{7.34}$$

where $\hat{\mathbf{g}}_1 = (1,0,0)$, $\hat{\mathbf{g}}_2 = (0,1,0)$, and $\hat{\mathbf{g}}_3 = (0,0,1)$, and Im denotes the imaginary part. Again, the salient feature of Eq.(7.34) is that the expectation value of the exponential is invariant with respect to the choice of cell. Thus, a general equation for the expectation value of the position operator in supercells of arbitrary symmetry is,

$$r_{\alpha,n} = -\sum_{\beta} \frac{\overleftrightarrow{h}_{\alpha\beta}}{2\pi} \text{Im } \log z_{\alpha,n} \ . \tag{7.35}$$

We now proceed to determine the weights ω_I as defined in the sum rule Eq. (7.30) for supercells of general symmetry. Recall that the metric, $\overleftrightarrow{\mathbf{g}}$ will contain at most six independent entries as defined by the case of least symmetry, triclinic. Thus, Eq. (7.30) is a linear set of six equations with six unknowns. We have freedom to choose the six Miller indices, $\hat{\mathbf{g}}^I$ of which we are to take the linear combinations of. For computational convenience of computing z_i we choose the first six indices that take you from one to the next point in the Brillouin zone. Namely, $\hat{\mathbf{g}}^1 = (1,0,0)$, $\hat{\mathbf{g}}^2 = (0,1,0)$, $\hat{\mathbf{g}}^3 = (0,0,1)$, $\hat{\mathbf{g}}^4 = (1,1,0)$, $\hat{\mathbf{g}}^5 = (1,0,1)$, $\hat{\mathbf{g}}^6 = (0,1,1)$. With this choice of $\hat{\mathbf{g}}^i$ the explicit system of equations based on Eq. (7.30) takes the following simple form,

$$\begin{pmatrix} 1 & 0 & 0 & 1 & 1 & 0 \\ 0 & 0 & 0 & 1 & 0 & 0 \\ 0 & 0 & 0 & 0 & 1 & 0 \\ 0 & 1 & 0 & 1 & 0 & 1 \\ 0 & 0 & 0 & 0 & 0 & 1 \\ 0 & 0 & 1 & 0 & 1 & 1 \end{pmatrix} \begin{pmatrix} \omega_1 \\ \omega_2 \\ \omega_3 \\ \omega_4 \\ \omega_5 \\ \omega_6 \end{pmatrix} = \begin{pmatrix} g_{11} \\ g_{12} \\ g_{13} \\ g_{22} \\ g_{23} \\ g_{33} \end{pmatrix} \tag{7.36}$$

Thus, the solution to Eq. (7.36) yields the following set of general weights,

$$\begin{aligned} \omega_1 &= g_{11} - g_{12} - g_{13} \\ \omega_2 &= g_{22} - g_{12} - g_{23} \\ \omega_3 &= g_{33} - g_{13} - g_{23} \\ \omega_4 &= g_{12} \\ \omega_5 &= g_{13} \\ \omega_6 &= g_{23} \end{aligned} \tag{7.37}$$

Eq. (7.37) indeed reduces to the specific cases computed in Ref.[91]. However, here, the case for triclinic symmetry is also included. Thus, with knowledge of the cell parameters, in conjunction with Eq. (7.31) allows one to compute the maximally localized WF.

Lecture 8

Chemical Reactions with CPMD

8.1 Simulated Annealing

By adding a friction term, Car–Parrinello molecular dynamics can be turned into a damped second order dynamics scheme.
The friction can be applied both to the nuclear degrees of freedom and the electronic coordinates. The resulting dynamics equation are a powerful method to simultaneously optimize the atomic structure and the Kohn–Sham orbitals [37, 109]. Harmonic reference system integration and plane wave dependent electron masses, are especially helpful in this context, as the derived dynamics does not have a direct physical relevance.
Introducing a friction force proportional to the constants $\gamma_{\rm n}$ and $\gamma_{\rm e}$ the equations of motion can readily be integrated using the velocity Verlet algorithm. The friction terms translate into a simple rescaling of the velocities at the beginning and end of the time step according to

$$\begin{aligned}
\dot{\mathbf{R}}_I(t) &= \gamma_{\rm n}\dot{\mathbf{R}}_I(t) \\
\dot{\mathbf{c}}_i(t) &= \gamma_{\rm e}\dot{\mathbf{c}}_i(t) \\
\texttt{VELOCITY} &\quad \texttt{VERLET UPDATE} \\
\dot{\mathbf{R}}_I(t+\delta t) &= \gamma_{\rm n}\dot{\mathbf{R}}_I(t+\delta t) \\
\dot{\mathbf{c}}_i(t+\delta t) &= \gamma_{\rm e}\dot{\mathbf{c}}_i(t+\delta t)\ .
\end{aligned}$$

It was shown [37, 109] that this scheme leads to efficient optimizations of all degrees of freedom and a combination with geometrical constraints is straightforward.
One advantage of the velocity Verlet integrator is that it can be easily combined with multiple time scale algorithms [22] and still results in reversible dynamics. The most successful implementation of a multiple time scale scheme in connection with the plane wave–pseudopotential method is the harmonic reference system idea [110, 22]. The high frequency motion of the plane waves with large kinetic energy is used as a reference system for the integration. The dynamics of this reference system is harmonic and can

be integrated analytically. In addition, this can be combined with the basic notion of a preconditioner already introduced in the section on optimizations. The electronic mass used in the Car–Parrinello scheme is a fictitious construct and it is allowed to generalize the idea by introducing different masses for different "classical" degrees of freedom [111, 109, 22],

$$\mu(\mathbf{G}) = \begin{cases} \mu & \mathbf{H}(\mathbf{G},\mathbf{G}) \leq \alpha \\ (\mu/\alpha)\ (\frac{1}{2}G^2 + \mathbf{V}(\mathbf{G},\mathbf{G})) & \mathbf{H}(\mathbf{G},\mathbf{G}) \geq \alpha \end{cases} , \tag{8.1}$$

where $\mathbf{H}$ and $\mathbf{V}$ are the matrix elements of the Kohn–Sham matrix and the potential respectively. The reference electron mass is μ. With the preconditioned masses and the harmonic reference system, the equations of motion of the system are

$$\mu(\mathbf{G})\ddot{c}_i(\mathbf{G}) = -\lambda(\mathbf{G})c_i(\mathbf{G}) + \delta\Phi_i(\mathbf{G}) + \sum_j \Lambda_{ij}c_j(\mathbf{G}) \ . \tag{8.2}$$

where $\delta\Phi_i(\mathbf{G})$ is the force on orbital i minus $-\lambda(\mathbf{G})$. From Eq. (8.2) it is easy to see that the frequencies $\omega(\mathbf{G}) = \sqrt{\lambda(\mathbf{G})/\mu(\mathbf{G})}$ are independent of $\mathbf{G}$ and that there is only one harmonic frequency equal to $\sqrt{\alpha/\mu}$. The revised formulas for the integration of the equations of motion for the velocity Verlet algorithm can be found in the literature [22]. The implications of the $\mathbf{G}$ vector dependent masses can be seen by revisiting the formulas for the characteristic frequencies of the electronic system. The masses μ are chosen such that all frequencies ω_{ij} are approximately the same, thus optimizing both, adiabaticity and maximal time step. The disadvantage of this method is that the average electron mass seen by the nuclei is drastically enhanced, leading to renormalization corrections [112] on the masses M_I that are significantly higher than in the standard approach and not as simple to estimate by an analytical expression.

8.2 Rare Events

A problem that is frequently encountered in simulations of chemical reactions is that of computing the free energy profile along a reaction path on a potential energy surface characterized by a reaction coordinate q. Not only does the free energy profile provide a thermodynamic picture along the reaction path, but it also permits determination of activation energies and estimation of associated rate constants via classical or quantum transition state theory. In many instances, a multidimensional free energy profile or surface characterized by a set of reaction coordinates may be of particular interest. However, the ability to characterize a process by a reaction coordinate or coordinates generally assumes some prior knowledge of the process under consideration. This is not always the case and one has to choose alternative methods like transition path sampling [95] or bias potential methods [96, 97] discussed in the subsequent sections.

Statistical mechanics provides a means whereby free energy profiles can be determined directly from ensemble averages. In the case of a classical N–particle system at temperature T, a reaction coordinate q is expressible as a function $q = q(\mathbf{r_1}, \ldots, \mathbf{r_N})$ of the N Cartesian position vectors $\{\mathbf{r_1}, \ldots, \mathbf{r_N}\}$ of the N particles. The free energy profile, $F(q')$, is then defined by

$$F(q') = -\frac{1}{\beta} \ln P(q') \ , \tag{8.3}$$

where

$$P(q') = \langle \delta(q(\mathbf{r_1}, \ldots, \mathbf{r_N}) - q') \rangle \tag{8.4}$$

is the probability density for the reaction coordinate to take the value q' and $\beta = 1/kT$. Analogous formulas hold for multidimensional free energy profiles. In principle, the probability distribution in Eq. 8.4 can be computed directly from a molecular dynamics simulation. However if the reaction path described by q corresponds to a rare event with a high activation energy, then the use of direct simulation techniques is infeasible due to the presence of very low probability regions in the configuration space. Consequently special techniques such as umbrella sampling [3], thermodynamic integration in conjection with the "blue moon ensemble" method [98, 99], guiding or bias potentials [96, 97, 100], nonequilibrium techniques [101], projection methods [102], and variable transformation approaches [103] have been developed. With the exception of the latter two, these approaches do not directly yield the probability distribution. Rather, they are based on the introduction of a bias on the configuration space which artificially drives the system into low probability regions. Averages must, then, be performed by applying appropriate unbiasing factors or reweighting procedures. In addition, the umbrella and blue moon methods, which use restraints/constraints to bias the phase space, require that separate simulations be performed at each value of the reaction coordinate and that weighted histogram or thermodynamic integration methods be applied in order to construct the free energy profile. Despite the enhancement of sampling efficiency caused by the bias, free energy calculations remain computationally very intensive and relatively complex to perform.

8.2.1 Thermodynamic Integration

Geometrical constraints are used in classical simulations to freeze fast degrees of freedom in order to allow for larger time steps. Mainly distance constraints are used for instance to fix intramolecular covalent bonds. These type of applications of constraints is of lesser importance in *ab initio* molecular dynamics. However, in the simulation of rare events such as many reactions, constraints play an important role together with the method of thermodynamic integration [3]. The "blue–moon" ensemble method [98, 99] enables one to compute the potential of mean force. This potential can be obtained directly from the average force of constraint and a geometric correction term during a molecular dynamics

simulation as follows:

$$\mathcal{F}(\xi_2) - \mathcal{F}(\xi_1) = \int_{\xi_1}^{\xi_2} d\xi' \left\langle \frac{\partial \mathcal{H}}{\partial \xi} \right\rangle_{\xi'}^{\text{cond.}} \quad , \tag{8.5}$$

where $\mathcal{F}$ is the free energy and $\xi(\mathbf{r})$ a one–dimensional reaction coordinate, $\mathcal{H}$ the Hamiltonian of the system and $\langle \cdots \rangle_{\xi'}^{\text{cond.}}$ the conditioned average in the constraint ensemble [98]. By way of the blue moon ensemble, the statistical average is replaced by a time average over a constrained trajectory with the reaction coordinate fixed at special values, $\xi(\mathbf{R}) = \xi'$, and $\dot{\xi}(\mathbf{R}, \dot{\mathbf{R}}) = 0$. The quantity to evaluate is the mean force

$$\frac{d\mathcal{F}}{d\xi'} = \frac{\left\langle \mathrm{Z}^{-1/2} \left[-\lambda + k_{\mathrm{B}} T \mathrm{G} \right] \right\rangle_{\xi'}}{\left\langle \mathrm{Z}^{-1/2} \right\rangle_{\xi'}} \quad , \tag{8.6}$$

where λ is the Lagrange multiplier of the constraint,

$$\mathrm{Z} = \sum_I \frac{1}{M_I} \left(\frac{\partial \xi}{\partial \mathbf{R}_I} \right)^2 \quad , \tag{8.7}$$

and

$$\mathrm{G} = \frac{1}{\mathrm{Z}^2} \sum_{I,J} \frac{1}{M_I M_J} \frac{\partial \xi}{\partial \mathbf{R}_I} \cdot \frac{\partial^2 \xi}{\partial \mathbf{R}_I \partial \mathbf{R}_J} \cdot \frac{\partial \xi}{\partial \mathbf{R}_J} \quad , \tag{8.8}$$

where $\langle \cdots \rangle_{\xi'}$ is the unconditioned average, as directly obtained from a constrained molecular dynamics run with $\xi(\mathbf{R}) = \xi'$ and

$$\mathcal{F}(\xi_2) - \mathcal{F}(\xi_1) = \int_{\xi_1}^{\xi_2} d\xi' \, \frac{d\mathcal{F}}{d\xi'} \tag{8.9}$$

finally defines the free energy difference. For the special case of a simple distance constraint $\xi(\mathbf{R}) = |\mathbf{R}_I - \mathbf{R}_J|$ the parameter Z is a constant and $\mathrm{G} = 0$.
The RATTLE algorithm, allows for the calculation of the Lagrange multiplier of arbitrary constraints on geometrical variables within the velocity Verlet integrator. The following algorithm is implemented in the `CPMD` code. The constraints are defined by

$$\sigma^{(i)}(\{\mathbf{R}_I(t)\}) = 0 \quad , \tag{8.10}$$

and the velocity Verlet algorithm can be performed with the following steps.

$$\begin{aligned} \dot{\tilde{\mathbf{R}}}_I &= \dot{\mathbf{R}}_I(t) + \frac{\delta t}{2M_I} \mathbf{F}_I(t) \\ \tilde{\mathbf{R}}_I &= \mathbf{R}_I(t) + \delta t \, \dot{\tilde{\mathbf{R}}}_I \\ \mathbf{R}_I(t+\delta t) &= \tilde{\mathbf{R}}_I + \frac{\delta t^2}{2M_I} \mathbf{g}_{\mathrm{p}}(t) \end{aligned}$$

$$
\begin{aligned}
\text{calculate} \qquad & \mathbf{F}_I(t+\delta t) \\
\dot{\mathbf{R}}'_I &= \dot{\tilde{\mathbf{R}}}_I + \frac{\delta t}{2M_I}\mathbf{F}_I(t+\delta t) \\
\dot{\mathbf{R}}_I(t+\delta t) &= \dot{\mathbf{R}}'_I + \frac{\delta t}{2M_I}\mathbf{g}_{\mathrm{v}}(t+\delta t) \ ,
\end{aligned}
$$

where the constraint forces are defined by

$$
\mathbf{g}_{\mathrm{p}}(t) = -\sum_i \lambda^i_{\mathrm{p}} \frac{\partial \sigma^{(i)}(\{\mathbf{R}_I(t)\})}{\partial \mathbf{R}_I} \tag{8.11}
$$

$$
\mathbf{g}_{\mathrm{v}}(t) = -\sum_i \lambda^i_{\mathrm{v}} \frac{\partial \sigma^{(i)}(\{\mathbf{R}_I(t)\})}{\partial \mathbf{R}_I} \ . \tag{8.12}
$$

The Lagrange multiplier have to be determined to ensure that the constraint on the positions and velocities are exactly fulfilled at the end of the time step. For the position, the constraint condition is

$$
\sigma^{(i)}(\{\mathbf{R}_I(t+\delta t)\}) = 0 \ . \tag{8.13}
$$

Eq. (8.13) is in general a system of nonlinear equations in the Lagrange multipliers λ^i_{p}. These equations can be solved using a generalized Newton algorithm [13] that can be combined with a convergence acceleration scheme based on the direct inversion in the iterative subspace method [31, 108]. The error vectors for a given set of Lagrange multipliers λ are calculated from

$$
\mathbf{e}_i(\lambda) = -\sum_j \mathbf{J}^{-1}_{ij}(\lambda)\sigma^{(j)}(\lambda) \ . \tag{8.14}
$$

The Jacobian $\mathbf{J}$ is defined by

$$
\begin{aligned}
\mathbf{J}_{ij}(\lambda) &= \frac{\partial \sigma^{(i)}(\lambda)}{\partial \lambda^j} && (8.15)\\
&= \sum_I \frac{\partial \sigma^{(i)}(\lambda)}{\partial \mathbf{R}_I(\lambda)} \frac{\partial \mathbf{R}_I(\lambda)}{\partial \lambda^j} && (8.16)\\
&= -\sum_I \frac{\delta t^2}{2M_I}\mathbf{f}^{\mathrm{c}}_I(\lambda)\mathbf{f}^{\mathrm{c}}_I(0) \ , && (8.17)
\end{aligned}
$$

where $\mathbf{f}^{\mathrm{c}}_I(\lambda) = \sum_i \lambda^i \partial\sigma^{(i)}/\partial\mathbf{R}_I$. Typically only a few iterations are needed to converge the Lagrange multipliers to an accuracy of 1×10^{-8}.
The constraint condition for the velocities can be cast into a system of linear equations. Again, as in the case of the orthonormality constraints in the Car–Parrinello method, the Lagrange multiplier for the velocity update can be calculated exactly without making use of an iterative scheme. Defining the derivative matrix

$$
\mathbf{A}_{iI} = \frac{\partial \sigma^{(i)}}{\partial \mathbf{R}_I} \ , \tag{8.18}
$$

the velocity constraints are

$$\dot{\sigma}^{(i)}(t+\delta t) = 0 \tag{8.19}$$

$$\sum_I \frac{\partial \sigma^{(i)}}{\partial \mathbf{R}_I}\dot{\mathbf{R}}_I = 0 \tag{8.20}$$

$$-\sum_j \left(\sum_I \frac{\delta t^2}{2M_I}\mathbf{A}_{iI}\mathbf{A}_{jI}\right)\lambda_j^{\mathrm{v}} = \sum_I \mathbf{A}_{iI}\dot{\mathbf{R}}'_I \ . \tag{8.21}$$

The only information needed to implement a new type of constraint are the formulas for the functional value and its derivative with respect to the nuclear coordinates involved in the constraint.

8.2.2 Adiabatic Free Energy Sampling

This method [104, 105] is based on the creation of a dynamical adiabatic separation between the reaction coordinate and remaining degrees of freedom. In particular, a dynamical scheme is constructed in which the reaction coordinate evolves slowly relative to the other degrees of freedom and is simultaneously maintained at a high temperature. The latter condition ensures that all activation barriers along the reaction path can be easily crossed and can be enforced by coupling the reaction coordinate to its own heat bath or thermostat. The former condition permits the remaining degrees of freedom to fully relax in response to the motion of the reaction coordinate and ,thereby, sample a large portion of their configuration space as the reaction coordinate slowly evolves. An analysis of the resulting dynamics reveals that the free energy profile will be given by Eq. 8.3 with β replaced by $\beta_s = 1/kT_s$, where T_s is the temperature of the reaction coordinate. This approach eliminates biasing from the simulation procedure and the need for post processing of the output data.
Let us consider the case where a straightforward partitioning of the system into a reactive subsystem (S) and the environment (E) is possible. A general separation of degrees of freedom will require a slightly more elaborate formulation. For each subsystem, positions $\mathbf{q}_i^{\mathrm{S}}, \mathbf{q}_j^{\mathrm{E}}$, momenta $\mathbf{p}_i^{\mathrm{S}}, \mathbf{p}_j^{\mathrm{E}}$, and masses $M_i^{\mathrm{S}}, M_j^{\mathrm{E}}$ are defined and the number of atoms in the subsystems is N^{S} and N^{E}. The Hamiltonian of the system is then

$$H(\mathbf{q},\mathbf{p}) = \sum_i^{N^{\mathrm{S}}} \frac{\left(\mathbf{p}_i^{\mathrm{S}}\right)^2}{2M_i^{\mathrm{S}}} + \sum_j^{N^{\mathrm{E}}} \frac{\left(\mathbf{p}_j^{\mathrm{E}}\right)^2}{2M_j^{\mathrm{E}}} + +V\left(\mathbf{q}^{\mathrm{S}}, \mathbf{q}^{\mathrm{E}}\right) \ . \tag{8.22}$$

Each subsystem is then coupled to its own thermostat with a target temperature T^{S} and T^{E}. The crucial step, which is needed to obtain the dynamics of the reactive system on the physical free energy surface at the specific temperature, is the rescaling of the atomic masses so that $M^{\mathrm{S}}/M^{\mathrm{E}} \ll 1$. This ensures that the frequency spectra of the subsystems do not overlap. In particular the reactive system is varying slowly, as compared to the

environment. This has two consequences: 1) The systems are decoupled and are in equilibrium although they are at different temperatures; 2) the slowly moving system feels the average force of the environment, which is at the physical temperature, and its dynamics is performed on this free energy surface. Note that this separation of systems is analogous to the two systems used in the Car–Parrinello method.
The fast degrees of freedom $\mathbf{q}_j^{\mathrm{E}}, \mathbf{p}_j^{\mathrm{E}}$ sample the canonical distribution at temperature T^{E} for every configuration $\mathbf{q}_j^{\mathrm{S}}, \mathbf{p}_j^{\mathrm{S}}$ of the reactive system. The dynamics of the slow degrees of freedom approximates the one resulting from a Hamiltonian with the effectively averaged potential. This potential $\bar{V}\left(\mathbf{q}^{\mathrm{S}}\right)$ is, for a full decoupling given by

$$\exp\left[-\beta^{\mathrm{E}}\bar{V}\left(\mathbf{q}^{\mathrm{S}}\right)\right] = \frac{\int \exp\left[-\beta^{\mathrm{E}}V\left(\mathbf{q}^{\mathrm{S}},\mathbf{q}^{\mathrm{E}}\right)\right] d\mathbf{q}^{\mathrm{E}}}{\int \exp\left[-\beta^{\mathrm{E}}V\left(\mathbf{q}^{\mathrm{S}},\mathbf{q}^{\mathrm{E}}\right)\right] d\mathbf{q}^{\mathrm{E}}d\mathbf{q}^{\mathrm{S}}} \quad . \tag{8.23}$$

This potential of mean force equals the physical free energy surface of the reactive system. An enhanced canonical sampling of this free energy surface can be obtained by choosing $T^{\mathrm{S}} > T^{\mathrm{E}}$. Because we have assumed adiabatic evolution, ergodic behavior, and hence equilibrium sampling, the probability distribution of the full system in configuration space is given by

$$\rho\left(\mathbf{q}^{\mathrm{S}},\mathbf{q}^{\mathrm{E}}\right) = \frac{\exp\left[-(\beta^{\mathrm{S}}-\beta^{\mathrm{E}})\bar{V}\left(\mathbf{q}^{\mathrm{S}}\right)\right]}{\int \exp\left[-\beta^{\mathrm{S}}\bar{V}\left(\mathbf{q}^{\mathrm{S}}\right)\right] d\mathbf{q}^{\mathrm{S}}} \times \frac{\exp\left[-\beta^{\mathrm{E}}V\left(\mathbf{q}^{\mathrm{S}},\mathbf{q}^{\mathrm{E}}\right)\right]}{\int \exp\left[-\beta^{\mathrm{E}}V\left(\mathbf{q}^{\mathrm{S}},\mathbf{q}^{\mathrm{E}}\right)\right] d\mathbf{q}^{\mathrm{E}}d\mathbf{q}^{\mathrm{S}}} \quad . \tag{8.24}$$

This probability distribution can be used to calculate all thermodynamic properties of the physical system from a trajectory generated within the adiabatically decoupled system. Efficiency and accuracy of this method depends on the choice of subsystems and the free parameters $M^{\mathrm{S}}/M^{\mathrm{E}}$ and the temperature T^{S}.

8.2.3 Bias Potential Methods

A long–standing problem of molecular dynamics is that its utility is limited to processes that occur on a time scale of nanoseconds or less. This is especially true for *ab initio* molecular dynamics where the time scale is typically only a few tens of picoseconds.
For many systems, the dynamics can be characterized as a sequence of infrequent transitions from one potential basin or state to another. In these cases, longer times scales can be accessed using transition state theory (TST), an elegant approach with a long history [3]. In TST, one takes the transition rate between states as the flux through a dividing surface separating the states. This flux is an equilibrium property of the system, and so does not require that actual dynamics be performed. TST assumes that each crossing of the dividing surface corresponds to a true reactive event, in which the system passes from one state to another and then loses all memory of this transition before the next event. In actuality, some surface crossings can be dynamically connected, i.e. if

the time between two successive crossings does not exceed the correlation time of the system. Because of this correlated dynamical behavior the TST rate constant is only approximate, but the exact rate can be recovered by computing a dynamical correction factor from short–duration trajectories initiated at the dividing surface [106]. If the TST dividing surface is chosen carefully, the TST rate constant is often an extremely good approximation to the true rate. This fact, along with the conceptual simplicity and accuracy of the harmonic approximation to TST [107], has led to the widespread use of TST for problems in many fields.

However, the utility of TST in treating infrequent–event dynamics has always rested on two crucial assumptions; that one knows in advance what the different states of the system will be, and that one can construct reasonable dividing surfaces along the boundaries between the states, or can find saddle points. Often, however, the understanding of the states to which a system will evolve is incomplete. Indeed, determining the future configurations may be the primary motivation of the atomistic simulation. Even worse, presumptions about how the system will evolve may be incorrect, so that important pathways are overlooked. These problems are especially severe in condensed systems or other systems with many degrees of freedom that are tightly coupled, e.g. in complex solvents like membranes and other biological systems.

Let us consider [104] a system described by a Hamiltonian $H(\mathbf{q},\mathbf{p})$ at an inverse temperature $\beta = 1/k_{\mathrm{B}}T$. The thermodynamic average of a function $f(\mathbf{q},\mathbf{p})$ is defined by through the 6–dimensional phase space integral

$$\begin{aligned} \langle f(\mathbf{q},\mathbf{p})\rangle_{\beta H} &= \lim_{\Delta t\to\infty}\frac{1}{\Delta t}\int_0^{\Delta t} f(\mathbf{q}(t),\mathbf{p}(t))dt & (8.25)\\ &= \frac{\int\int f(\mathbf{q},\mathbf{p})e^{-\beta H(\mathbf{q},\mathbf{p})}d\mathbf{p}d\mathbf{q}}{\int\int e^{-\beta H(\mathbf{q},\mathbf{p})}d\mathbf{p}d\mathbf{q}}\ . & (8.26)\end{aligned}$$

If the original Hamiltonian is changed to a new Hamiltonian $H'(\mathbf{q},\mathbf{p})$ and inverse temperature β' the phase space integral $\langle f(\mathbf{q},\mathbf{p})\rangle_{\beta H}$ can be calculated by using

$$\begin{aligned} \langle f(\mathbf{q},\mathbf{p})\rangle_{\beta H} &= \frac{\int\int f(\mathbf{q},\mathbf{p})e^{-\beta H(\mathbf{q},\mathbf{p})}d\mathbf{p}d\mathbf{q}}{\int\int e^{-\beta H(\mathbf{q},\mathbf{p})}d\mathbf{p}d\mathbf{q}}\\ &= \frac{\int\int\left[f(\mathbf{q},\mathbf{p})e^{\beta' H'-\beta H}\right]e^{-\beta' H'}d\mathbf{p}d\mathbf{q}}{\int\int e^{-\beta' H'}d\mathbf{p}d\mathbf{q}}\times\frac{\int\int e^{-\beta' H'}d\mathbf{p}d\mathbf{q}}{\int\int\left[e^{\beta' H'-\beta H}\right]e^{-\beta' H'}d\mathbf{p}d\mathbf{q}} & (8.27)\\ &= \langle f(\mathbf{q},\mathbf{p})e^{\beta' H'-\beta H}\rangle_{\beta' H'}\frac{1}{\langle e^{\beta' H'-\beta H}\rangle_{\beta' H'}} & (8.28)\end{aligned}$$

The last equality shows that the average of the function f of the system with Hamiltonian H can be obtained as a function of the averages of two different functions $f(\mathbf{q},\mathbf{p})e^{\beta' H'-\beta H}$ and $e^{\beta' H'-\beta H}$, of a system based on the Hamiltonian H'. If H' is chosen in an appropriate way the new averages converge faster than the original one. The technique will work efficiently as long as sufficiently many configurations sampled with the the Hamiltonian

Figure 8.1: Schematic illustration of a one–dimensional potential V (solid line) defining state A, and the biased potential $V + \Delta V_b$ (dashed line), which defines state A_b. The potentials are equivalent at the transition state boundaries (indicated by vertical lines), so the relative probability of escape to the left vs. right is the same for both states, although the escape rates are enhanced for state A_b. [97]

H' are also significant for the system with Hamiltonian H, so that the reweighting factor $e^{\beta' H' - \beta H}$ is non vanishing during a considerable part of the trajectory.
We introduce [97] a bias potential $\Delta V_b(\mathbf{q})$ (see Fig. 8.2.3) that is added to the original Hamiltonian and defines the new Hamiltonian of the system $H'(\mathbf{q}, \mathbf{p}) = H(\mathbf{q}, \mathbf{p}) + \Delta V_b(\mathbf{q})$. Assume that $\Delta V_b(\mathbf{q})$ is chosen such that it is zero in the transition state regions, that it does not block any escape paths, nor introduce any new, significant wells into the system. We further assume that TST is exact for both systems. Under this assumptions we find the following property for the escape rates from states A and A_b (as defined in Fig. 8.2.3)

$$\frac{k^{\mathrm{TST}}_{A\to B}}{k^{\mathrm{TST}}_{A\to C}} = \frac{k^{\mathrm{TST}}_{A_b\to B}}{k^{\mathrm{TST}}_{A_b\to C}} \quad . \tag{8.29}$$

If now also states B and C have bias potentials there escape rates will be enhanced, and the system evolves, at an accelerated pace, from state to state in a sequence representative of the exact dynamics. That is , the probability of any given sequence of states visited is exactly the same for the biased dynamics as for the exact dynamics.

Lecture 9

Linear Response

9.1 Adiabatic Density–Functional Perturbation Theory

The total energy and charge density are basic quantities of DFT, and give access to a wide number of experimental observables. Most of these quantities can be derived from derivatives of the energy or density with respect to external perturbations. As an example, the force exerted on a nucleus is equal to minus the derivative of the total energy of the system. The calculation of such energy derivatives can be done by finite–difference methods: the total energy is obtained at slightly different values of the external perturbation, then the derivative of the total energy curve with respect to the small disturbance is calculated numerically. Although this is a very convenient method, the recent practice has shown that perturbative techniques within DFT are more powerful. Such techniques are very similar to the treatment of perturbations within Hartree–Fock theory (the coupled–perturbed Hartree–Fock formalism) [113]. Such techniques were discovered and rediscovered within DFT many times. They are based either on the Sternheimer equation, Green's functions, sum–over–states techniques, or on the Hylleras variational technique. Generalizations to arbitrary order of perturbations, based on the $2n+1$ theorem of perturbation theory and on generalized Sternheimer equations were also proposed.

9.2 Coupled Perturbed Kohn–Sham Equations

Let us consider the extended Kohn–Sham energy functional

$$\mathcal{E}^{\mathrm{KS}}[\{\Phi_i\}] = E^{\mathrm{KS}}[\{\Phi_i\}] + \lambda E^{\mathrm{pert.}}[\{\Phi_i\}] + \sum_{ij} \Lambda_{ij} \left(\langle \Phi_i \mid \Phi_j \rangle - \delta_{ij} \right) \quad . \tag{9.1}$$

All quantities are expanded in powers of λ in the form

$$X(\lambda) = X^{(0)} + \lambda X^{(1)} + \lambda^2 X^{(2)} + \cdots \quad , \tag{9.2}$$

Table 9.1: List of some properties related to derivatives of the total energy. ϵ_α is an external electrical field, x_i a displacement of a nuclei, B_α a magnetic field, m_i the nuclear magnetic moment.

Derivative	Observable
$\frac{d^2E}{d\epsilon_\alpha d\epsilon_\beta}$	polarizability
$\frac{d^2E}{dx_i dx_j}$	harmonic force constants
$\frac{d^2E}{dx_i d\epsilon_\alpha}$	dipole derivatives, infrared intensities
$\frac{d^2E}{dx_i d\epsilon_\alpha d\epsilon_\beta}$	polarizability derivative, Raman intensities
$\frac{d^2E}{dB_\alpha dB_\beta}$	magnetazibility
$\frac{d^2E}{dm_i dB_\beta}$	nuclear magnetic shielding tensor

where X can be the Kohn–Sham energy E_{KS}, the Kohn–Sham orbitals $\Phi_i(\mathbf{r})$, the electron density $n(\mathbf{r})$, the Lagrange multipliers Λ, or the Kohn–Sham Hamiltonian H_{KS}.
Because the Kohn–Sham energy satisfies a variational principle under constraints, it is possible to derive a constraint variational principle for the $2n$th order derivative of the energy with respect to the nth order derivative of the wavefunctions $\Phi_i(\mathbf{r})$ [115, 114]: when the expansion of the wavefunction up to an order of $n-1$ is known, the variational principle for the $2n$th order derivative of the energy is as follows:

$$E^{(2n)} = \min_{\Phi_i^{(n)}} \left(\mathcal{E} \left[\sum_k \lambda^k \phi_i^{(k)} \right] \right)^{(2n)} \tag{9.3}$$

under the constraint, in the parallel transport gauge

$$\sum_{k=0}^{n} \langle \Phi_i^{(n-k)} \mid \Phi_j^{(k)} \rangle = 0 \tag{9.4}$$

for all occupied states i and j. The requirement that the constraint condition (orthogonality in our case) is fulfilled at every order in the perturbation was used to derive the above equations. It turns out that there is a certain degree of arbitrariness in the definition of the Lagrange multipliers. By adding additional conditions that leave energy invariant a special gauge for the Lagrange multipliers is chosen. The best known of such a gauge is the canonical gauge for the zeroth order wavefunction in Hartree–Fock and Kohn–Sham theory. In this gauge the matrix of Lagrange multipliers is diagonal. For the perturbation treatment at hand the parallel transport gauge defined above is most convenient. The explicit expressions for $E^{(2n)}$ can be derived by introducing Eq. 9.1 into Eq. 9.3. For zeroth order we get back the Kohn–Sham equations

$$\mathcal{H}^{(0)} \mid \Phi_i^{(0)} \rangle = \sum_j \Lambda_{ij} \mid \Phi_j^{(0)} \rangle \ , \tag{9.5}$$

and for second order the following expression is obtained

$$
\begin{aligned}
E^{(2)}\left[\{\Phi_i^{(0)}\},\{\Phi_i^{(1)}\}\right] &= \sum_{ij}\langle\Phi_i^{(1)} \mid \mathcal{H}^{(0)}\delta_{ij}+\Lambda_{ij} \mid \Phi_j^{(1)}\rangle \\
&+\sum_i\left\{\langle\Phi_i^{(1)} \mid \frac{\delta E^{\rm pert}}{\delta\langle\Phi_i \mid}+\frac{\delta E^{\rm pert}}{\delta \mid \Phi_i\rangle} \mid \Phi_i^{(1)}\rangle\right\} \\
&+\frac{1}{2}\int\int \mathcal{K}(\mathbf{r},\mathbf{r}')\; n^{(1)}(\mathbf{r})\; n^{(1)}(\mathbf{r}')\; d\mathbf{r}\; d\mathbf{r}' \\
&+\int \frac{d}{d\lambda}\left.\frac{\delta E_{\rm Hxc}}{\delta n(\mathbf{r})}\right|_{n^{(0)}} n^{(1)}(\mathbf{r})\; d\mathbf{r}+\frac{1}{2}\left.\frac{d^2E_{\rm Hxc}}{d\lambda^2}\right|_{n^{(0)}} \quad , \qquad (9.6)
\end{aligned}
$$

where the first–order wavefunctions are varied under the constraints

$$\langle\Phi_i^{(0)} \mid \Phi_j^{(1)}\rangle = 0 \;\; , \qquad (9.7)$$

for all occupied states i and j. The density and the first order density are given by

$$n^{(0)}(\mathbf{r}) = \sum_i f_i \mid \Phi_i^{(0)}(\mathbf{r}) \mid^2 \qquad (9.8)$$

$$n^{(1)}(\mathbf{r}) = \sum_i f_i[\Phi_i^{(0)\star}(\mathbf{r})\Phi_i^{(1)}(\mathbf{r})+\Phi_i^{(1)\star}(\mathbf{r})\Phi_i^{(0)}(\mathbf{r})] \;\; . \qquad (9.9)$$

Further, we have introduced the zeroth order Kohn–Sham Hamiltonian

$$\mathcal{H}^{(0)}[\{\Phi_i^{(0)}\}] = \frac{1}{2}\nabla^2+\mathcal{V}_{\rm ext}^{(0)}(\mathbf{r})+\int\frac{n^{(0)}(\mathbf{r}')}{\mid\mathbf{r}-\mathbf{r}'\mid}d\mathbf{r}'+\left.\frac{\delta E_{\rm xc}}{\delta n(\mathbf{r})}\right|_{n^{(0)}} \quad , \qquad (9.10)$$

the combined Hartree and exchange–correlation energy

$$E_{\rm Hxc}[n] = \frac{1}{2}\int\int\frac{n^{(0)}(\mathbf{r})n^{(0)}(\mathbf{r}')}{\mid\mathbf{r}-\mathbf{r}'\mid}d\mathbf{r}'d\mathbf{r}+E_{\rm xc}[n] \;\; , \qquad (9.11)$$

and the second order energy kernel

$$\mathcal{K}(\mathbf{r},\mathbf{r}') = \left.\frac{\delta^2E_{\rm Hxc}[n]}{\delta n(\mathbf{r})\delta n(\mathbf{r}')}\right|_{n^{(0)}} \quad . \qquad (9.12)$$

Since $E^{(2)}$ is variational with respect to $\Phi_i^{(1)}$ the Euler–Lagrange, or in this case self–consistent Sternheimer equations [116, 117] can be deduced

$$\mathcal{P}_c\sum_j\left(\mathcal{H}^{(0)}\delta_{ij}+\Lambda_{ij}^{(0)}\right)\mathcal{P}_c \mid \Phi_j^{(1)}\rangle = -\mathcal{P}_c\mathcal{H}^{(1)} \mid \Phi_i^{(0)}\rangle \;\; , \qquad (9.13)$$

where $\mathcal{P}_c$ is the projector upon the unoccupied states

$$\mathcal{P}_c = 1-\sum_i \mid \Phi_i^{(0)}\rangle\langle\Phi_i^{(0)} \mid \qquad (9.14)$$

and the first order Hamiltonian $\mathcal{H}^{(1)}$ is given by

$$\mathcal{H}^{(1)} = \frac{\delta E^{\text{pert}}}{\delta \langle \Phi_i \mid} + \int \mathcal{K}(\mathbf{r},\mathbf{r}')\; n^{(1)}(\mathbf{r}')\; d\mathbf{r}' + \frac{d}{d\lambda}\; \frac{\delta E_{\text{Hxc}}}{\delta n(\mathbf{r})}\bigg|_{n^{(0)}} \quad . \tag{9.15}$$

Eq. 9.13 can either be considered as a set of equations for $\{\Phi_i^{(1)}\}$ that have to be solved self–consistently or as one linear system of the size $N \times M$, where N is the number of occupied orbitals and M the number of basis functions.

9.2.1 Exchange-Correlation Functionals

The evaluation of the kernel function $\mathcal{K}(\mathbf{r},\mathbf{r}')$ requires the second functional derivative of the exchange and correlation functionals. In the case of LDA functionals this is easily done, however, its evaluation is more complex for GC functionals, which can be written in the form:

$$E_{xc} = \int d\mathbf{r}\; F_{xc}\left[n(\mathbf{r}), \nabla n(\mathbf{r})\right]. \tag{9.16}$$

The calculus of variations yields the following expression in terms of first and second derivatives of $n^{(1)}$[118]:

$$\begin{aligned} V_{xc}^{(1)}(\mathbf{r}) \;=\; & \frac{\partial^2[F_{xc}\,[n,\nabla n]]}{\partial n^2}\bigg|_{n^{(0)}} n^{(1)}(\mathbf{r}) - \sum_{\alpha} \frac{\partial}{\partial \mathbf{r}_\alpha}\left[\frac{\partial^2[F_{xc}\,[n,\nabla n]]}{\partial n \partial(\partial_\alpha n)}\bigg|_{n^{(0)}}\right] n^{(1)}(\mathbf{r}) \\ & - \sum_{\alpha,\beta} \frac{\partial}{\partial \mathbf{r}_\alpha}\left[\frac{\partial^2[F_{xc}\,[n,\nabla n]]}{\partial(\partial_\alpha n)\partial(\partial_\beta n)}\bigg|_{n^{(0)}}\right] \frac{\partial n^{(1)}(\mathbf{r})}{\partial \mathbf{r}_\beta} \\ & - \sum_{\alpha,\beta} \left[\frac{\partial^2[F_{xc}\,[n,\nabla n]]}{\partial(\partial_\alpha n)\partial(\partial_\beta n)}\bigg|_{n^{(0)}}\right] \frac{\partial^2 n^{(1)}(\mathbf{r})}{\partial \mathbf{r}_\alpha \partial \mathbf{r}_\beta}. \end{aligned} \tag{9.17}$$

The evaluation of these terms is rather cumbersome and alternatively a finite difference approach can be used:

$$\begin{aligned} & \frac{1}{2}\int d\mathbf{r} \int d\mathbf{r}' n^{(1)}\left(\mathbf{r}'\right) \frac{\delta^2 E_{xc}}{\delta n(\mathbf{r}')\delta n(\mathbf{r})} n^{(1)}\left(\mathbf{r}\right) \qquad (9.18) \\ = \;& \frac{1}{2}\lim_{\varepsilon\to 0} \frac{E_{xc}\left[n^{(0)}\left(\mathbf{r}\right) + \varepsilon n^{(1)}\left(\mathbf{r}\right)\right] + E_{xc}\left[n^{(0)}\left(\mathbf{r}\right) - \varepsilon n^{(1)}\left(\mathbf{r}\right)\right] - 2E_{xc}\left[n^{(0)}\left(\mathbf{r}\right)\right]}{\varepsilon^2}. \end{aligned}$$

and therefore

$$V_{xc}^{(1)} = \lim_{\varepsilon\to 0} \frac{V_{xc}\left(n^{(0)} + \varepsilon n^{(1)}\right) - V_{xc}\left(n^{(0)} - \varepsilon n^{(1)}\right)}{2\varepsilon} \tag{9.19}$$

In Eq.(9.19), accuracy requires the use of a small ε, but on the other hand, numerical stability favors a large ε. A good compromise can be achieved with a value of $\varepsilon \approx 10^{-3}$. The numerical approach can be more reliable and stable than the analytical expression.

In a plane wave approach it is also computationally cheaper: in fact in Eq.(9.17) one needs to evaluate $\partial n^{(1)}/\partial \mathbf{r}_\alpha$ and $\partial^2 n^{(1)}/\partial \mathbf{r}_\alpha \partial \mathbf{r}_\beta$, which require a total of 9 Fourier transforms to be compared with the 6 Fourier transforms of Eq.(9.19), not to mention the cost of evaluating the very complex functions in Eq.(9.17).

9.3 Nuclear Hessian

Harmonic vibrational frequencies of a system can be calculated as the eigenvalues of the dynamical matrix

$$D_{I\alpha,J\beta} = \frac{1}{\sqrt{M_I M_J}} \left(\frac{\partial^2 E_{\rm ion}}{\partial R_{I\alpha} \partial R_{J\beta}} + \frac{\partial^2 E_{KS}}{\partial R_{I\alpha} \partial R_{J\beta}} \right) \tag{9.20}$$

where we indicate the ions with $I, J = 1, N_{\rm atom}$ ($N_{\rm atom}$ is the number of ions) and the Cartesian coordinates with indeces $\alpha, \beta = 1, 2, 3$. The first term in this matrix can be calculated easily from $E_{\rm ion}$. The second term is due to the interaction of the electrons with the nuclei and can be calculated using density functional perturbation theory. We have to consider $3N_{\rm atom}$ perturbations, one for each small displacement of the atom I from its equilibrium position $\mathbf{R}_I$ in the direction α. The perturbative functional is given by:

$$E^{pert}[n] = \int d\mathbf{r}\; n(\mathbf{r}) \sum_{J=1}^{N_{\rm atom}} \frac{\partial V_{\rm ext}(\mathbf{r} - \mathbf{R}_J)}{\partial R_{I\alpha}} \delta_{IJ} \;\; , \tag{9.21}$$

where V_{ext} describes the ionic Coulomb potential that is in the case of norm–conserving pseudopotentials (Note that the above formula is for a local potential only)

$$V_{\rm ext}(\mathbf{r}) = V_{\rm loc}(\mathbf{r}) + \sum_L \mid p_L \rangle \omega_L \langle p_L \mid \tag{9.22}$$

where we assumed only one projector per angular momentum channel. Therefore the perturbation functional is

$$\begin{aligned} E^{pert}[n] \;\; = \;\; & \int d\mathbf{r}\; n(\mathbf{r}) \frac{\partial V_{loc}(\mathbf{r} - \mathbf{R}_I)}{\partial R_{I\alpha}} \\ & + \sum_L \sum_k \left(\langle \Phi_k \left| \frac{\partial p_L}{\partial R_{I\alpha}} \right\rangle \omega_L \langle p_L | \Phi_k \rangle + \langle \Phi_k | p_L \rangle \omega_L \left\langle \frac{\partial p_L}{\partial R_{I\alpha}} \right| \Phi_k \rangle \right) \;\; . \end{aligned} \tag{9.23}$$

The electronic term of the dynamic matrix can be calculated using the Hellmann-Feynman theorem generalized to the nonlocal potential:

$$\frac{\partial E_{KS}}{\partial R_{I\alpha}} = \sum_k \left\langle \Phi_k^{(0)} \right| \frac{\partial V_{\rm ext}}{\partial R_{I\alpha}} \left| \Phi_k^{(0)} \right\rangle \tag{9.24}$$

and taking the second derivative:

$$\begin{aligned}
\frac{\partial^2 E^{KS}}{\partial R_{I\alpha}\partial R_{J\beta}} &= \sum_k \left(\left\langle \Phi_k^{(0)} \right| \frac{\partial^2 V_{\text{ext}}}{\partial R_{I\alpha}\partial R_{J\beta}} \left| \Phi_k^{(0)} \right\rangle + \left\langle \Phi_{k,I\alpha}^{(1)} \right| \frac{\partial V_{\text{ext}}}{\partial R_{J\beta}} \left| \Phi_k^{(0)} \right\rangle + \left\langle \Phi_k^{(0)} \right| \frac{\partial V_{\text{ext}}}{\partial R_{J\beta}} \left| \Phi_{k,I\alpha}^{(1)} \right\rangle \right) \\
&= \sum_k \left[\left\langle \Phi_k^{(0)} \right| \frac{\partial^2 V_{loc}}{\partial R_{I\alpha}\partial R_{J\beta}} \left| \Phi_k^{(0)} \right\rangle + \sum_L \left(\langle \Phi_k^{(0)} \left| \frac{\partial^2 p_L}{\partial R_{I\alpha}\partial R_{J\beta}} \right\rangle \omega_L \langle p_L \mid \Phi_k^{(0)} \rangle \right. \right. \\
&\quad + \langle \Phi_k^{(0)} \mid p_L \rangle \omega_L \left\langle \frac{\partial^2 p_L}{\partial R_{I\alpha}\partial R_{J\beta}} \right| \Phi_k^{(0)} \rangle + 2 \langle \Phi_k^{(0)} \left| \frac{\partial p_L}{\partial R_{I\alpha}} \right\rangle \omega_L \left\langle \frac{\partial p_L}{\partial R_{\beta j}} \right| \Phi_k^{(0)} \rangle \Big) \\
&\quad + \left\langle \Phi_{k,I\alpha}^{(1)} \right| \frac{\partial V_{loc}}{\partial R_{J\beta}} \left| \Phi_k^{(0)} \right\rangle + \left\langle \Phi_k^{(0)} \right| \frac{\partial V_{loc}}{\partial R_{J\beta}} \left| \Phi_{k,I\alpha}^{(1)} \right\rangle \\
&\quad + \sum_L \left(\langle \Phi_{k,I\alpha}^{(1)} \left| \frac{\partial p_L}{\partial R_{J\beta}} \right\rangle \omega_L \langle p_L \mid \Phi_k^{(0)} \rangle + \langle \Phi_{k,I\alpha}^{(1)} \mid p_L \rangle \omega_L \left\langle \frac{\partial p_L}{\partial R_{J\beta}} \right| \Phi_k^{(0)} \rangle \right. \\
&\quad \left. \left. + \langle \Phi_k^{(0)} \left| \frac{\partial p_L}{\partial R_{J\beta}} \right\rangle \omega_L \langle p_L \mid \Phi_{k,I\alpha}^{(1)} \rangle + \langle \Phi_k^{(0)} \mid p_L \rangle \omega_L \left\langle \frac{\partial p_L}{\partial R_{\beta j}} \right| \Phi_{k,I\alpha}^{(1)} \rangle \right) \right] \qquad (9.25)
\end{aligned}$$

9.3.1 Selected Eigenmodes of the Hessian

Harmonic vibrational frequencies are calculated from the eigenvalues of the dynamical matrix. If only part of the eigenvalues are needed an iterative diagonalization scheme, e.g. Lanczos or Davidson diagonalization could be used. This might be useful in geometry optimization or in the location of saddle points, as well as when only certain type of vibrations are of interest, for example surface modes or hydrogen stretching modes. Iterative diagonalization scheme are based on matrix vector multiplication

$$\mathbf{a} = \mathbf{H}\mathbf{q} \ . \qquad (9.26)$$

This is of special interest when the calculation of the matrix $\mathbf{H}$ can be avoided and only an algorithm for the application of a vector to the matrix has to be available.
Let us consider a collective displacement [119]

$$\mathbf{q} = \sum_{I,\alpha} q_{I\alpha} \mathbf{e}_{I\alpha} \ , \qquad (9.27)$$

where the indices I, α run over all atoms and coordinates x, y, z respectively, and $\mathbf{e}_{I\alpha}$ is a $3N_{\text{atom}}$ Cartesian unit vector. The matrix vector multiplication then becomes

$$\mathbf{a}_{J\beta} = \sum_{I\alpha} \frac{\partial^2 E}{\partial \mathbf{R}_{J\beta} \partial \mathbf{R}_{I\alpha}} q_{I\alpha} \ . \qquad (9.28)$$

This can be calculated using density functional perturbation theory where we again assumed only one projector per angular momentum channel. Therefore the perturbation

functional is

$$\begin{aligned} E^{pert}[n] &= \int d\mathbf{r}\; n(\mathbf{r}) \sum_{I\alpha} q_{I\alpha} \frac{\partial V_{ext}(\mathbf{r}-\mathbf{R}_I)}{\partial R_{I\alpha}} \\ &= \int d\mathbf{r}\; n(\mathbf{r}) \sum_{I\alpha} q_{I\alpha} \left[\frac{\partial V_{loc}(\mathbf{r}-\mathbf{R}_I)}{\partial R_{I\alpha}} \right. \\ &\quad \left. + \sum_k \sum_L \left(\langle \Phi_k \left| \frac{\partial p_L}{\partial R_{I\alpha}} \right\rangle \omega_L \langle p_L | \Phi_k \rangle + \langle \Phi_k | p_L \rangle \omega_L \left\langle \frac{\partial p_L}{\partial R_{I\alpha}} \right| \Phi_k \rangle \right) \right] \quad . (9.29) \end{aligned}$$

Using this perturbation expression the response Φ_i^q of the Kohn–Sham wavefunction to the collective displacement $q_{I,\alpha}$ can be calculated. And with the response function the matrix vector multiplication becomes

$$\begin{aligned} \mathbf{a}_{J\beta} &= \sum_{I\alpha} \frac{\partial^2 E}{\partial R_{J\beta} \partial R_{I\alpha}} q_{I\alpha} = \frac{\partial^2 E}{\partial R_{J\beta} \partial q} \\ &= \sum_k \left(\sum_{I\alpha} q_{I\alpha} \left\langle \Phi_k^{(0)} \right| \frac{\partial^2 V_{\text{ext}}}{\partial R_{I\alpha} \partial R_{J\beta}} \left| \Phi_k^{(0)} \right\rangle \right. \\ &\quad \left. + \left\langle \Phi_{k,q}^{(1)} \right| \frac{\partial V_{\text{ext}}}{\partial R_{J\beta}} \left| \Phi_k^{(0)} \right\rangle + \left\langle \Phi_k^{(0)} \right| \frac{\partial V_{\text{ext}}}{\partial R_{J\beta}} \left| \Phi_{k,q}^{(1)} \right\rangle \right) \\ &= \sum_k \left[\sum_{I\alpha} q_{I\alpha} \left\langle \Phi_k^{(0)} \right| \frac{\partial^2 V_{loc}}{\partial R_{I\alpha} \partial R_{J\beta}} \left| \Phi_k^{(0)} \right\rangle \right. \\ &\quad + \sum_L \sum_{I\alpha} q_{I\alpha} \left(\langle \Phi_k^{(0)} \left| \frac{\partial^2 p_L}{\partial R_{I\alpha} \partial R_{J\beta}} \right\rangle \omega_L \langle p_L \mid \Phi_k^{(0)} \rangle \right. \\ &\quad \left. + \langle \Phi_k^{(0)} \mid p_L \rangle \omega_L \left\langle \frac{\partial^2 p_L}{\partial R_{I\alpha} \partial R_{J\beta}} \right| \Phi_k^{(0)} \rangle + 2 \langle \Phi_k^{(0)} \left| \frac{\partial p_L}{\partial R_{I\alpha}} \right\rangle \omega_L \left\langle \frac{\partial p_L}{\partial R_{\beta j}} \right| \Phi_k^{(0)} \rangle \right) \\ &\quad + \left\langle \Phi_{k,q}^{(1)} \right| \frac{\partial V_{loc}}{\partial R_{J\beta}} \left| \Phi_k^{(0)} \right\rangle + \left\langle \Phi_k^{(0)} \right| \frac{\partial V_{loc}}{\partial R_{J\beta}} \left| \Phi_{k,q}^{(1)} \right\rangle \\ &\quad + \sum_L \left(\langle \Phi_{k,q}^{(1)} \left| \frac{\partial p_L}{\partial R_{J\beta}} \right\rangle \omega_L \langle p_L \mid \Phi_k^{(0)} \rangle + \langle \Phi_{k,q}^{(1)} \mid p_L \rangle \omega_L \left\langle \frac{\partial p_L}{\partial R_{J\beta}} \right| \Phi_k^{(0)} \rangle \right. \\ &\quad \left. \left. + \langle \Phi_k^{(0)} \left| \frac{\partial p_L}{\partial R_{J\beta}} \right\rangle \omega_L \langle p_L \mid \Phi_{k,q}^{(1)} \rangle + \langle \Phi_k^{(0)} \mid p_L \rangle \omega_L \left\langle \frac{\partial p_L}{\partial R_{\beta j}} \right| \Phi_{k,q}^{(1)} \rangle \right) \right] \end{aligned} \quad (9.30)$$

9.4 Polarizability

As discussed in the introduction, a case in which the perturbation cannot be expressed in a Hamiltonian form is that of an external electric field, which couples with the electric polarization $\mathbf{P}^{ele} = e\langle \mathbf{r} \rangle$ in a periodic system. The latter using the modern theory of

polarization in the Γ only sampling of the Brillouin zone can be written in terms of Berry phase φ_μ[83]:

$$\varphi_\mu = \mathrm{Im} \log \det \mathbf{Q}^{(\mu)}, \tag{9.31}$$

where the matrix $\mathbf{Q}^{(\mu)}$ is defined as

$$\mathbf{Q}^{(\mu)}_{i,j} = \left\langle \Phi_i \left| e^{i\mathbf{G}_\mu \cdot \mathbf{r}} \right| \Phi_j \right\rangle \quad , \tag{9.32}$$

$\mathbf{G}_\mu$ is the smallest vector in a periodically repeated cubic cell in the direction μ. Eq.(9.31) can be generalized to cells of arbitrary shape. This formula is in principle valid in the limit of an infinite dimension of the cell, but in a non conducting material this is a good approximation even with relatively small supercells. P^{ele}_μ is then given by:

$$P^{ele}_\mu = \frac{2\,|e|}{|G_\mu|}\varphi_\mu. \tag{9.33}$$

This induces a perturbation in the Kohn–Sham functional of the type:

$$\lambda E^{pert}\left[\{|\Phi_i\rangle\}\right] = -\mathbf{E}\cdot\mathbf{P}^{ele} = -\sum_\nu E_\nu \frac{2\,|e|}{|\mathbf{G}_\nu|}\mathrm{Im}\log\det\left\langle \Phi_i \left| e^{i\mathbf{G}_\nu\cdot\mathbf{r}}\right| \Phi_j\right\rangle. \tag{9.34}$$

In this case the perturbative parameter is E_ν and $|\Phi_i\rangle \simeq |\varphi^{(0)}_i\rangle - E_\nu|\Phi^{\nu(1)}_i\rangle$ The derivative $\delta E^{pert}\ /\delta\langle\varphi^{(0)}_i|$ and its ket conjugate can be evaluated using the formula for the derivative of a matrix A with respect to a generic variable x:

$$\frac{d}{dx}\ln\ \det A = \mathrm{Tr}\ \frac{dA_{ij}}{dx}A^{-1}_{ji}. \tag{9.35}$$

The perturbative term becomes:

$$\frac{2\,|e|}{|\mathbf{G}_\nu|}\mathrm{Im}\left[\sum_{i,j}\left(\left\langle\Phi^{\nu(1)}_i\left|e^{i\mathbf{G}_\nu\cdot\mathbf{r}}\right|\Phi^{(0)}_j\right\rangle + \left\langle\Phi^{(0)}_i\left|e^{i\mathbf{G}_\nu\cdot\mathbf{r}}\right|\phi^{\nu(1)}_j\right\rangle\right)\mathbf{Q}^{(\nu)-1}_{j,i}\right]. \tag{9.36}$$

Using this perturbative term we can calculate the first order correction to the wavefunctions $\{\Phi^{(1)}_i\}$. This allows to evaluate the induced dipole moment in the μ direction:

$$\begin{aligned}\delta P^{ele}_\mu &= \frac{2\,|e|}{|\mathbf{G}_\mu|}\delta\Phi_\mu \\ &= -\sum_\nu \frac{2\,|e|}{|\mathbf{G}_\nu|}\mathrm{Im}\left[\sum_{i,j}\left(\left\langle\Phi^{\nu(1)}_i\left|e^{i\mathbf{G}_\mu\cdot\mathbf{r}}\right|\Phi^{(0)}_j\right\rangle + \left\langle\Phi^{(0)}_i\left|e^{i\mathbf{G}_\mu\cdot\mathbf{r}}\right|\Phi^{\nu(1)}_j\right\rangle\right)\mathbf{Q}^{(\nu)-1}_{j,i}\right]\end{aligned} \tag{9.37}$$

and the polarizability $\alpha_{\mu,\nu} = -\partial P_\mu/\partial E_\nu$:

$$\alpha_{\mu,\nu} = \frac{2\,|e|}{|\mathbf{G}_\nu|}\mathrm{Im}\left[\sum_{i,j}\left(\left\langle\Phi^{\nu(1)}_i\left|e^{i\mathbf{G}_\mu\cdot\mathbf{r}}\right|\Phi^{(0)}_j\right\rangle + \left\langle\Phi^{(0)}_i\left|e^{i\mathbf{G}_\mu\cdot\mathbf{r}}\right|\Phi^{\nu(1)}_j\right\rangle\right)\mathbf{Q}^{(\nu)-1}_{j,i}\right]. \tag{9.38}$$

9.5 NMR Chemical Shifts

The *ab-initio* calculation of chemical shifts has become more and more popular, and over the years, many methods have been developed in the quantum chemistry community to perform such computations. A good review of the various approaches and recent developments in this field is given in [120]. One major problem that appears in these calculations is the choice of the gauge. While being in principle a cyclic variable, gauge can significantly affect the results in an actual calculation. To minimize this effect, several solutions have been proposed: in the GIAO method (Gauge Including Atomic Orbitals, [121]), one transforms the gauge of the basis set functions to the position of their nuclei, whereas in the IGLO method (Individual Gauges for Localized Orbitals, [122]), the gauges of the final wavefunctions are transformed to their centers of charge. The CSGT method (Continuous Set of Gauge Transformations, [123]) finally defines a gauge which depends on the position where the induced current is to be calculated. However, there is another issue that restricts the applicability of the existing implementations of these methods to isolated systems. The Hamiltonian, which represents the magnetic field, contains the position operator. In an extended system, which would typically be treated under periodic boundary conditions, this operator is ill-defined. In particular, this position operator and therefore the perturbation Hamiltonian operator do not have any periodicity, as would be required for periodic boundary conditions.
Mauri et al. have presented a formalism which allows the calculation of chemical shifts and other magnetic properties in extended systems using periodic boundary conditions [124]. This formulation is based on a magnetic field which is modulated in space. To return to the experimental situation of an homogeneous field, the limit of infinite modulation wavelength is evaluated numerically. This is done using a small, but finite wavevector.

An alternative method by Sebastiani and Parrinello [125] for extended systems in periodic boundary conditions takes advantage of the exponential decay properties of localized Wannier orbitals [126, 127] and treats these localized orbitals as virtually isolated. For the gauge problem, a particular variant of the CSGT method mentioned above [123] is adapted to these localized orbitals.

9.5.1 Chemical shifts and susceptibilities

When a magnetic field is applied to a medium, it induces a current due to the modification of the electronic ground state. This electronic current distribution induces an additional inhomogeneous magnetic field. The chemical shift tensor is defined as the proportionality factor between the induced and the externally applied magnetic field at the positions of the nuclei:

$$\sigma(\mathbf{R}) \;=\; \frac{\partial \mathbf{B}^{\mathrm{ind}}(\mathbf{R})}{\partial \mathbf{B}^{\mathrm{ext}}}. \tag{9.39}$$

The induced field is determined by the total electronic current $\mathbf{j}(\mathbf{r})$ through

$$\mathbf{B}^{\mathrm{ind}}(\mathbf{r}) \;=\; \frac{\mu_0}{4\pi}\int d^3r'\;\frac{\mathbf{r}'-\mathbf{r}}{|\mathbf{r}'-\mathbf{r}|^3}\times\mathbf{j}(\mathbf{r}'), \tag{9.40}$$

where μ_0 is the permeability of the vacuum. In periodic system also the current density will be periodic and we can calculate Eq. (9.40) in reciprocal space from the Fourier transform of the current:

$$\mathbf{B}^{\mathrm{ind}}(\mathbf{G}\neq 0) \;=\; -\mu_0\, i\,\frac{\mathbf{G}}{|\mathbf{G}|^2}\;\times\;\mathbf{j}(\mathbf{G}). \tag{9.41}$$

The $\mathbf{G}=0$ component of the field depends on the bulk magnetic susceptibility tensor, χ, and the shape of the sample:

$$\mathbf{B}^{\mathrm{ind}}(\mathbf{G}=0) \;=\; \kappa\,\chi\,\mathbf{B}^{\mathrm{ext}}. \tag{9.42}$$

In the case of a spherical system, the prefactor κ is given by $\kappa = 2/3$. The bulk susceptibility χ can also be expressed as a function of the orbital electronic current as

$$\chi \;=\; \frac{\mu_0}{2\Omega}\,\frac{\partial}{\partial\mathbf{B}^{\mathrm{ext}}}\int_\Omega d^3r\;\mathbf{r}\times\mathbf{j}(\mathbf{r}), \tag{9.43}$$

where the integral is done over one unit cell of volume Ω. A single cell is sufficient since the integral is invariant under translations of any lattice vector $\mathbf{R}_L$ because of

$$\mathbf{j}(\mathbf{r}+\mathbf{R}_L) \;=\; \mathbf{j}(\mathbf{r}) \tag{9.44}$$

$$\text{and}\quad \int_\Omega d^3r\;\mathbf{j}(\mathbf{r}) \;=\; 0. \tag{9.45}$$

Therefore, the integral over the complete sample can be written as the sum of integrals over unit cells, and all these integrals are equal. The molar susceptibility is related to χ through $\chi^m = \Omega N_L \chi$ with the Avogadro number N_L.
The standard procedure to obtain the orbital electronic current density $\mathbf{j}$ is perturbation theory. The field $\mathbf{B}$ is represented by a vector potential $\mathbf{A}$ satisfying $\mathbf{B} = \nabla\times\mathbf{A}(\mathbf{r})$. A typical choice for $\mathbf{A}$ in the case of a homogeneous magnetic field is

$$\mathbf{A}(\mathbf{r}) \;=\; -\frac{1}{2}\;(\mathbf{r}-\mathbf{R})\times\mathbf{B} \tag{9.46}$$

with a cyclic variable $\mathbf{R}$, the gauge origin. The perturbation Hamiltonians at first and second order in the field strength are given by:

$$\mathcal{H}^{(1)} \;=\; \frac{e}{m}\,\mathbf{p}\cdot\mathbf{A}(\mathbf{r}) \tag{9.47}$$

$$\mathcal{H}^{(2)} \;=\; \frac{e^2}{2m}\,\mathbf{A}(\mathbf{r})\cdot\mathbf{A}(\mathbf{r}), \tag{9.48}$$

with the momentum operator $\mathbf{p}$ and the charge e and mass m of the electron. The first order perturbation gives rise to a correction in the electronic ground state with respect to the unperturbed system:

$$\Phi = \Phi^{(0)} + B\Phi^{(1)}. \tag{9.49}$$

This correction $\Phi^{(1)}$ is responsible for the induced current, which can be obtained as:

$$\begin{aligned} \mathbf{j}(\mathbf{r}') &= \frac{e^2}{m}\,\mathbf{A}(\mathbf{r}')\,|\Phi^{(0)}(\mathbf{r}')|^2 \\ &\quad + \frac{e}{m}\langle\Phi^{(0)}|\Big[\mathbf{p}|\mathbf{r}'\rangle\langle\mathbf{r}'| + |\mathbf{r}'\rangle\langle\mathbf{r}'|\mathbf{p}\Big]|\Phi^{(1)}\rangle. \end{aligned} \tag{9.50}$$

9.5.2 The gauge origin problem

The current density, Eq. (9.50), written in terms of the orbital contributions $\mathbf{j}_k$, can be separated into the so-called dia– and paramagnetic terms:

$$\begin{aligned} \mathbf{j}(\mathbf{r}') &= \sum_k \mathbf{j}_k(\mathbf{r}') \quad = \quad \sum_k \mathbf{j}_k^{\mathrm{d}}(\mathbf{r}') + \mathbf{j}_k^{\mathrm{p}}(\mathbf{r}') \\ \mathbf{j}_k^{\mathrm{d}}(\mathbf{r}') &= \frac{e^2}{m}\,\mathbf{A}(\mathbf{r}')\,|\Phi_k^{(0)}(\mathbf{r}')|^2 \\ \mathbf{j}_k^{\mathrm{p}}(\mathbf{r}') &= \frac{e}{m}\,\langle\Phi_k^{(0)}|\Big[\mathbf{p}|\mathbf{r}'\rangle\langle\mathbf{r}'| + |\mathbf{r}'\rangle\langle\mathbf{r}'|\mathbf{p}\Big]|\Phi_k^{(1)}\rangle \end{aligned} \tag{9.51}$$

Both contributions individually depend on the gauge, whereas the total current $\mathbf{j}$ is gauge-independent. However, the two contributions are large numbers and have opposite signs. For our choice of the vector potential, Eq. (9.46), $\mathbf{A}(\mathbf{r})$ is linear in the gauge origin $\mathbf{R}$. Therefore, the diamagnetic current $\mathbf{j}_k^{\mathrm{d}}$ grows linearly in $\mathbf{R}$, and $\mathbf{j}_k^{\mathrm{p}}$ must compensate for this in order to fulfill the invariance of the total current. Thus, for large distances $|\mathbf{r}-\mathbf{R}|$, the current density $\mathbf{j}$ results from the cancellation of two large terms. In a computer simulation using a finite basis set, the gauge invariance of $\mathbf{j}$ is no longer numerically verified.

Many techniques have been developed to minimize this problem for isolated molecules [121, 122, 123]. For periodic systems the probably most natural approach is the so-called "$\mathbf{R} = \mathbf{r}$" – variant of the CSGT method [123]. For each point $\mathbf{r}'$ in space, the current density is calculated with the gauge origin $\mathbf{R}$ being set equal to $\mathbf{r}'$. This method makes the diamagnetic part vanish analytically:

$$\mathbf{j}_k^{\mathrm{d}}(\mathbf{r}') = 0, \tag{9.52}$$

such that cancellations of large numbers no longer occur. In practice, the current is computed as

$$\begin{aligned} \mathbf{j}_k(\mathbf{r}') &= \frac{e}{m}\,\langle\Phi_k^{(0)}|\left(\mathbf{p}|\mathbf{r}'\rangle\langle\mathbf{r}'| + |\mathbf{r}'\rangle\langle\mathbf{r}'|\mathbf{p}\right) \\ &\quad \Big[|\Phi_k^{\mathbf{r}\times\mathbf{p}}\rangle - \mathbf{r}'\times|\Phi_k^{\mathbf{p}}\rangle\Big]\cdot\mathbf{B}. \end{aligned} \tag{9.53}$$

Here, $|\Phi_k^{\mathbf{r}\times\mathbf{p}}\rangle$ and $|\Phi_k^{\mathbf{p}}\rangle$ are the first order perturbation wavefunctions for the special perturbation Hamiltonians:

$$|\Phi_k^{\mathbf{r}\times\mathbf{p}}\rangle \;\mapsto\; \mathcal{H}^{(1)} = \mathbf{r}\times\mathbf{p} \tag{9.54}$$

$$|\Phi_k^{\mathbf{p}}\rangle \;\mapsto\; \mathcal{H}^{(1)} = \mathbf{p}. \tag{9.55}$$

This formulation avoids actually calculating distinct wavefunctions $\Phi^{(1)}$ for each point $\mathbf{r}'$ in space. Denoting the perturbation theory Green's function:

$$\mathcal{G}_{lk} \;=\; -\left(\mathcal{H}^{(0)}\,\delta_{kl} - \langle\Phi_k^{(0)}|\mathcal{H}^{(0)}|\Phi_l^{(0)}\rangle\right)^{-1}, \tag{9.56}$$

we can formally express the first order perturbation wavefunctions for an arbitrary perturbation operator $\mathcal{O}$ as:

$$|\Phi_k^{\mathcal{O}}\rangle \;=\; \sum_l \mathcal{G}_{kl}\,\mathcal{O}\,|\Phi_l^{(0)}\rangle \tag{9.57}$$

where $\mathcal{O}$ is either $\mathbf{p}$ or $\mathbf{r}\times\mathbf{p}$. By expanding Eq. (9.57) in the basis of the unperturbed unoccupied orbitals, one would obtain the well-known sum-over-states expression for the first order perturbation wavefunction.
We do not use this Green's function formulation in the actual calculation, but rather perform a variational energy minimization (see section 9.5.4). Eq. (9.57) serves only as a compact notation to obtain a closed expression for the current density:

$$\begin{aligned}\mathbf{j}_k(\mathbf{r}') \;=\; & \frac{e}{m}\sum_l \langle\Phi_k^{(0)}|\left(\mathbf{p}|\mathbf{r}'\rangle\langle\mathbf{r}'| + |\mathbf{r}'\rangle\langle\mathbf{r}'|\mathbf{p}\right) \\ & \left[\mathcal{G}_{kl}\,\mathbf{r}\times\mathbf{p}\,|\Phi_l^{(0)}\rangle - \mathcal{G}_{kl}\,\mathbf{r}'\times\mathbf{p}\,|\Phi_l^{(0)}\rangle\right]\cdot\mathbf{B}.\end{aligned} \tag{9.58}$$

In this formulation, it becomes apparent that any simultaneous translation of the relative origin for the operator $\mathbf{r}$ and the gauge $\mathbf{R} = \mathbf{r}'$ automatically cancel each other out. In particular, the current is invariant under arbitrary orbital-specific translations $\mathbf{d}_l$:

$$\begin{aligned}\mathbf{j}_k(\mathbf{r}') \;=\; & \frac{e}{m}\sum_l \langle\Phi_k^{(0)}|\left(\mathbf{p}|\mathbf{r}'\rangle\langle\mathbf{r}'| + |\mathbf{r}'\rangle\langle\mathbf{r}'|\mathbf{p}\right) \\ & \left[\mathcal{G}_{kl}\,(\mathbf{r}-\mathbf{d}_l)\times\mathbf{p}\,|\Phi_l^{(0)}\rangle - \mathcal{G}_{kl}\,(\mathbf{r}'-\mathbf{d}_l)\times\mathbf{p}\,|\Phi_l^{(0)}\rangle\right]\cdot\mathbf{B}.\end{aligned} \tag{9.59}$$

This formulation looks somewhat similar to the well-known IGLO gauge transformation (individual gauges for localized orbitals, [122]), but it is not the same. Our physical gauge is always the $\mathbf{R} = \mathbf{r}'$ version of the CSGT method. However, this gauge still leaves the freedom to translate the coordinate system individually for each orbital, according to Eq. (9.59). A straightforward application of Eq. (9.59) would be too expensive. In fact, it would require one inversion of the Hamiltonian per real space mesh point $\mathbf{r}'$. However,

Figure 9.1: Two localized orbitals with specific position operators.

the second term of $\mathbf{j}_k$ can be rewritten as

$$\begin{aligned} -\frac{e}{m} \sum_l \langle \Phi_k^{(0)}| \left(\mathbf{p}|\mathbf{r}'\rangle\langle\mathbf{r}'| + |\mathbf{r}'\rangle\langle\mathbf{r}'|\mathbf{p} \right) \mathcal{G}_{kl} \, (\mathbf{r}' - \mathbf{d}_l) \times \, \mathbf{p} \, |\Phi_l^{(0)}\rangle \cdot \mathbf{B} \\ = \; -\frac{e}{m} \sum_l \langle \Phi_k^{(0)}| \left(\mathbf{p}|\mathbf{r}'\rangle\langle\mathbf{r}'| + |\mathbf{r}'\rangle\langle\mathbf{r}'|\mathbf{p} \right) (\mathbf{r}' - \mathbf{d}_k) \times \, \mathcal{G}_{kl} \, \mathbf{p} \, |\Phi_l^{(0)}\rangle \cdot \mathbf{B} \\ +\Delta\mathbf{j}_k(\mathbf{r}') \end{aligned} \tag{9.60}$$

where

$$\Delta\mathbf{j}_k(\mathbf{r}') \;=\; -\frac{e}{m} \sum_l \langle \Phi_k^{(0)}| \left(\mathbf{p}|\mathbf{r}'\rangle\langle\mathbf{r}'| + |\mathbf{r}'\rangle\langle\mathbf{r}'|\mathbf{p} \right) \, \mathcal{G}_{kl} \, (\mathbf{d}_k - \mathbf{d}_l) \times \, \mathbf{p} \, |\Phi_l^{(0)}\rangle \cdot \mathbf{B}. \tag{9.61}$$

The evaluation the first term of Eq. (9.60) can be done at the computational cost of one total energy calculation, while $\Delta\mathbf{j}_k$ requires one such calculation per electronic state k. At first sight, the sum $\Delta\mathbf{j} = \sum_k \Delta\mathbf{j}_k$ seems to be equal to zero, since the inner operator is antisymmetric in k, l. But since the momentum operators in Eq. (9.61) do not commute with the Green's function, $\Delta\mathbf{j}$ does not vanish unless all $\mathbf{d}_l$ are equal. However, for many systems $\Delta\mathbf{j}$ can be neglected.

9.5.3 The position operator problem

We first localize the wavefunctions by means of a unitary rotation in the occupied subspace. This is a technique well-known in quantum chemistry, where it is used to determine the location and the nature of chemical bonds. The rotation is chosen such that the spatial extension of the wavefunctions is minimal, yielding so-called maximally localized Wannier functions [126]. The extension is characterized by the second moment Δ_2 of the orbitals:

$$\Delta_2 \;=\; \sum_k \langle \Phi_k|\mathbf{r}^2|\Phi_k\rangle - \langle \Phi_k|\mathbf{r}|\Phi_k\rangle^2. \tag{9.62}$$

In a periodic system, special care is required to define the position operator properly. A solution to this problem in terms of a Berry phase approach [92] has been given by Marzari et al. [87]. A practical scheme to calculate maximally localized Wannier orbitals has recently been presented by Berghold et al. [128]. It can be shown that in an insulator, the resulting localized wavefunctions decay exponentially [127]. If the unit cell is chosen such that the lattice parameter is larger than the decay length, the orbital is significantly different from zero only within a limited region of the cell, and it practically vanishes everywhere else.
The next step is to assign individual *virtual cells* to these Wannier orbitals. The virtual cells are chosen such that for the corresponding wavefunction, the cell walls are located in

that region of space where the orbital density is close to zero over a certain range. Then, the position operator is defined normally running from $-L/2$ to $+L/2$ inside the virtual cell. At the walls, it makes a smooth transition back from $+L/2$ to $-L/2$, yielding a saw-tooth shape (see fig. 9.1). This jump is not sharp in order to avoid components of very high frequency in the operator. As a consequence of this definition, the position operator now matches the periodic boundary conditions, since it is identical in every virtual cell and all its replica.
This transformation does not affect the orbitals gauge. If it would, additional terms in the perturbation Hamiltonian and the wavefunction orthonormality relations, as in the IGLO method, would appear. The crucial difference is that no individual orbital gauge origins are used; the gauge is always "$\mathbf{R} = \mathbf{r}'$". Instead, an individual reference system is defined for both $\mathbf{r}$ and $\mathbf{R}$ simultaneously, as described by the relative origins $\mathbf{d}_k$ in Eq. (9.59).
The problem that arises for this construction is that the new operator has a completely unphysical shape around the borders of the virtual cell, where it makes its jump (at $x = nL$). But by choosing the virtual cells as described above, the unphysical transitions lie in those regions of space where the wavefunction vanishes. As a consequence, the problematic part of the operator is only applied where it has no effect anyway.
Hence, the saw-tooth shape of the position operator as indicated by fig. 9.1 is a reasonable approximation as long as the wavefunctions are sufficiently localized.
However, this represents a certain restriction for this method. We require that the decay length be significantly smaller than the lattice constant of the simulation box, as mentioned above. Only in such a case can the virtual cell be chosen with its borders in a region of vanishing density. It follows that for a system with truly delocalize orbitals, like a metal, this approach is not applicable. In such a system, the decay of the Wannier orbitals is only algebraic, and the necessary cell size would far exceed the computationally tractable volume.

9.5.4 Density functional perturbation theory

We can now use density functional perturbation theory introduced before to calculate the response orbitals. The derivation has strong analogies with other variational schemes used in quantum chemistry. In particular, it is similar to the stationary perturbation theory by Kutzelnigg [129] which is used in the IGLO implementation. We start from a functional for the second-order energy of the system which is variational in the first order perturbation wavefunctions $\Phi^{(1)}$:

$$\begin{aligned} E^{(2)} &= \sum_{kl} \langle \Phi_k^{(1)} | \mathcal{H}^{(0)}\, \delta_{kl} - \lambda_{kl} | \Phi_l^{(1)} \rangle \\ &\quad + \sum_k \left[\langle \Phi_k^{(1)} | \mathcal{H}^{(1)} | \Phi_k^{(0)} \rangle + \langle \Phi_k^{(0)} | \mathcal{H}^{(1)} | \Phi_k^{(1)} \rangle \right] \\ &\quad + \frac{1}{2} \int \mathrm{d}^3 r\, \mathrm{d}^3 r'\, \frac{\delta^2 E_{\mathrm{Hxc}}}{[n^{(0)}]} \delta n(\mathbf{r}) \delta n(\mathbf{r}')\ \ n^{(1)}(\mathbf{r}) n^{(1)}(\mathbf{r}'). \end{aligned} \tag{9.63}$$

The second order energy is variational in the first order perturbation wavefunctions under the orthogonality constraint:

$$\frac{\delta E^{(2)}}{\delta \Phi^{(1)}} = 0. \tag{9.64}$$

In our case, the perturbation is a magnetic field. The energy functional simplifies considerably because the first order density analytically vanishes everywhere. The reason is that the perturbation Hamiltonian and the first order wavefunctions are purely imaginary, and thus, the two terms in the response density cancel each other out. The matrix element of the magnetic perturbation Hamiltonian, Eq. (9.47), in the position representation is given by:

$$\langle \mathbf{r}|\mathcal{H}^{(1)}|\mathbf{r}'\rangle = i\,\frac{\hbar e}{2m}\,\delta^3(\mathbf{r}-\mathbf{r}')\;\;(\mathbf{r}-\mathbf{R})\times\mathbf{B}\cdot\nabla. \tag{9.65}$$

It is purely imaginary, so that with real wavefunctions and a necessarily real energy, the first order orbitals $\Phi_k^{(1)}$ must be purely imaginary, too. Hence, the first order density vanishes analytically for magnetic perturbations, and the energy functional, Eq. (9.63), simplifies to:

$$\begin{aligned} E^{(2)} &= \sum_{kl} \langle \Phi_k^{(1)}|\mathcal{H}^{(0)}\,\delta_{kl} - \lambda_{kl}|\Phi_l^{(1)}\rangle \\ &\quad + \sum_k \left[\langle \Phi_k^{(1)}|\mathcal{H}^{(1)}|\Phi_k^{(0)}\rangle + \langle \Phi_k^{(0)}|\mathcal{H}^{(1)}|\Phi_k^{(1)}\rangle\right]. \end{aligned} \tag{9.66}$$

The stationarity condition on the energy, Eq. (9.64), can be written as an inhomogeneous system of coupled equations for the $\Phi_k^{(1)}$:

$$\sum_l \left(\mathcal{H}^{(0)}\,\delta_{kl} - \lambda_{kl}\right)|\Phi_l^{(1)}\rangle = -\mathcal{H}^{(1)}|\Phi_k^{(0)}\rangle. \tag{9.67}$$

9.5.5 Pseudopotential correction

In pseudopotential/ plane wave calculations no core orbitals are taken into account, and the valence wavefunctions have an incorrect shape in the core region. The chemical shift is extremely sensitive to precisely that region of space, because the interaction between nuclear spin and current is proportional to $1/r^2$. Thus, it is not clear a priori whether a pseudopotential implementation can give meaningful results at all. Often, the contribution of the core orbitals to the chemical shift is almost constant with respect to the chemical environment of the atom. In the recent investigation of Gregor *et al.* [130], it has been shown that this property can be exploited to correct for the frozen-core approximation. A simple additive constant is sufficient to reproduce the all-electron shieldings satisfactorily in many cases.

Lecture 10

Excited States

10.1 Restricted Open–shell Kohn–Sham Method

For large–gap systems with well separated electronic states it might be desirable to single out a particular state in order to allow the nuclei to move on the associated excited state potential energy surface. Approaches that rely on fractional occupation numbers such as ensemble density functional theories are difficult to adapt for cases where the symmetry and / or spin of the electronic state should be fixed [24]. An early approach in order to select a particular excited state was based on introducing a "quadratic restoring potential" which vanishes only at the eigenvalue of the particular state [131].
A method that combines Roothaan's symmetry–adapted wavefunctions with Kohn–Sham density functional theory was proposed in Ref. [132] and used to simulate a photoisomerization via molecular dynamics. Viewed from Kohn–Sham theory this approach consists in building up the spin density of an open–shell system based on a symmetry–adapted wavefunction that is constructed from spin–restricted determinants (the "microstates"). Viewed from the restricted open–shell Hartree–Fock theory *à la* Roothaan it amounts essentially to replacing Hartree–Fock exchange by an approximate exchange–correlation density functional. This procedure leads to an orbital–dependent density functional which was formulated explicitely for the first–excited singlet state S_1 in Ref. [132]. The relation of this approach to previous theories is discussed in some detail in Ref. [132]. In particular, the success of the closely–related Ziegler–Rauk–Baerends "sum methods" [134, 135] was an important stimulus. More recently several papers [136, 137, 133] appeared that are similar in spirit to the method of Ref. [132]. The approach of Refs. [133] can be viewed as a generalization of the special case (S_1 state) worked out in Ref. [132] to arbitrary spin states. In addition, the generalized method [133] was derived within the framework of density functional theory, whereas the wavefunction perspective was the starting point in Ref. [132].
In the following, the method is outlined with the focus to perform molecular dynamics in the S_1 state. Promoting one electron from the HOMO to the LUMO in a closed–shell system

Figure 10.1: Four possible determinants $|t_1\rangle$, $|t_2\rangle$, $|m_1\rangle$ and $|m_2\rangle$ as a result of the promotion of a single electron from the HOMO to the LUMO of a closed shell system, see text for further details. Taken from Ref. [132].

Figure 10.2: Four patterns of spin densities n_t^α, n_t^β, n_m^α, and n_m^β corresponding to the two spin–restricted determinants $|t\rangle$ and $|m\rangle$ sketched in Fig. 10.1, see text for further details. Taken from Ref. [132].

with $2n$ electrons assigned to n doubly occupied orbitals (that is spin–restricted orbitals that have the same spatial part for both spin up α and spin down β electrons) leads to four different excited wavefunctions or determinants, see Fig. 10.1 for a sketch. Two states $|t_1\rangle$ and $|t_2\rangle$ are energetically degenerate triplets t whereas the two states $|m_1\rangle$ and $|m_2\rangle$ are not eigenfunctions of the total spin operator and thus degenerate mixed states m ("spin contamination"). Note in particular that the m states do not correspond – as is well known – to singlet states despite the suggestive occupation pattern in Fig. 10.1. However, suitable Clebsch–Gordon projections of the mixed states $|m_1\rangle$ and $|m_2\rangle$ yield another triplet state $|t_3\rangle$ and the desired first excited singlet or S_1 state $|s_1\rangle$. Here, the ansatz [132] for the total energy of the S_1 state is given by

$$E_{S_1}\left[\{\phi_i\}\right] \;=\; 2E_m^{\mathrm{KS}}\left[\{\phi_i\}\right] - E_t^{\mathrm{KS}}\left[\{\phi_i\}\right] \tag{10.1}$$

where the energies of the mixed and triplet determinants

$$E_m^{\mathrm{KS}}[\{\phi_i\}] \;=\; T_{\mathrm{s}}[n] + \int d\mathbf{r}\;\; V_{\mathrm{ext}}(\mathbf{r})n(\mathbf{r}) + \frac{1}{2}\int d\mathbf{r}\;\; V_{\mathrm{H}}(\mathbf{r})n(\mathbf{r}) + E_{\mathrm{xc}}[n_m^\alpha, n_m^\beta] \tag{10.2}$$

$$E_t^{\mathrm{KS}}[\{\phi_i\}] \;=\; T_{\mathrm{s}}[n] + \int d\mathbf{r}\;\; V_{\mathrm{ext}}(\mathbf{r})n(\mathbf{r}) + \frac{1}{2}\int d\mathbf{r}\;\; V_{\mathrm{H}}(\mathbf{r})n(\mathbf{r}) + E_{\mathrm{xc}}[n_t^\alpha, n_t^\beta] \tag{10.3}$$

are expressed in terms of (restricted) Kohn–Sham spin–density functionals constructed from the set $\{\phi_i\}$, cf. Eq. (2.1). The associated S_1 wavefunction is given by

$$|\,s_1\left[\{\phi_i\}\right]\rangle = \sqrt{2}\,|\,m\left[\{\phi_i\}\right]\rangle - |\,t\left[\{\phi_i\}\right]\rangle \tag{10.4}$$

where the "microstates" m and t are both constructed from the same set $\{\phi_i\}$ of $n+1$ spin–*restricted* orbitals. Using this particular set of orbitals the total density

$$n(\mathbf{r}) \;=\; n_m^\alpha(\mathbf{r}) + n_m^\beta(\mathbf{r}) = n_t^\alpha(\mathbf{r}) + n_t^\beta(\mathbf{r}) \tag{10.5}$$

is of course identical for both the m and t determinants whereas their spin densities clearly differ, see Fig. 10.2. Thus, the decisive difference between the m and t functionals Eq. (10.2) and Eq. (10.3), respectively, comes exclusively from the exchange–correlation

functional $E_{\rm xc}$, whereas kinetic, external and Hartree energy are identical by construction. Note that this basic philosophy can be generalized to other spin–states by adapting suitably the microstates and the corresponding coefficients in Eq. (10.1) and Eq. (10.4). Having defined a density functional for the first excited singlet state the corresponding Kohn–Sham equations are obtained by varying Eq. (10.1) using Eq. (10.2) and Eq. (10.3) subject to the orthonormality constraint $\sum_{i,j=1}^{n+1}\Lambda_{ij}(\langle\phi_i \mid \phi_j\rangle - \delta_{ij})$. Following this procedure the equation for the doubly occupied orbitals $i = 1, \ldots, n-1$ reads

$$\begin{aligned}
\Big\{ & -\frac{1}{2}\nabla^2 + V_{\rm H}(\mathbf{r}) + V_{\rm ext}(\mathbf{r}) \\
+ & V_{\rm xc}^{\alpha}[n_m^{\alpha}(\mathbf{r}), n_m^{\beta}(\mathbf{r})] + V_{\rm xc}^{\beta}[n_m^{\alpha}(\mathbf{r}), n_m^{\beta}(\mathbf{r})] \\
- & \frac{1}{2}V_{\rm xc}^{\alpha}[n_t^{\alpha}(\mathbf{r}), n_t^{\beta}(\mathbf{r})] - \frac{1}{2}V_{\rm xc}^{\beta}[n_t^{\alpha}(\mathbf{r}), n_t^{\beta}(\mathbf{r})]\Big\}\phi_i(\mathbf{r}) = \sum_{j=1}^{n+1}\Lambda_{ij}\phi_j(\mathbf{r})
\end{aligned} \tag{10.6}$$

whereas

$$\begin{aligned}
\Big\{ & \frac{1}{2}\Big[-\frac{1}{2}\nabla^2 + V_{\rm H}(\mathbf{r}) + V_{\rm ext}(\mathbf{r})\Big] \\
+ & V_{\rm xc}^{\alpha}[n_m^{\alpha}(\mathbf{r}), n_m^{\beta}(\mathbf{r})] - \frac{1}{2}V_{\rm xc}^{\alpha}[n_t^{\alpha}(\mathbf{r}), n_t^{\beta}(\mathbf{r})]\Big\}\phi_{\rm a}(\mathbf{r}) = \sum_{j=1}^{n+1}\Lambda_{aj}\phi_j(\mathbf{r})\ ,
\end{aligned} \tag{10.7}$$

and

$$\begin{aligned}
\Big\{ & \frac{1}{2}\Big[-\frac{1}{2}\nabla^2 + V_{\rm H}(\mathbf{r}) + V_{\rm ext}(\mathbf{r})\Big] \\
+ & V_{\rm xc}^{\beta}[n_m^{\alpha}(\mathbf{r}), n_m^{\beta}(\mathbf{r})] - \frac{1}{2}V_{\rm xc}^{\alpha}[n_t^{\alpha}(\mathbf{r}), n_t^{\beta}(\mathbf{r})]\Big\}\phi_{\rm b}(\mathbf{r}) = \sum_{j=1}^{n+1}\Lambda_{bj}\phi_j(\mathbf{r})\ .
\end{aligned} \tag{10.8}$$

are two *different* equations for the two singly–occupied open–shell orbitals a and b, respectively, see Fig. 10.1. Note that these Kohn–Sham–like equations feature an orbital–dependent exchange–correlation potential where $V_{\rm xc}^{\alpha}[n_m^{\alpha}, n_m^{\beta}] = \delta E_{\rm xc}[n_m^{\alpha}, n_m^{\beta}]/\delta n_m^{\alpha}$ and analogues definitions hold for the β and t cases.
The set of equations Eq. (10.6)–(10.8) could be solved by diagonalization of the corresponding "restricted open–shell Kohn–Sham Hamiltonian" or alternatively by direct minimization of the associated total energy functional. The algorithm proposed in Ref. [138], allows to properly and efficiently minimize such orbital–dependent functionals including the orthonormality constraints.

10.2 Time–Dependent Density Functional Theory

In recent years time–dependent density functional theory (TDDFT) has been laid on rigorous foundations [139, 140]. However, its roots go back to the time–dependent Thomas–Fermi theory by Bloch [141]. Like the original time–independent theory the formalism rests on two basic theorems:

- Every observable can be calculated from the density alone, i.e. each observable can be written as a functional of the density.
- The density of the interacting system can be obtained as the density of an auxiliary system of non–interacting particles moving in an effective local single–particle potential, the Kohn–Sham potential.

The time–dependent Kohn–Sham formalism can be summarized as follows: the density of the interacting system can be obtained from

$$n(\mathbf{r},t) = \sum_{i=1}^{N} \mid \Phi_i(\mathbf{r},t) \mid^2 \tag{10.9}$$

with orbitals $\Phi_i(\mathbf{r},t)$ satisfying the time–dependent Kohn–Sham equation

$$i\frac{\partial}{\partial t}\Phi_i(\mathbf{r},t) = \left(-\frac{1}{2}\nabla^2 + V_{\rm s}[n](\mathbf{r},t)\right)\Phi_i(\mathbf{r},t) \ . \tag{10.10}$$

The single–particle potential $V_{\rm s}$ is written as

$$V_{\rm s}[n](\mathbf{r},t) = V_{\rm ext}(\mathbf{r},t) + \int d\mathbf{r}\ \frac{n(\mathbf{r}',t)}{\mid \mathbf{r}-\mathbf{r}' \mid} + V_{\rm xc}[n](\mathbf{r},t) \ , \tag{10.11}$$

where $V_{\rm ext}(\mathbf{r},t)$ is the external time–dependent field. The last equations defines the exchange and correlation potential $V_{\rm xc}$, a quantity that in practicle applications has to be approximated. The simplest possible approximation is the adiabatic local density approximation

$$V_{\rm xc}^{\rm ALDA}(\mathbf{r},t) = V_{\rm xc}^{\rm LDA}[n(\mathbf{r},t)] \tag{10.12}$$

and its gradient corrected generalizations.
Most applications of TDDFT have been done in the linear response regime. However, also direct applications of the TDDFT equations have been used for the simulation of the interaction of matter with ultra–intense laser pulses or to simulate the time evolution of complex systems.

10.3 Excited States from Linear Response

Linear response to the time–dependent Kohn–Sham equations can be derived along the same line as in the time–independent case. However, here a slightly different route will be followed.
In an orthonormal basis $\{\varphi_p(\mathbf{r})\}$ the starting point for the derivation of the excitation energies is the time–dependent Kohn–Sham equation[139]

$$\sum_q \{F_{pq\sigma}P_{qr\sigma} - P_{pq\sigma}F_{qr\sigma}\} = i\frac{\partial P_{pr\sigma}}{\partial t} \tag{10.13}$$

together with the idem–potency condition

$$\sum_q P_{pq\sigma} P_{qr\sigma} = P_{pr\sigma} \tag{10.14}$$

where F and P are the Kohn–Sham Hamiltonian and density matrices, respectively, p, q, r are basis set indices and σ denotes spin. The Hamiltonian matrix elements are

$$\begin{aligned} F_{pq\sigma} &= \int \varphi_p^\star(\mathbf{r}) \left(-\frac{1}{2}\nabla^2 + \sum_A \frac{-Z_A}{\mid \mathbf{r} - \mathbf{R}_A \mid} \right. \\ &\quad \left. + \int \frac{n(\mathbf{r}')}{\mid \mathbf{r} - \mathbf{r}' \mid} d\mathbf{r}' + \frac{\partial E_{\mathrm{XC}}}{\partial n_\sigma(\mathbf{r})} \right) \varphi_q(\mathbf{r}) d\mathbf{r}, \end{aligned} \tag{10.15}$$

where the adiabatic approximation for the exchange and correlation term was used. The spin density $n_\sigma(\mathbf{r})$ is related to the density matrix in the usual way

$$n_\sigma(\mathbf{r}) = \sum_{pq} P_{pq\sigma}\ \varphi_p(\mathbf{r}) \varphi_q^\star(\mathbf{r}). \tag{10.16}$$

Initially the system is assumed to be in a stationary state, which is described by the Hamiltonian $F^0_{pq\sigma}$ and density matrix $P^0_{pq\sigma}$. Then we apply an oscillatory perturbation

$$g_{pq\sigma} = \frac{1}{2} \left[f_{pq\sigma} \exp\left(-i\omega t\right) + f^\star_{pq\sigma} \exp\left(i\omega t\right) \right]. \tag{10.17}$$

The linear response of the density matrix P^1 to the applied perturbation is

$$P_{pq\sigma} = P^0_{pq\sigma} + P^1_{pq\sigma} \tag{10.18}$$

with

$$P^1_{pq\sigma} = \frac{1}{2} \left[d_{pq\sigma} \exp\left(-i\omega t\right) + d^\star_{qp\sigma} \exp\left(i\omega t\right) \right]. \tag{10.19}$$

The first order change in the Hamiltonian consists of the applied perturbation $g_{pq\sigma}$ and the part induced by the linear response of the density matrix

$$F_{pq\sigma} = F^0_{pq\sigma} + g_{pq\sigma} + \sum_{rs\tau} \frac{\partial F^0_{pq\sigma}}{\partial P^0_{rs\tau}} P^1_{rs\tau}. \tag{10.20}$$

Substituting Eqs. (10.17) to (10.20) to the time-dependent Kohn–Sham Eq. (10.13) and collecting terms which are multiplied by the factor $\exp\left(-i\omega t\right)$ we obtain

$$\sum_q \left[F^0_{pq\sigma} d_{qr\sigma} - d_{pq\sigma} F^0_{qr\sigma} + \left(f_{pq\sigma} + W_{pq\sigma}\right) P^0_{qr\sigma} - P^0_{pq\sigma} \left(f_{qr\sigma} + W_{qr\sigma}\right) \right] = \omega d_{pr\sigma}, \tag{10.21}$$

where we have used the definition

$$W_{pq\sigma} = \sum_{st\tau} \frac{\partial F^0_{pq\sigma}}{\partial P^0_{st\tau}} d_{st\tau}. \tag{10.22}$$

The idem–potency conditions to first order are

$$\sum_q P^0_{pq\sigma} P^0_{qr\sigma} = P^0_{pr\sigma}, \tag{10.23}$$

$$\sum_q P^0_{pq\sigma} d_{qr\sigma} + d_{pq\sigma} P^0_{qr\sigma} = d_{pr\sigma}. \tag{10.24}$$

Expansion of the wavefunction to first order

$$\phi_{n\sigma}(\mathbf{r}) = \phi^0_{n\sigma}(\mathbf{r}) + \frac{1}{2}\left\{\phi^{-1}_{n\sigma}(\mathbf{r}) \exp(-i\omega t) + \phi^{+1}_{n\sigma}(\mathbf{r}) \exp(i\omega t)\right\} \tag{10.25}$$

in the basis set

$$\phi^0_{n\sigma}(\mathbf{r}) = \sum_p c^0_{pn\sigma} \varphi_p(\mathbf{r}) \tag{10.26}$$

$$\phi^{-1}_{n\sigma}(\mathbf{r}) = \sum_p c^{-1}_{pn\sigma} \varphi_p(\mathbf{r}) \tag{10.27}$$

$$\phi^{+1}_{n\sigma}(\mathbf{r}) = \sum_p c^{+1}_{pn\sigma} \varphi_p(\mathbf{r}) \tag{10.28}$$

defines the coefficients c^0, c^{-1}, c^{+1}. Expanding the density we get expressions for the zeroth and first order density matrices

$$P^0_{pq\sigma} = \sum_n c^0_{pn\sigma} (c^0_{qn\sigma})^\star \tag{10.29}$$

$$d_{pq\sigma} = \sum_n c^0_{pn\sigma} (c^{+1}_{qn\sigma})^\star + c^{-1}_{pn\sigma} (c^0_{qn\sigma})^\star \tag{10.30}$$

$$(d_{qp\sigma})^\star = \sum_n c^0_{pn\sigma} (c^{-1}_{qn\sigma})^\star + c^{+1}_{pn\sigma} (c^0_{qn\sigma})^\star \ . \tag{10.31}$$

From the idem–potency conditions for the density matrices orthogonality conditions for the wavefunctions can be derived.

$$\sum_q (c^0_{qn\sigma})^\star c^0_{qm\sigma} = \delta_{nm} \tag{10.32}$$

$$\sum_q (c^0_{qn\sigma})^\star c^{+1}_{qm\sigma} + (c^{-1}_{qn\sigma})^\star c^0_{qm\sigma} = 0 \tag{10.33}$$

There are different possibilities to fulfill the orthogonality condition for the first order wavefunction. In the following we will use the conditions (parallel transport gauge)

$$\sum_q (c^0_{qn\sigma})^\star c^{+1}_{qm\sigma} = 0 \tag{10.34}$$

$$\sum_q (c^{-1}_{qn\sigma})^\star c^0_{qm\sigma} = 0 \tag{10.35}$$

This means that the response orbitals are chosen orthogonal to the occupied subspace. These definitions are substituted in Eq. (10.21).

$$\begin{aligned}
&\sum_n \sum_q \Big[F^0_{pq\sigma} \left(c^0_{qn\sigma} (c^{+1}_{rn\sigma})^\star + c^{-1}_{qn\sigma} (c^0_{rn\sigma})^\star \right) - \left(c^0_{pn\sigma} (c^{+1}_{qn\sigma})^\star + c^{-1}_{pn\sigma} (c^0_{qn\sigma})^\star \right) F^0_{qr\sigma} \\
&+ \left(f_{pq\sigma} + W_{pq\sigma} \right) c^0_{qn\sigma} (c^0_{rn\sigma})^\star - c^0_{pn\sigma} (c^0_{qn\sigma})^\star \left(f_{qr\sigma} + W_{qr\sigma} \right) \Big] \\
= \; & \sum_n \omega \left(c^0_{pn\sigma} (c^{+1}_{rn\sigma})^\star + c^{-1}_{pn\sigma} (c^0_{rn\sigma})^\star \right)
\end{aligned} \tag{10.36}$$

The Kohn–Sham Hamiltonian projected on the occupied orbitals is defined as

$$\Gamma_{nm\sigma} = \sum_{pq} (c^0_{qn\sigma})^\star F^0_{qp\sigma} c^0_{pm\sigma}. \tag{10.37}$$

Multiplying Eq. (10.36) from the left with $(c^0_{pm\sigma})^\star$ and summing over p, we get after some rearrangements

$$\sum_q F^0_{rq\sigma} c^{+1}_{qm\sigma} - \sum_n c^{+1}_{rn\sigma} \Gamma^0_{nm\sigma} + \sum_{pq} \left(\delta_{rp} - P^0_{rp\sigma} \right) \left(f_{pq\sigma} + W_{pq\sigma} \right) c^0_{qm\sigma} = -\omega c^{+1}_{rm\sigma}. \tag{10.38}$$

If we now redo this procedure, but starting by multiplying Eq. (10.36) from the right with $c^0_{rm\sigma}$ and summing over r, we get a similar equation for c^{-1}. Finally, both equations can be written in short form

$$\sum_q F^0_{rq\sigma} c^{\pm 1}_{qm\sigma} - \sum_n c^{\pm 1}_{rn\sigma} \Gamma^0_{nm\sigma} + \sum_{pq} \left(\delta_{rp} - P^0_{rp\sigma} \right) \left(f_{pq\sigma} + W_{pq\sigma} \right) c^0_{qm\sigma} = \mp \omega c^{\pm 1}_{rm\sigma}. \tag{10.39}$$

Next, we introduce linear combination of the response vectors

$$x_{pn\sigma} = c^{+1}_{pn\sigma} + c^{-1}_{pn\sigma} \tag{10.40}$$

$$y_{pn\sigma} = c^{+1}_{pn\sigma} - c^{-1}_{pn\sigma} \tag{10.41}$$

and rewrite, for real wave functions

$$\begin{aligned}
W_{pq\sigma} &= \sum_{st\tau} \frac{\partial F_{pq\sigma}}{\partial P_{st\tau}} d_{st\tau} \\
&= \sum_{st\tau} \frac{\partial F_{pq\sigma}}{\partial P_{st\tau}} \left(\sum_n c^0_{sn\tau} (c^{+1}_{tn\tau})^\star + c^{-1}_{sn\tau} (c^0_{tn\tau})^\star \right) \\
&= \sum_{st\tau} \frac{\partial F_{pq\sigma}}{\partial P_{st\tau}} \left(\sum_n x_{sn\tau} (c^0_{tn\tau})^\star \right) \\
&= W_{pq\sigma}(x).
\end{aligned}$$

With this new definitions, we can add and subtract the Eqs.(10.39) and get

$$\begin{aligned} \sum_q F^0_{rq\sigma} x_{qm\sigma} - \sum_n x_{rn\sigma}\Gamma^0_{nm\sigma} & & \\ +2\sum_{pq}\left(\delta_{rp} - P^0_{rp\sigma}\right)\left(f_{pq\sigma} + W_{pq\sigma}(x)\right)c^0_{qm\sigma} &= -\omega y_{rm\sigma} & (10.42)\\ \sum_q F^0_{rq\sigma} y_{qm\sigma} - \sum_n y_{rn\sigma}\Gamma^0_{nm\sigma} &= -\omega x_{rm\sigma}, & (10.43) \end{aligned}$$

or in compact form

$$\begin{aligned} \sum_{qn\tau}\left\{\left(A_{rm\sigma,qn\tau} + B_{rm\sigma,qn\tau}\right)x_{qn\tau} + \omega\delta_{rq}\delta_{nm}\delta_{\sigma\tau}y_{qn\tau}\right\} &= b_{rm\sigma} & (10.44)\\ \sum_{qn\tau}\left\{\left(A_{rm\sigma,qn\tau} - B_{rm\sigma,qn\tau}\right)y_{qn\tau} + \omega\delta_{rq}\delta_{nm}\delta_{\sigma\tau}x_{qn\tau}\right\} &= 0 & (10.45) \end{aligned}$$

Solving the first equation for $\mathbf{y}$ and introducing the result into the second equation leads to the final system of equations

$$\begin{aligned} \left\{\left(\mathbf{A}-\mathbf{B}\right)\left(\mathbf{A}+\mathbf{B}\right) - \omega^2\mathbf{1}\right\}\mathbf{x} &= \left(\mathbf{A}-\mathbf{B}\right)\mathbf{b} & (10.46)\\ \left\{\left(\mathbf{A}+\mathbf{B}\right)\left(\mathbf{A}-\mathbf{B}\right) - \omega^2\mathbf{1}\right\}\mathbf{y} &= -\omega\mathbf{b} & (10.47) \end{aligned}$$

where the matrices $\mathbf{A}$ and $\mathbf{B}$ are defined by

$$\begin{aligned} A_{rm\sigma,qn\tau} &= F^0_{rq\sigma}\delta_{nm}\delta_{\sigma\tau} - \tilde{F}^0_{nm\sigma}\delta_{rq}\delta_{\sigma\tau} \\ &\quad + \sum_{spt}\left(\delta_{rp} - P^0_{rp\sigma}\right)\frac{\partial F^0_{ps\sigma}}{\partial P^0_{qt\tau}}c^0_{sm\sigma}(c^0_{tn\tau})^\star & (10.48)\\ B_{rm\sigma,qn\tau} &= \sum_{spt}\left(\delta_{rp} - P^0_{rp\sigma}\right)\frac{\partial F^0_{ps\sigma}}{\partial P^0_{qt\tau}}c^0_{sm\sigma}(c^0_{tn\tau})^\star & (10.49) \end{aligned}$$

and the vector $\mathbf{b}$

$$b_{rm\sigma} = \sum_{qp}\left(\delta_{rp} - P^0_{rp\sigma}\right)f_{pq\sigma}c^0_{qm\sigma} \tag{10.50}$$

The polarizability tensor is defined by

$$\alpha_{\mu\nu}(-\omega;\omega) = -\mathbf{x}_\mu{}^T\mathbf{f}^\nu. \tag{10.51}$$

Solving formally Eq.(10.46) for $\mathbf{x}$ yields

$$\mathbf{x}_\mu = \left[\left(\mathbf{A}-\mathbf{B}\right)\left(\mathbf{A}+\mathbf{B}\right) - \omega^2\mathbf{1}\right]^{-1}\left(\mathbf{A}-\mathbf{B}\right)\mathbf{b}^\mu \tag{10.52}$$

that can be rewritten using the spectral representation

$$\left[\left(\mathbf{A}-\mathbf{B}\right)\left(\mathbf{A}+\mathbf{B}\right) - \omega^2\mathbf{1}\right] = \mathbf{U}\left(\mathbf{\Lambda} - \omega^2\mathbf{1}\right)\mathbf{V}^T \tag{10.53}$$

where $\mathbf{\Lambda}$ is the diagonal matrix of eigenvalues.

$$\mathbf{x}_\mu = \mathbf{U}\left[\mathbf{\Lambda} - \omega^2\mathbf{1}\right]^{-1}\mathbf{V}^T\left(\mathbf{A}-\mathbf{B}\right)\mathbf{b}^\mu \tag{10.54}$$

$$\alpha_{\mu\nu}(-\omega;\omega) = -\left[\left(\mathbf{A}-\mathbf{B}\right)\mathbf{b}^\mu\right]^T\mathbf{V}\left[\mathbf{\Lambda} - \omega^2\mathbf{1}\right]^{-1}\mathbf{U}^T\mathbf{f}^\nu. \tag{10.55}$$

Excitation energies are defined as the poles of this equation and oscillator strengths are calculated by comparing to the definition

$$\bar{\alpha} = \frac{1}{3}\mathrm{Tr}(\alpha) = \sum_i \frac{f_i}{\omega_i^2 - \omega^2} \tag{10.56}$$

From this we get the final results

$$\left(\mathbf{A}-\mathbf{B}\right)\left(\mathbf{A}+\mathbf{B}\right)\mathbf{x}_i = \omega^2\mathbf{x}_i \tag{10.57}$$

$$\left(\mathbf{A}+\mathbf{B}\right)\left(\mathbf{A}-\mathbf{B}\right)\mathbf{y}_i = \omega^2\mathbf{y}_i \tag{10.58}$$

with $\mathbf{x}$ and $\mathbf{y}$ the right and left normalized eigenfunctions, $\mathbf{y}^T\mathbf{x} = 1$.

$$f_i = -\frac{1}{3}\sum_\mu\left[\left(\mathbf{A}-\mathbf{B}\right)\mathbf{b}^\mu\right]^T\mathbf{x}_i\mathbf{y}_i^T\mathbf{f}^\mu \tag{10.59}$$

10.3.1 Tamm-Dancoff Approximation

In the Tamm-Dancoff approximation to the TDDFT equation, the linear response amplitudes c^{+1} are neglected and we get the following equation with the above definitions for the symbols

$$\left(\mathbf{A} - \omega\mathbf{1}\right)\mathbf{x}_\mu = \mathbf{b}^\mu. \tag{10.60}$$

From this we get

$$\alpha_{\mu\nu}(-\omega;\omega) = -(\mathbf{b}^\mu)^T\mathbf{X}\left[\mathbf{\Lambda} - \omega\mathbf{1}\right]^{-1}\mathbf{X}^T\mathbf{f}^\nu. \tag{10.61}$$

The excitation energies are calculated from

$$\mathbf{A}\mathbf{x}_i = \omega\mathbf{x}_i \tag{10.62}$$

and oscillator strength from

$$f_i = -\frac{1}{3}\omega_i\sum_\mu(\mathbf{b}^\mu)^T\mathbf{x}_i\mathbf{x}_i^T\mathbf{f}^\mu \tag{10.63}$$

References

[1] E. Fermi, J. Pasta, and S. Ulam, Los Alamos preprint LA-1940 (1955).
E. Fermi, Collected Papers II, 978 (1965).
B.J. Alder and T.E. Wainwright, J. Chem. Phys., **26**, 1208 (1957).
B.J. Alder and T.E. Wainwright, J. Chem. Phys., **31**, 459 (1959).
A. Rahman, Phys. Rev., **136A**, 405 (1964).
L. Verlet, Phys. Rev., **159**, 98 (1967).

[2] M. P. Allen and D. J. Tildesley, *Computer Simulation of Liquids* (Clarendon Press, Oxford, 1987; reprinted 1990).

[3] D. Frenkel and B. Smit, *Understanding Molecular Simulation – From Algorithms to Applications* (Academic Press, San Diego, 1996).

[4] G. Ciccotti and W.G. Hoover (editors). *Proceedings of the 97th international school of Physics "Enrico Fermi" on Molecular–Dynamics Simulations of Statistical–Mechanical Systems.* North–Holland, Amsterdam, 1986.

[5] M. Meyer and V. Pontikis, *Proceedings of the NATO ASI on Computer Simulation in Material Science* Kluwer, Dordrecht, 1991.

[6] M. P. Allen and D. J. Tildesley, *Proceedings of the NATO ASI on Computer Simulation in Chemical Physics.* Kluwer, Dordrecht, 1993.

[7] D. Marx, in *Classical and Quantum Dynamics in Condensed Phase Simulations* Chapt. 15, eds. B. J. Berne, G. Ciccotti, and D. F. Coker (World Scientific, Singapore, 1998).

[8] D. Marx and J. Hutter, *Ab Initio Molecular Dynamics: Theory and Implementation*, in *Modern Methods and Algorithms of Quantum Chemistry* pp. 301–449, Editor: J. Grotendorst (John von Neumann Institute for Computing, Forschungszentrum Jülich 2000)

[9] H. Goldstein, *Klassische Mechanik* (Aula–Verlag, Wiesbaden, 1987).

[10] M.E. Tuckerman and G.J. Martyna, J. Phys. Chem. B, **104** 159 (2000).

[11] R. Kubo, M. Toda, N. Hashitsume, Statistical Physics II, Springer–Verlag, Berlin 1978.

[12] B.J. Berne and G.D. Harp, Adv. Chem. Phys. **17** 63 (1970).

[13] W. H. Press, S. A. Teukolsky, W. T. Vetterling, and B. P. Flannery, *Numerical Recipes – The Art of Scientific Computing*, (Cambridge University Press, Cambridge, 1992).

[14] W. C. Swope, H. C. Andersen, P. H. Berens, and K. R. Wilson, J. Chem. Phys. **76**, 637 (1982).

[15] H. C. Andersen, J. Comput. Phys. **52**, 24 (1983).

[16] S. Nosé and M. L. Klein, Mol. Phys. **50**, 1055 (1983). S. Nosé, Mol. Phys. **52**, 255 (1984). S. Nosé, J. Chem. Phys. **81**, 511 (1984). S. Nosé, Prog. Theor. Phys. Suppl. **103**, 1 (1991).

[17] M. Parrinello and A. Rahman, Phys. Rev. Lett. **45**, 1196 (1980).

[18] H. C. Andersen, J. Chem. Phys. **72**, 2384 (1980).

[19] G. J. Martyna, D. J. Tobias, and M. L. Klein, J. Chem. Phys. **101**, 4177 (1994).

[20] W. G. Hoover, Phys. Rev. A **31**, 1695 (1985).

[21] G. J. Martyna, M. L. Klein, and M. Tuckerman, J. Chem. Phys. **97**, 2635 (1992).

[22] M. E. Tuckerman and M. Parrinello, J. Chem. Phys. **101**, 1302 (1994).
M. E. Tuckerman and M. Parrinello, J. Chem. Phys. **101**, 1316 (1994).
J. Hutter, M. E. Tuckerman, and M. Parrinello, J. Chem. Phys. **102**, 859 (1995).

[23] R. G. Parr and W. Yang, *Density–Functional Theory of Atoms and Molecules* (Oxford University Press, Oxford, 1989).

[24] R. M. Dreizler and E. K. U. Gross, *Density–Functional Theory* (Springer, Berlin, 1990);

[25] P. Hohenberg and W. Kohn, Phys. Rev. **136**, B864 (1964).

[26] W. Kohn and L. J. Sham, Phys. Rev. **140**, A1133 (1965).

[27] M. Sprik, in *Classical and Quantum Dynamics in Condensed Phase Simulations*, Chapt. 13, eds. B. J. Berne, G. Ciccotti, and D. F. Coker (World Scientific, Singapore, 1998).

[28] R. Car and M. Parrinello, Phys. Rev. Lett. **55**, 2471 (1985).

[29] G. Pastore, E. Smargiassi, and F. Buda, Phys. Rev. A **44**, 6334 (1991).
G. Pastore, in *Monte Carlo and Molecular Dynamics of Condensed Matter Systems*, Chapt. 24, p. 635, eds. K. Binder and G. Ciccotti (Italien Physical Society SIF, Bologna, 1996).

[30] F. A. Bornemann and C. Schütte, Numer. Math. **78**, 359 (1998).
F. A. Bornemann and C. Schütte, Numer. Math. **83**, 179 (1999).

[31] P. Pulay, Chem. Phys. Lett. **73**, 393 (1980).
J. Hutter, H. P. Lüthi, and M. Parrinello, Comput. Mat. Sci. **2**, 244 (1994).

[32] `CPMD Version 3.5:` developed by J. Hutter et al., Max–Planck–Institut für Festkörperforschung and IBM Zurich Research Laboratory (1995–2002).
www.cpmd.org

[33] W. E. Pickett, Comput. Phys. Rep. **9**, 115 (1989).

[34] G. P. Srivastava and D. Weaire, Adv. Phys. **36**, 463 (1987).

[35] D. J. Singh, *Plane waves, Pseudopotentials and the* LAPW *Method* (Kluwer, Dordrecht, 1994).

[36] D. K. Remler and P. A. Madden, Molec. Phys. **70**, 921 (1990).

[37] M. C. Payne, M. P. Teter, D. C. Allan, T. A. Arias, and J. D. Joannopoulos, Rev. Mod. Phys. **64**, 1045 (1992).

[38] G. Galli and M. Parrinello, in *Computer Simulations in Materials Science*, p. 282, eds. M. Meyer and V. Pontikis (Kluwer, Dordrecht, 1991).

[39] G. Galli and A. Pasquarello, in *Computer Simulation in Chemical Physics*, eds. M. P. Allen and D. J. Tildesley (Kluwer, Dordrecht, 1993).

[40] N. W. Ashcroft and N. D. Mermin, *Solid State Physics* (Saunders College Publishing, Philadelphia, 1976).

[41] J. A. White and D. M. Bird, Phys. Rev. B **50**, 4954 (1994).

[42] D.R. Hamann, M. Schlüter, and C. Chiang, Phys. Rev. Lett. **43**, 1494 (1979)

[43] G.B. Bachelet, D.R. Hamann, and M. Schlüter, Phys. Rev. B, **26**, 4199 (1982)

[44] G.P. Kerker, J. Phys. C: Solid State Phys., **13**, L189 (1980).

[45] N. Troullier and J.L. Martins, Phys. Rev. B, **43**, 1993 (1991).

[46] A.M. Rappe, K.M. Rabe, E. Kaxiras, and J.D. Joannopoulos, Phys. Rev. B, **41**, 1227 (1990).
J.S. Lin, A. Qteish, M.C. Payne, and V. Heine, Phys. Rev. B, **47**, 4174 (1993).

[47] L. Kleinman and D.M. Bylander, Phys. Rev. Lett., **48**, 1425 (1982).

[48] P.E. Blöchl, Phys. Rev. B, **41**, 5414 (1990).

[49] D. Vanderbilt, Phys. Rev. B, **41**, 7892 (1990).

[50] X. Gonze, R. Stumpf, and M. Scheffler, Phys. Rev. B, **44**, 8503 (1991).

[51] S. Goedecker, M. Teter, and J. Hutter, Phys. Rev. B, **54**, 1703 (1996).
C. Hartwigsen, S. Goedecker, and J. Hutter, Phys. Rev. B, **58**, 3641 (1998).

[52] S. G. Louie, S. Froyen, and M. L. Cohen, Phys. Rev. B **26**, 1738 (1982).

[53] D. Vanderbilt, Phys. Rev. B **41**, 7892 (1990).

[54] G. Kresse and D. Joubert, Phys. Rev. B **59**, 1758 (1999).

[55] M. Valiev and J.H. Weare, J. Phys. Chem. A **103**, 10588 (1999).

[56] K. Laasonen, A. Pasquarello, R. Car, C. Lee, and D. Vanderbilt, Phys. Rev. B, **47**, 10142 (1993).

[57] G. Kresse and J. Hafner, J. Phys.: Condens. Matter **6**, 8245 (1994).

[58] A. Alavi, J. Kohanoff, M. Parrinello, and D. Frenkel, Phys. Rev. Lett. **73**, 2599 (1994). A. Alavi, in *Monte Carlo and Molecular Dynamics of Condensed Matter Systems*, Chapt. 25, p. 648, eds. K. Binder and G. Ciccotti (Italien Physical Society SIF, Bologna, 1996).

[59] J. Cao and B. J. Berne, J. Chem. Phys. **99**, 2902 (1993).

[60] P. L. Silvestrelli, A. Alavi, M. Parrinello, and D. Frenkel, Phys. Rev. Lett. **77**, 3149 (1996). P. L. Silvestrelli, A. Alavi, and M. Parrinello, Phys. Rev. B **55**, 15 515 (1997). P. L. Silvestrelli, A. Alavi, M. Parrinello, and D. Frenkel, Phys. Rev. B **56**, 3806 (1997). P. L. Silvestrelli and M. Parrinello, J. Appl. Phys. **83**, 2478 (1998).

[61] M. D. Feit, J. A. Fleck, Jr., and A. Steiger, J. Comput. Phys. **47**, 412 (1982).

[62] N. D. Mermin, Phys. Rev. **137**, A1441 (1965).

[63] S. Goedecker, Rev. Mod. Phys. **71**, 1085 (1999).

[64] M. J. Gillan, J. Phys.: Condens. Matter **1**, 689 (1989).

[65] G. W. Fernando, G.–X. Qian, M. Weinert, and J. W. Davenport, Phys. Rev. B **40**, 7985 (1989).

[66] M. Weinert and J. W. Davenport, Phys. Rev. B **45**, 13 709 (1992).

[67] G. Kresse and J. Hafner, Phys. Rev. B **47**, 558 (1993). G. Kresse and J. Furthmüller, Phys. Rev. B **54**, 11 169 (1996).

[68] M. P. Grumbach, D. Hohl, R. M. Martin, and R. Car, J. Phys.: Condens. Matter **6**, 1999 (1994).

[69] N. Marzari, D. Vanderbilt, and M. C. Payne, Phys. Rev. Lett. **79**, 1337 (1997).

[70] G. Makov and M. C. Payne, Phys. Rev. B **51**, 4014 (1995).

[71] J. Bernholc, N. O. Lipari, and S. T. Pantelides, Phys. Rev. B **21**, 3545 (1980).

[72] J.–Y. Yi, D. J. Oh, J. Bernholc, and R. Car, Chem. Phys. Lett. **174**, 461 (1990).

[73] G. Lauritsch and P.–G. Reinhard, Int. J. Mod. Phys. C **5**, 65 (1994).

[74] P. E. Blöchl, J. Chem. Phys. **103**, 7422 (1995).

[75] R. W. Hockney, Methods Comput. Phys. **9**, 136 (1970).

[76] R. N. Barnett and U. Landman, Phys. Rev. B **48**, 2081 (1993).

[77] J. W. Eastwood and D. R. K. Brownrigg, J. Comp. Phys. **32**, 24 (1979).

[78] G. J. Martyna and M. E. Tuckerman, J. Chem. Phys. **110**, 2810 (1999).

[79] J. J. Mortensen and M. Parrinello, J. Phys. Chem. B **104**, 2901 (2000).

[80] A. M. Rappe, J. D. Joannopoulos, and P. A. Bash, J. Am. Chem. Soc. **114**, 6466 (1992).

[81] R. Resta, Ferroelectrics **136**, 51 (1992).
R.D. King–Smith and D. Vanderbilt, Phys. Rev. B **47**, 1651 (1993).
R. Resta, Europhys. Lett. **22**, 133 (1993).

[82] R. Resta, Rev. Mod. Phys. **66**, 899 (1994).
G. Ortiz and R.M. Martin, Phys. Rev. B **49**, 14202 (1994).

[83] A. Shapere and F. Wilczek, Eds., *Geometric Phases in Physics*, World Scientific, Singapore, 1989.

[84] B. Guillot, J. Chem. Phys. **95**, 1543 (1991).

[85] P.A. Egelstaff, Adv. Phys. **11**, 203 (1962).
J. Borysow, M. Moraldi, and L. Frommhold, Mol. Phys. **56**, 913 (1985).

[86] G. H. Wannier, Phys. Rev. **52**, 191, (1937).

[87] N. Marzari and D. Vanderbilt, Phys. Rev. B **56**, 12847, (1997).

[88] S. F. Boys, Rev. Mod. Phys. **32**, 296, (1960).

[89] I. Souza and R. M. Martin, Phys. Rev. Lett. **81**, 4452, (1998).

[90] P. L. Silvestrelli, N. Marzari, D. Vanderbilt and M. Parrinello, Solid State Com. **107**, 7, (1998).

[91] P. L. Silvestrelli, Phys. Rev. B **59**, 9703, (1999).

[92] R. Resta, Phys. Rev. Lett. **80**, 1800, (1998).

[93] R. Resta, Phys. Rev. Lett. **82**, 370, (1999).

[94] J. M. Lighthill, *Introduction to Fourier Analysis and Generalized Functions* (Cambridge University Press, Cambridge, 1958).

[95] C. Dellago, P. G. Bolhuis, F. S. Csajka, D. J. Chandler, J. Chem. Phys., **108**, 1964, (1998).
P. G. Bolhuis, C. Dellago, D. J. Chandler, Faraday Discuss., **110**, 42, (1998).

[96] T. Huber, A.E. Torda, and W.F. van Gunsteren, J. Comput. Chem. **8**, 695 (1994).
H. Grubmüller, Phys. Rev. E **52**, 2893 (1995).
A.F. Voter, Phys. Rev. Lett. **78**, 3908, (1997).

[97] A.F. Voter, J. Chem. Phys. **106**, 4665 (1997).

[98] M. Sprik and G. Ciccotti, J. Chem. Phys. **109**, 7737 (1998).

[99] E. A. Carter, G. Ciccotti, J. T. Hynes, and R. Kapral, Chem. Phys. Lett. **156**, 472 (1989).

[100] J. VandeVondele and U. Röthlisberger, J. Chem. Phys. **113**, 4863 (2000).

[101] D.A. Hendrix and C. Jarzynski, J. Chem. Phys. **114**, 5974 (2001).

[102] S. Melchionna, Phys. Rev. E **62**, 8762 (2000).

[103] Z.W. Zhu, M.E. Tuckerman, S.O. Samuelson, and G.J. Martyna, Phys. Rev. Lett. **88**, art. no. 10020 (2002).

[104] J. VandeVondele and U. Röthlisberger, J. Phys. Chem. B **106**, 203 (2002).

[105] L. Rosso, P. Mináry, Zhongwei Zhu, and M.E. Tuckerman, J. Chem. Phys. **116**, 4389 (2002).

[106] J.B. Anderson, Adv. Chem. Phys. **91**, 381 (1995).

[107] G.H. Vinyard, J. Phys. Chem. Solids **3**, 121 (1957).

[108] C. Császár and P. Pulay, J. Mol. Struc. **114**, 31 (1984).

[109] F. Tassone, F. Mauri, and R. Car, Phys. Rev. B **50**, 10 561 (1994).

[110] M. C. Payne, J. D. Joannopoulos, D. C. Allan, M. P. Teter, and D. Vanderbilt, Phys. Rev. Lett. **56**, 2656 (1986).

[111] M. Pearson, E. Smargiassi, and P. Madden, J. Phys. Condens. Matter **5**, 3221 (1993).

[112] P. E. Blöchl, Phys. Rev. B **50**, 17953 (1994).

[113] P.W. Langhoff, S.T. Epstein, and M. Karplus, Rev. Mod. Phys. **44**, 602 (1972).

[114] X. Gonze, Phys. Rev. A **52**, 1086 (1995).
X. Gonze, Phys. Rev. A **52**, 1096 (1995).

[115] O. Sinanoglu, J. Chem. Phys. **34**, 1237 (1961).

[116] X. Gonze, Phys. Rev. B **55**, 10337 (1997).

[117] R.M. Sternheimer, Phys. Rev. B **96**, 951 (1954).

[118] A. Dal Corso, S. Baroni and R. Resta, Phys. Rev. B **49**, 5323 (1994).

[119] F. Filippone, S. Meloni, and M. Parrinello, J. Chem. Phys. **115**, 636 (2001).
F. Filippone and M. Parrinello, Chem. Phys. Lett. **345**, 179 (2001).

[120] T. Helgaker, M. Jaszunski, and K. Ruud, Chem. Rev. **99**, 293 (1999).

[121] R. Ditchfield, J. Chem. Phys. **56**, 5688 (1972).

[122] W. Kutzelnigg, Isr. J. Chem. **19**, 193 (1980).

[123] T.A. Keith and R.F.W. Bader, Chem. Phys. Lett. **210**, 223 (1993).

[124] F. Mauri and S. Louie, Phys. Rev. Lett. **76**, 4246 (1996).
F. Mauri, B. Pfrommer, and S. Louie, Phys. Rev. Lett. **77**, 5300 (1996).

[125] D. Sebastiani and M. Parrinello, J. Phys. Chem. A **105**, 1951 (2001).

[126] G.H. Wannier, Phys. Rev. **52**, 191 (1937).

[127] W. Kohn, Phys. Rev. **115**, 809 (1959).

[128] G. Berghold, C.J. Mundy, A.H. Romero, J. Hutter, and M. Parrinello, Phys. Rev. B **61**, 10040 (2000).

[129] W. Kutzelnigg, Theor. Chim. Acta **83**, 263 (1992).

[130] T. Gregor, F. Mauri, and R. Car, J. Chem. Phys. **111**, 1815 (1999).

[131] R. Car, in *Monte Carlo and Molecular Dynamics of Condensed Matter Systems*, Chapt. 23, p. 601, eds. K. Binder and G. Ciccotti (Italien Physical Society SIF, Bologna, 1996).

[132] I. Frank, J. Hutter, D. Marx, and M. Parrinello, J. Chem. Phys. **108**, 4060 (1998).

[133] M. Filatov and S. Shaik, Chem. Phys. Lett. **288**, 689 (1998).
M. Filatov and S. Shaik, J. Chem. Phys. **110**, 116 (1999).
M. Filatov and S. Shaik, Chem. Phys. Lett. **304**, 429 (1999).

[134] T. Ziegler, A. Rauk, and E. J. Baerends, Theor. Chim. Acta **43**, 261 (1977).

[135] C. Daul, Int. J. Quantum Chem. **52**, 867 (1994).

[136] J. Gräfenstein, E. Kraka, and D. Cremer, Chem. Phys. Lett. **288**, 593 (1998).

[137] Á. Nagy, Phys. Rev. A **57**, 1672 (1998).

[138] S. Goedecker and C. J. Umrigar, Phys. Rev. A **55**, 1765 (1997).

[139] E. Runge and E.K.U. Gross, Phys. Rev. Lett. **52**, 997 (1984)

[140] E.K.U. Gross, J.F. Dobson, and M. Petersilka, *Density functional theory of time–dependent phenomena* in "Density Functional Theory, ed. R.F. Nalewajski, Springer Series "Topics in Current Chemistry", 1996.

[141] F. Bloch, Z. Physik, bf 81, 363 (1933).